Design synthesis and evaluation of novel boronic acid based fluorescent sensors

Bosch, Laurence Isabelle

Award date:
2004

Awarding institution:
University of Bath

DESIGN SYNTHESIS AND EVALUATION OF NOVEL BORONIC ACID BASED FLUORESCENT SENSORS

Submitted by Laurence Isabelle Bosch

for the degree of PhD

of the University of Bath

2004

Signature 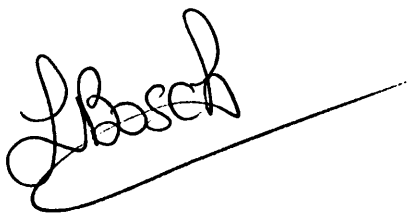

Date 26. 03. 2004

ProQuest LLC
789 East Eisenhower Parkway
P.O. Box 1346
Ann Arbor, MI 48106-1346

"Lucky is he who can understand the causes of things "

Virgil (70-19BC)

Abstract

The ability to detect biologically important molecules is of paramount importance in a wide range of medicinal and industrial environments. Sensors with the capacity to selectively detect chosen molecules and signal this presence by altering their optical signature have attracted considerable interest in recent years. In the last decade, there has been an explosion in the use of boronic acid technology for the molecular recognition of saccharides. Whilst a number of successful sensors have been reported, there has been, to date, only a little activity in the development of ICT (Internal Charge Transfer) systems using the boronic acid moiety.

Twenty boronic acid based sensors for saccharides and fluoride have been prepared. All the sensors can be classified into three different series: monoboronic acid (11), diboronic acid (6) and monoboronic acid with a benzocrown ether moiety (3).

The main fluorophore used in the monoboronic acid series is an aniline fluorophore. One of the systems is a TICT (Twisted Internal Charge Transfer) system. This system contains an intra-molecular boron-nitrogen (B-N) bond and displays dual fluorescence, due to both LE (Locally Excited) and TICT states. Two other ICT systems have no intra-molecular B-N bond and only display fluorescence due to the LE state.

One of the dibronic acid ICT sensors is a TICT system and displays enhanced selectivity for D-glucose, due to optimal spacing of boronic acid groups and forms a 1:1 rigid complex. A Higher stability constant for D-fructose is observed with boronic acid groups in *meta*-position, while the largest fluorescence enhancement is observed with boronic acid groups in *para*-position.

The boronic acid ICT sensors' interaction with halides has also been evaluated. All the sensors studied display changes in fluorescence upon addition of potassium fluoride to solutions of the sensors in methanol, with selectivity for fluoride over other halide ions.

Résumé

La capacité à détecter des molécules biologiquement actives est de la plus haute importance pour un grand nombre d'applications médicales et industrielles. Les sondes fluorescentes, qui ont la capacité de détecter sélectivement les molécules et de signaler leur présence en altérant leur signature optique, ont vu leur intérêt considérablement accru au cours des dernières années. Ainsi, l'utilisation de la technologie des acides boroniques en reconnaissance moléculaire de sucres est en constante augmentation. Cependant, bien qu'un certain nombre de sondes fluorescentes aient été mises au point avec succès, peu de travaux ont été effectués concernant le développement de systèmes ICT (Internal Charge Transfert) possédant un groupement acide boronique.

C'est dans cet objectif que nous avons préparé et étudié 20 sondes fluorescentes possédant un motif acide boronique, pour la reconnaissance des sucres et des ions fluorures. Ces sondes peuvent être classées en trois catégories : 11 sondes possèdant un seul groupement acide boronique, 6 sondes deux groupements acides boroniques, et 3 sondes un groupement acide boronique possédant une unité benzo-éther couronne.

Le principal fluorophore utilisé dans la première série (un seul motif acide boronique) est l'aniline. Nous avons montré qu'une de ces sondes était un système TICT (Twisted Internal Charge Transfert). Ce système contient une liaison intramoléculaire B-N et présente une double fluorescence, due à la présence de deux états LE (Locally excited) et TICT lors de l'addition de sucres. Nous avons également montré que deux autres systèmes ICT, n'ayant pas de liaison intramoléculaire B-N, présentent seulement une fluorescence due à l'état LE.

L'étude des sondes fluorescentes de la deuxième série (deux motifs acides boroniques) a montré qu'une seule de ces sondes était également un système TICT et présentait une forte sélectivité pour le D-glucose, due à un espacement optimal des deux motifs acides boroniques et à la formation d'un complexe rigide 1:1. Nous avons également observé une plus haute constante de stabilité pour le D-fructose lorsque les groupements acides boroniques étaient en position *méta* par rapport au pont CH_2, alors qu'une augmentation significative de fluorescence a été observée lorsque les groupements acides boroniques étaient en position *para*.

Enfin, une étude de l'interaction de ces nouvelles sondes fluorescentes ICT avec les ions halogénures a été effectuée. Toutes les sondes étudiées ont présenté des changements en fluorescence lors de l'addition de fluorure de potassium dans le méthanol, mettant en évidence une sélectivité pour le fluorure sur les autres ions halogénés.

Acknowledgements

I would like to thank many people for their help and encouragement over the past three years. First of all I would like to thank my supervisor Dr Tony James for giving me the opportunity of doing a PhD in the first place, studying both in England and Japan and also for his guidance, help and support along way. Due to his so approachable nature, I could not have asked for a better boss.

I am also very grateful to Professor Itaru Hamachi, for his guidance and welcome during my stay in his laboratory in Japan and also to Professor Thomas Fyles, for his collaboration here in Bath and after, and for his hospitality in Ottawa.

Thanks also go to the past and present members of the legendary BART (Boronic Acid Research Team) for their help and team spirit: Dr Susumu Arimori, Dr Christopher Ward, Dr Karine Frimat, Dr Giuseppe Consiglio, Dr Suvi Koskela, Dr Jianzhang Zhao, Dr Sukhdeep Kaur, Dr Vijay Kumar, and Marcus Phillips.

I also wish to thank Beckman-Coulter and the University of Bath, for funding my PhD. I wish to thank the analytical and technical staff of the university for their expertise, especially Mrs Sarah Elkins for all her help and support.

Thank you to Dr Mary Mahon, Prof. K C Molloy and Dr G Kociok-Köhn, for crystal structure analysis.

I also want to thank the people who proof read this manuscript! Sukhdeep, Vijay, Vincent, Rachel, Dawn, Marcus, Diane, and Christine.

This PhD has also allowed me to meet a number of great people. Thanks go to all the people in my lab past and present Jay, Gary, Phill, Karine, Giuseppe and especially to Vincent for his friendship who spent all the three years working next to me, Petra for our tea break, Upul, Rodolphe for our chat, Belinda, Leonardo, Nicolas, Luke, and all the organic section, Selma, Christelle, Jean-Philippe, Joe, Cath, Claudia, Phil, Kelly, Diane, Koko, Duncan, Steve "La fleur", Steves, Fred, Mikes, Rachel, Chris, Luke Piers, Christine....

A big, big thanks go to the Samba and 1001 Nights who kept me dancing and staying in rhythm: Trisha, Halina, Amanda, Corina, Javina, Caroline, Niki, Serpil, Chararеh (Persian dance) and a very special thank you to Iara (for her Samba class!) and for all the nights out, laughs and rehearsals for shows.
This was an amazing time!!!!!

A big thanks to Francesco, Sean, Emma, Samar, Mahmoud and Hratch, for their friendship and the time spent with them during the weekend escaping from chemistry.

Finally, I would like to extend my thanks to my family, my parents and Arnaud for their love, support and encouragement.

Un Grand Merci à Tous!!!

Table of Contents

List of Abbreviations

Ar	Aromatic
brs	Broad singlet
CT	Charge transfer
δ	Chemical shift
d	Doublet
d app	Apparent doublet
dd	Doublet of doublet
dec	Decomposed
e^-	Electron
EF	Enhancement factor
eq	Equivalent
ET	Energy transfer
EtOH	Ethanol
FAB	Fast atom bombardment
g	Gram
h	Hour
hν	Light
HCl	Hydrochloric acid
HOMO	Highest occupied molecular orbital
HRMS	High-resolution mass spectroscopy
ICT	Internal charge transfer
IR	Infra-red
J	Coupling constant
K	Stability constant
KCl	Potassium chloride
KH_2PO_4	Potassium phosphate
LE	Locally excited
LUMO	Lowest unoccupied molecular orbital
M	Multiplet
m-	*Meta-*
M	$mol.dm^{-3}$

M^{-1}	$mol^{-1}.dm^3$
MeOH	Methanol
mg	Milligram
MHz	Megahertz
ml	Milliliter
mM	$mmol.dm^{-3}$
mmol	Millimoles
mp	Melting point
mV	Millivolt
m/z	Mass to charge ratio
$NaBH_4$	Sodium borohydride
NaCl	Sodium chloride
Na_2HPO_4	*Di*-sodium hydrogen *ortho*phosphate
NaOH	Sodium hydroxide
nm	Nanometer
NMR	Nuclear magnetic resonance
p-	*Para-*
PET	Photo-induced electron transfer
$PhCH_3$	Toluene
ppm	Parts per million
rt	Room temperature
s	Singlet
TICT	Twisted internal charge transfer
THF	Tetrahydrofuran
UV-Vis	Ultra violet-visible
v/v	Volume for volume
w/w	Weight for weight
wt	Weight
°C	Degree centigrade
λ_{em}	Emission wavelength
λ_{ex}	Excitation wavelength
%	Percentage
Φ	Quantum yield

Chapter 1

Introduction

"Savoir s'étonner à propos est le premier pas fait sur la route de la découverte"

Louis Pasteur (1822-1895)

1.1 Overview

Molecular recognition is defined as a process, which involves not only binding but also the selection of a certain substrate, by a certain receptor molecule with a chemical or physical purpose. This process is therefore based on the interaction between a substrate and a receptor, which possesses the specific electronic and geometrical characteristics required for this interaction. For this recognition to be of practical use to analytical chemists, some measurable signal must be generated when it takes place. The recognizing molecule must have not only a receptor moiety but also a signaling one. The molecular recognition process that takes place, when binding of the substrate to the receptor group occurs, produces a supermolecule (substrate-receptor-signaling unit).[1]

Applying the principles contained in the definition of the molecular recognition is an important key for the design of sensors. This section will introduce the concepts used in the design of chemosensors, and to provide a general summary of boronic acid fluorescent sensors for saccharides and fluoride.

1.2 Definition of a Sensor

A sensor is a device, which interacts with a guest and gives a signal in response of this host-guest binding event (Figure 1).

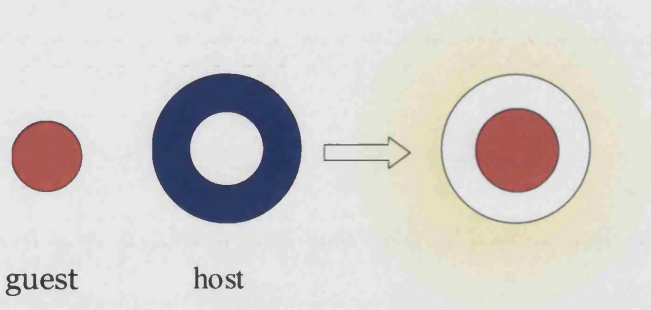

Figure 1: The action of a sensor: signalling as a result of a guest binding to a host (receptor).

Different methods to signal the binding event are available, fluorescence, absorbance or electrochemically. Fluorescence will only be explained in the next section.

1.3 Principle of Fluorescence

Nicolas Monardes, a spanish physician and botanist, observed fluorescence for the first time in 1565, when he noticed a strange blue glimmer from water contained in a cup made from a specific wood (*Ligirium nephiticiem*). However, the understanding of fluorescence became clear only in the late 19th century with George Stokes' work. He was the first one to establish that fluorescence emission was emitted at a longer wavelength than the excitation wavelength.

Figure 2 shows the different absorption and emission processes which can occur in a molecule (Jablonski diagram).[2]

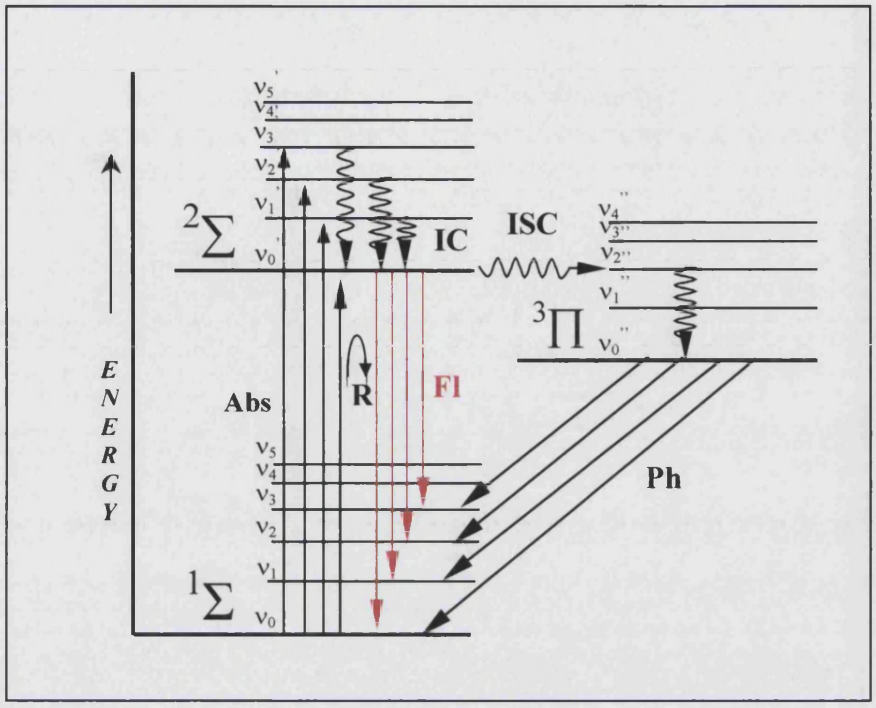

Figure 2: A molecular energy level diagram showing absorption (Abs), resonance fluorescence (R), fluorescence (Fl), internal conversion (IC), intersystem crossing (ISC) and phosphorescence (Ph).

The ground singlet state and the triplet state of the electronic energy level of the molecule are presented as $^1\Sigma$ and $^3\Pi$, respectively. The first excited state is presented by $^2\Sigma$. Each electronic level has a series of vibrational states labelled ν_1, ν_2, ν_3 .... for the ground state and ν_1', ν_2', ν_3'... for the first excited state.[3] The simplest type of fluorescence is the resonance fluorescence (R), in which the radiation emitted is of the same wavelength as the exciting radiation. Fluorescence (Fl) is the emission of a photon, which results from the return to the lower level at a longer wavelength (i.e. lower energy). The missing energy in fluorescence corresponds to nonradiative or internal conversion (IC) transitions shown as wavy lines within the excited state in Figure 2. This energy is lost in collision with other atoms or molecules as kinetic energy of motion or in other excited vibrational states in other particles. Phosphorescence (Ph) is the result of the emission from a triplet to a singlet state. Because it is a forbidden

transition it will only occur very slowly requiring up to 1 second or even longer. However, in the fluorescence emission, both states are singlets corresponding to an allowed and very rapid transition (less than 10^{-8} seconds).

Finally, the advantage of fluorescence sensors for saccharides lies in the inherent sensitivity of the fluorescence technique. The high sensitivity of fluorescence allows the detection of single molecules. Consequently, only a small amount of the sensor is required (typically 10^{-6} mol.dm^{-3}) offsetting the synthetic cost of such sensors. Moreover, fluorescence spectrometers are widely available and inexpensive.
Fluorescence allows a plethora of applications in molecule-molecule recognition events in chemistry and biology. Optical fibres are already used in medical field for continuous monitoring.

1.4 Glucose Sensors

1.4.1 Context of Research

Saccharides play many important and essential roles in living organisms. They are involved in a variety of functions in glycobiology: in cell recognition, cell adhesion, many aspects of the immune response and in regulation of hormonal activity. However, the more common one is the detection of the presence and concentration of biologically important sugars, which have recently gained much attention.

D-glucose for example, is the main source of energy for living organisms. Human blood contains three monosaccharides with different concentrations: D-glucose (0.3-1 mmol.dm^{-3}), D-fructose ($\leq$0.1 mmol.dm^{-3}) and D-galactose ($\leq$0.1 mmol.dm^{-3}). Recent research provides clear evidence that a tight control of blood sugar (glucose) levels in diabetics sharply reduces the risk of long term complications of the disease

(blindness, kidney failure, heart attack). Also, the breakdown in the transport of glucose in humans has been related to cystic fibrosis and cancer. [4]

Industrial processes also require the monitoring of the concentration of sugars in fermentations during the brewing and when analysing the purity of synthetic drugs.[5, 6]

1.4.2 Biosensors

In the medicinal and industrial fields the majority of the methods used for the detection of glucose are based on the glucose oxidase (GOD) enzyme: enzyme-based biosensor.[7] In this case, voltammetric techniques are used for detection purpose: Glucose oxidase (GOD) catalyses the oxidation of glucose to gluconic acid. The basic reaction of oxidation of the aldehyde group to a carboxylic acid group produces two electrons, which are accepted by an electron acceptor, usually molecular oxygen, which produces a peroxide.

The overall reaction is decribed as follows:

$$\text{glucose} + \text{GOD}_{\text{oxidized}} \longrightarrow \text{gluconic acid} + \text{GOD}_{\text{reduced}}$$

$$\text{GOD}_{\text{reduced}} + O_2 + 2H^+ \longrightarrow \text{GOD}_{\text{oxidized}} + H_2O_2$$

Monitoring either the production of hydrogen peroxide or the decrease in the amount of oxygen enables the determination of the glucose concentration.

The production of hydrogen peroxide is monitored by anodic oxidation at a fixed potential (e.g. +600 mV versus (Ag/AgCl)). The current measured, is directly related to the concentration of glucose in the original sample. This biosensor works well in industry for the detection of the glucose concentration in food, such as ice cream, glucose syrup.....[7]

An alternative method uses an oxygen probe to monitor the decrease in the amount of oxygen in the sample after oxidation of the glucose.

This glucose biosensor has also been used for the determination of glucose in whole blood for diabetics. However, in a media such as whole blood, the presence of metabolites (such as ascorbic acid) can interfere with the detection of oxygen or hydrogen peroxide, in such cases a mediator, ferrocene derivative (Figure 3), is used to mediate the redox process.

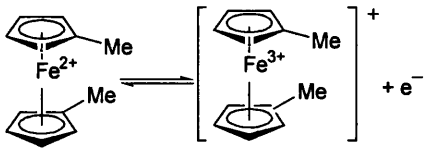

Dimethylferrocene $FeCp_2Me_2$ — Dimethylferricinium ion $FeCp_2Me_2^+$

Figure 3: Oxidation of dimethylferrocene

In the glucose oxidase catalysed oxidation of glucose the ferricinium ion acts as the electron acceptor and eliminates the need for oxygen. The overall reaction is presented below:

$$\text{glucose} + GOD_{oxidized} \longrightarrow \text{gluconic acid} + GOD_{reduced}$$

$$GOD_{reduced} + 2FeCpMe_2^+ \longrightarrow GOD_{oxidized} + 2FeCpMe_2 + 2H^+$$

In this method, the potential is held at the one required for the oxidation of the dimethylferrocene to dimethylferricinium ion (+160 mV). Each equivalent of glucose, which is oxidized, produces the same equivalent of reduced form of GOD, which reacts with the dimethylferricinium ion to produce the same equivalent of dimethylferrocene.

This is immediately oxidised back to the dimethylferricinium ion at the set potential. The current measured is proportional to the concentration of glucose present.

Another glucose biosensor is also available using a different class of enzyme, glucose dehydrogenase and is based on the cofactor, Nicotinamide Adenine Dinucleotide, NAD^+/ NADH see below:

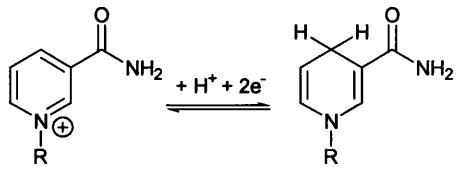

NAD^+ NADH

R = adenosine diphosphoribose

This biosensor based on glucose dehydrogenase uses a graphite modified surface with Medola blue (7-dimethyl-amino-1,2-benzophenoxazinium ion see below).

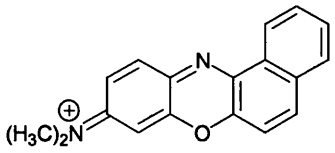

Medola blue

Compounds such as this bind strongly to the graphite and exchange electrons rapidly with the cofactor. The structure of the Medola blue and the glucose dehydrogenase catalyse the oxidation of glucose in the presence of NAD^+ cofactor, the reaction is shown below.

$$\text{glucose} + NAD^+ + H_2O \xrightarrow[\text{Deshydrogenase}]{\text{Glucose}} \text{gluconic acid} + NADH$$

The amount of NADH formed is determined at the chemically modified electrode by oxidation using the appropriate potential and measuring the current. Unfortunately this reaction is irreversible and it is impossible to reuse the biosensor.

As we have just seen, there are a number of limitations using enzymes for the detection of glucose. The enzymatic nature of the glucose oxidase or dehydrogenase means that its inherent instability, its lifetime and also all these methods are sensitive to factors that influence either the enzyme activity or glucose transport.

1.4.3 Artificial Sensors

In nature, recognition of saccharides by enzymes occurs by the formation of hydrogen bonding[6] in the pocket of the enzyme. In lectins and bacterial periplasmic proteins the natural protein-carbohydrate recognition is generally established through a network of hydrogen bonds and complementary contact between nonplanar surfaces (Figure 4).

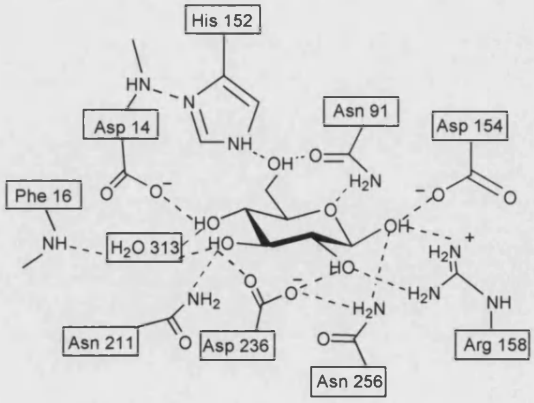

Figure 4: Intramolecular hydrogen bonds in the complex between D-glucose and "D-galactose-binding" bacterial periplasmic protein. [8, 9]

In antibodies the recognition is mediated by the use of main chain amides for hydrogen bonding and the most general hydrogen bonding motif is NH...OH...O=C. This motif highlights many possibilities and also the importance of cooperative hydrogen bonding by the sugar hydroxy groups.[9]

Non-covalent interactions

In the last 20 years, an alternative design has emerged, utilizing synthetic receptors. The idea to use artificial receptors instead of natural enzymes as glucose sensors has been driven by the need for stable, sterilisable and nonimmunogenic materials. The vast majority of these systems rely on hydrogen bonding interaction for the recognition of the guest species. A recent review described the progress of carbohydrate recognition through non-covalent interactions. [9] A few new examples in the literature have been chosen and presented below, to give a brief illustration of how hydrogen bonding has been used in saccharide recognition.

In 1998, Davis et al. synthesised the novel tricyclic cage (Figure 5a).[10] This carbohydrate receptor was inspired by carbohydrate-binding proteins, which commonly place aromatic surfaces against patches of carbohydrate CH groups while accepting the hydroxyl groups into networks of hydrogen bonds. The tricyclic cage receptor (Figure 5a) can bind the monosaccharide derivatives strongly and has a remarkable affinity and selectivity for all-equatorial β-glucosides (Figure 5b) against the α-anomer (Figure 5c) in chloroform even in the presence of 8% of CD_3OH.[10] In 2002, an "extended analogue" of the tricyclic cage (Figure 5a) was designed for disaccharide substrates (Figure 5d).[11] This new receptor is the first to distinguish clearly between disaccharides through noncovalent interactions. The tricyclic octaamide cage (Figure 5d) possesses a parallel

apolar surface linked through a spacer containing hydrogen bond donor and acceptor groups that can detect, selectively, the *n*-octyl-β-D-cellobioside (Figure 5e).

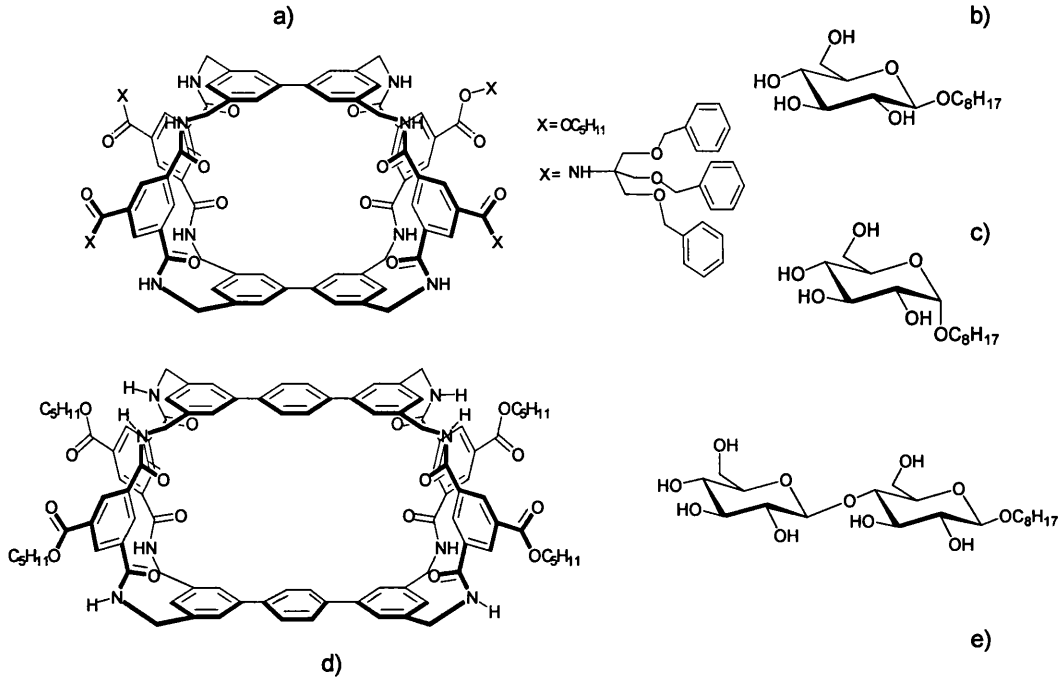

Figure 5: a) and d) Carbohydrate receptors by Davis b), c) and e) examples of saccharides

Pyridine based receptors have been explored by a number of groups for carbohydrate recognition purposes. Recently, Shinkai *et al.*, have synthesised a fused-pyridine receptor, which contained two carboxylate anions and four basic nitrogen atoms capable of forming both ionic and hydrogen-bonding interactions (Figure 6). [12] This receptor can bind with high affinity various aminoglycosides (D-glucosamine, D-galactosamine and D-mannosamine). The ammonium group interacts with one of the two carboxyl groups while the hydrogen-bonding interaction occurs between the hydroxyl groups of the saccharides and the other carboxyl group and/or nitrogen bases. An induced circular

dichroism (CD) is caused by the formation of a pseudo-cyclic 1:1 complex involving mutiple point interactions.

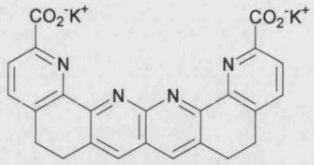

Figure 6: Shinkai pyrdine-based receptor.

In 2002, Sicking and co-workers have prepared acyclic pyridine-based receptors, which display a high α/β-anomer selectivity (Figure 7).[13] The interactions involve the amino-pyridine unit and thus affect the selectivity and affinity of the receptor in favour of the β-D-glucopyranoside with a marked β *versus* α selectivity. The pyridine unit participated in cooperative and bidentate hydrogen bonds with the sugars hydroxyls, similar to biological systems.

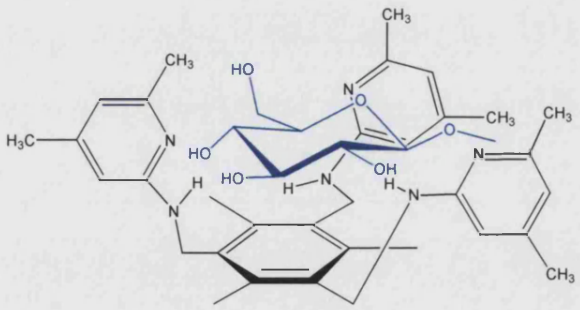

Figure 7: Example of pyridine-based receptor by Sicking and co-workers.

1,1'-binaphthyl-substituted macrocycles have been used by many groups with porphyrin or metalloporphyrin units, such as Kral and co-workers[14], or phosphates like Diederich and co-workers.[15]

Figure 8a shows the (Fe^{III}) metalloporphyrin macrocycle with four 1,1'-binaphthyl-substituents and eight phenolic hydroxyl groups which generate a binding site for saccharides.

The (Fe^{III}) metalloporphyrin macrocycle (Figure 8a) interacts more strongly with saccharides than its porphyrin analoguous and with a preference for disaccharides.

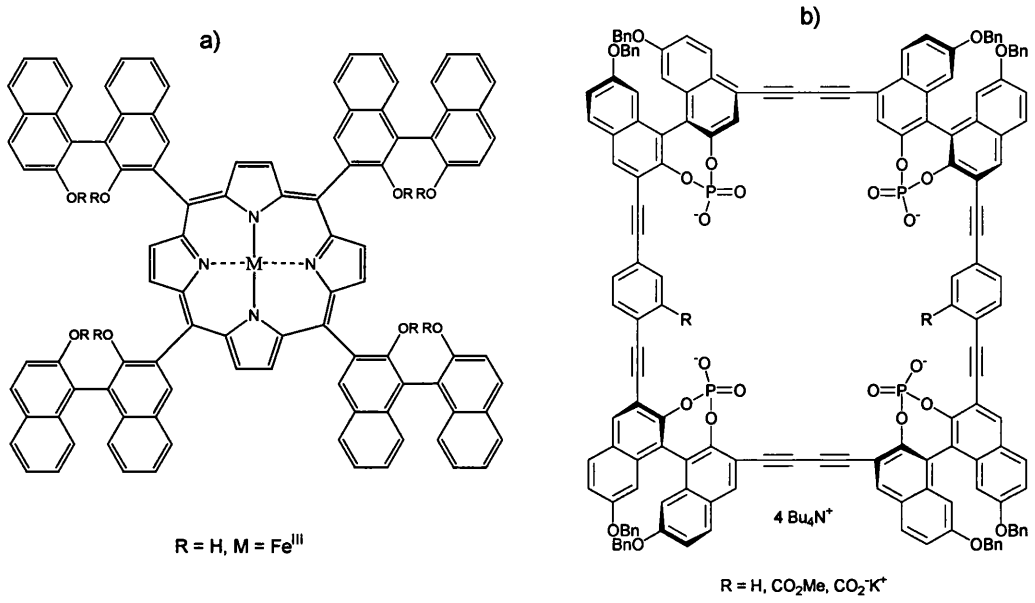

Figure 8: Examples of Macrocycles a) Kral and co-workers; b) Diederich and co-workers

Diederich's cyclophane receptor is based on phosphodiester residues (Figure 8b). This family of receptor binds very strongly disaccharides with phophodiester residues.

Other groups have used photoaffinity-labelling modification of a lectin surface to recognise saccharide[16] or peptide-bridged calixarenes.[17]

Some examples of synthetic receptors using hydrogen bonding have been presented. The efficiency of such interactions has been well demonstrated in non-aqueous systems, however, in aqueous media, competitive hydrogen bonding by the solvent is a serious drawback.[6]

To overcome the hydrogen-bonding drawback, artificial chemosensors based on boronic acids have been developed.[6]

Covalent interactions

Boronic acid background

In 1880, phenylboronic acid was first synthesised by Michaelis and Becker.[18] However this discovery remained unused until Kuivila *et al.*[19] published the first binding study of diols with boronic acid in 1954. They noticed that phenylboronic acid solubilised polyols including saccharides and the formation of a cyclic ester was postulated for the first time. This agreed with the known ability of boronate esters to form complexes with compounds containing polyhydroxyl groups. [20]

Later, in 1959, Lorand and Edwards[21] reported the first quantitative evaluation of interaction between saccharides and boronic acids. To clarify the structure of the phenylboronate anion, Lorand and Edwards investigated a range of diols after addition to phenylboronic acid at such a pH that is existed in equal quantities as its neutral and anionic forms, i.e. its pK_a. It was observed, using the method of pH depression, that the pH of the solution upon addition of a wide range of diols was reduced. This study lead to the first determination of the phenylboronic acid's affinity for diols. The conclusion of this study was that the phenylboronate anion has a tetrahedral, rather than trigonal structure as shown in Figure 9.

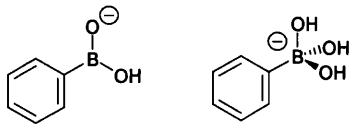

Figure 9: Proposed trigonal and tetrahedral forms of the phenylboronic acid anion.

In spite of the fact that the structure of the boronic acid-saccharide complex formed in aqueous solution is still disputed[22], the use of boronic acid in the design of sensors for saccharides has become increasingly important. [1,6, 18, 23, 24, 25, 26, 27]

Boronic acids rapidly and reversibly forms cyclic esters with diols in nonaqueous or basic aqueous media. The most common interactions are with *cis* 1,2 or 1,3-diols to generate five or six-membered rings respectively *via* two covalent bonds[6] (Scheme 1). The rigid vicinal *cis* diols of saccharides form more stable cyclic esters than simple acyclic diols such as ethylene glycol.

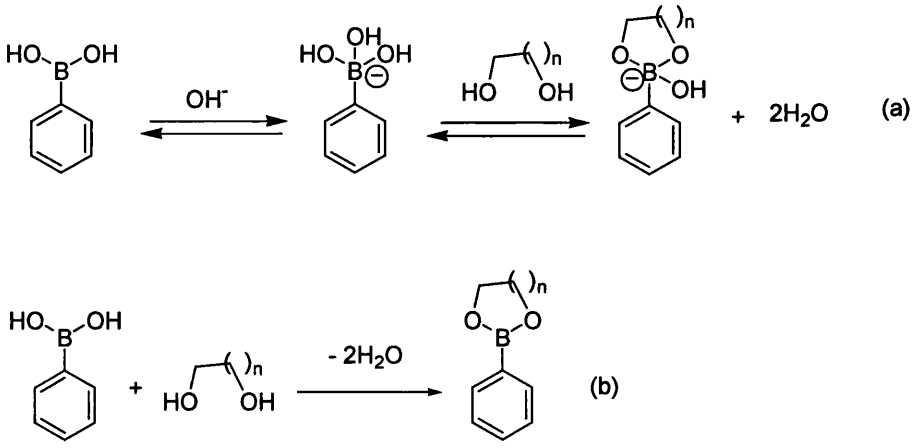

Scheme 1: Cyclic ester formation of phenylboronic acid with diols in (a) basic aqueous media and (b) aprotic media in the presence of dehydrating agent.

As described earlier, Lorand and Edwards determined the selectivity of phenylboronic acid[21] towards acyclic diols and saccharides. Table 1 reports a selection of results.

Table 1: Stability constant for some polyol-phenylboronic acid complexes.

Polyol	log K_a
D-Fructose	3.64
D-Galactose	2.44
D-Mannose	2.23
D-Glucose	2.04
Ethylene glycol	0.44

The selectivity order observed by Lorand and Edwards is common to all monoboronic acids.[6, 21]

With saccharides the choice of diol used in the formation of cyclic esters is complicated by the possibility of pyranose to furanose isomerisation of the saccharide moiety.

Usually free boronic acids have sp^2 hybridization and, therefore, the bond angle is 120° (Scheme 2a). However, when boronic acids bind to form cyclic ester, the bond angle is reduced to 108° (Scheme 2b). Since sp^3 hybridized orbitals have a tetrahedral geometry, with an ideal bond angle of 109°, formation of the boronate anion reduces the ring strain (Scheme 2c). The reduction of the bond angle from 120° to 108° changes the hybridization from sp^2 to closer to sp^3 hybridization. Therefore, the cyclic boronate ester formed is more acidic than the free boronic acid.

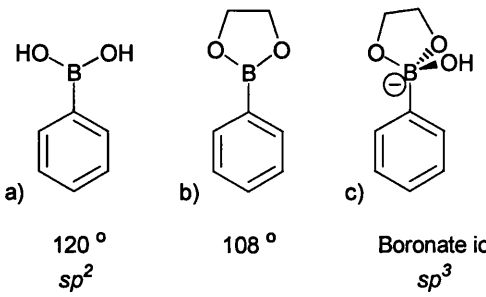

Scheme 2: O-B-O bond angle variation and hybridization form during boronic acid binding and anion formation.[28]

It is well known that the boron atom in boronic acids becomes more acidic when bound to saccharides.[21] The reduction of pK_a upon addition of saccharide is the base for the development of many sensors, but its definition is not well defined in this context. A better explanation would be to consider the boronic acid to have a water molecule loosely associated to the boron. At high pH, the associated water molecule is deprotonated and a tetrahedral boronate anion is formed. The binding of a saccharide to a boronic acid enhances the Lewis acidity of the boron, facilitating this deprotonation (Scheme 3).[29]

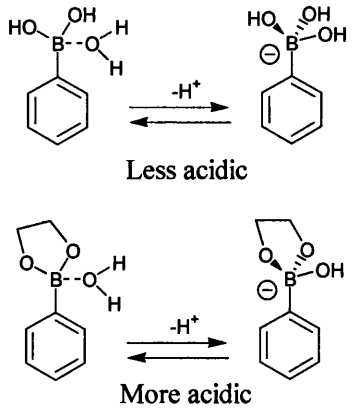

Scheme 3: qualitative description for the pKa of boronic acid.[29]

The formation of an sp^3-hybridized boronic acid is also possible by incorporation of a neighbouring tertiary amine (B-N bond) at neutral pH, and was first introduced by Wulff (Scheme 4).[30]

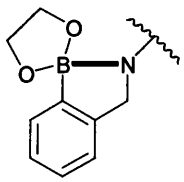

Scheme 4: sp^3 form with B-N bond at neutral pH

The B-N bond has been successfully used in the development of saccharide sensors. The interaction of the neighbouring amine with the boronic acid is strengthened on saccharide binding. The strength of this boronic acid-tertiary amine interaction can be used to detect the signal of the binding event by UV-Vis spectroscopy with colour sensors and by fluorescence spectroscopy with fluorescent sensors.[1, 24, 26, 27]

Further applications of boronic acid as receptor are presented in the next section.

Internal Charged Transfer (ICT)

Internal charge transfer (ICT) can be defined as an integrated system (Figure 10), where the fluorophore is directly attached to the receptor and acts as a donor acceptor system.[25] When the fluorophore is excited by light, a charge transfer (CT) occurs within the molecule.

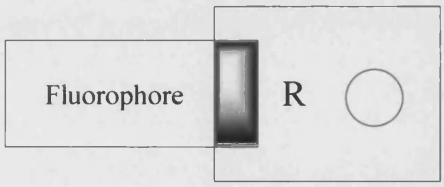

Figure 10: Integrated fluorophore-receptor, receptor (R).

The presence of electron donor and acceptor groups on opposite sides of the molecule, connected by a highly delocalised π electron system, is the key to observe dual fluorescence.

Lippert *et al.* 40 years ago, was the first one to discover dual fluorescence in compounds such as 4-(*N,N*-dimethylamino)benzonitrile (shown in Figure 11). The first model proposed by Graboswski *et al.*, commomnly named TICT for twisted internal charge

transfer, supposed the existence of two conformers for the intramolecular charge transfer excited state.[31]

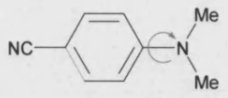

a) 4-(*N,N*-dimethylamino)benzonitrile

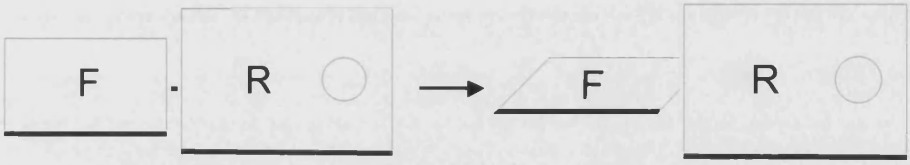

b) ICT TICT

Figure 11: example of Lippert compound, 4-(*N,N*-dimethylamino)benzonitrile and ICT to TICT tranformation.

Early systems

Early fluorescent sensors for saccharides were very simple molecules, based on fluorophore boronic acid. In 1992-1993, Yoon and Czarnik reported the first boronic acid sensor, 2-anthrylboronic acid and 9-anthrylboronic acid (Figure 12a and b). [32, 33]

In these two systems, the fluorophore is the anthracene unit. Both 2- and 9-anthrylboronic acid can be used to detect saccharides. The fluorescence of 2- and 9-anthrylboronic acid is quenched upon saccharide binding. It was observed that the pK_a of fluorophore boronic acid was lowered upon saccharide complexation. Therefore, since the pK_a value decreased upon addition of saccharide, the amount of fluorescence quenched at a fixed pH increased. So pK_a modulation reported saccharide recognition by the anthrylboronic acid system.

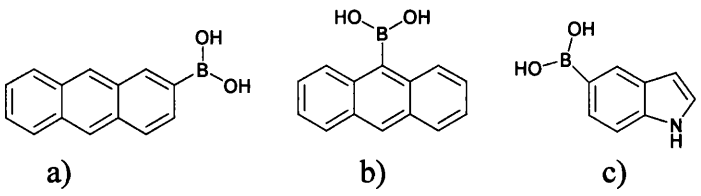

Figure 12: First ICT Fluorescent Sensors for Saccharides

Similarly, Aoyama showed that 5-indolylboronic acid (Figure 12c) undergoes fluorescence quenching upon complexation with monosaccharides and oligosaccharides.[34] The stability constant order for monosaccharides was as expected. However, if the length of the oligosaccharide is increased, an increase in stabilization due to an interaction with the indole was observed.

Shinkai *et al.*[35, 36] through a screening of eight aromatic boronic acids, have shown that the two arylboronic acid presented in Figure 13, are the more suitable candidates for the detection of saccharides due to the large fluorescence changes compared to 2-anthrylboronic acid used by Czarnik which displayed only a small fluorescence change.

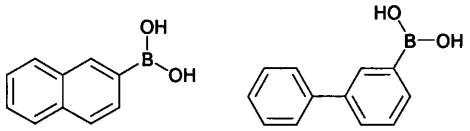

Figure 13: more suitable candidate from a screening of eight aromatic boronic acids

All of these systems were described originally as a photon induced electron transfer (PET) systems where the fluorescence is quenched by a boronate anion, using an "On-Off" process. However, a more reasonable explanation of the fluorescence quenching comes from the investigation of stilbene boronic acid (Figure 14a) by Shinkai *et al.*[37] in 1995 and as well by the detailed investigation of 4 stilbene systems (Figure 14a-d) by Lakowicz[38] in 2001. Principally, the neutral form of the boronic acid acts as an electron-

withdrawing group while the anionic form of the boronate ester acts as an electron-donating group. Upon saccharide binding, the boronic acid changes to its anionic form, and this is what causes the fluorescence spectral changes observed by both groups. This donor-acceptor system lead to the prospect of a new class of fluorescence probes for saccharide recognition.

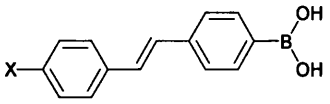

a) X = $N(CH_3)_2$
b) X = H
c) X = CN
d) X = OCH_3

Figure 14: Stilbene derivatives (a-d)

Therefore, the original fluorescent systems described have now been classified as ICT fluorophores rather than PET systems. The boronic acid is the acceptor group and no defined donor is present in these simple systems.

New systems

Very few ICT fluorescent respond to small anionic or neutral molecules.[25] Until recently only one example was reported in the literature.[39] The Shinkai group prepared an ICT fluorescent sensor for saccharides, based on the coumarin framework (Figure 15).

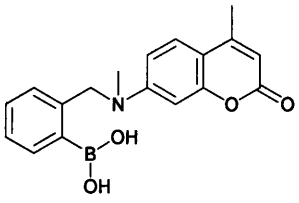

Figure 15: first elaborated ICT sensor

In this system, both fluorescence intensity and wavelength are affected since the nitrogen is directly connected to the chromophore. However, this system shows only a small shift in emission wavelength and in intensity of emission upon binding with D-fructose.

This result demonstrates that the coumarinium ICT system was insensitive to saccharide binding in spite of its clever molecular design. This was the first attempt to link a donor and an acceptor group for the designed construction of an ICT system.

Lakowicz utilizing the potential of the stilbene boronic acid (Figure 8a) and in an attempt to extend their usefulness, a number of analogous ICT systems [40] were prepared including polyene[41] (16a,b), diphenyloxazole[42] (16c), boron-dipyrromethene[43] (BODIPY) (16d) and chalcone[44] (16e, f) derivatives (Figure 16).

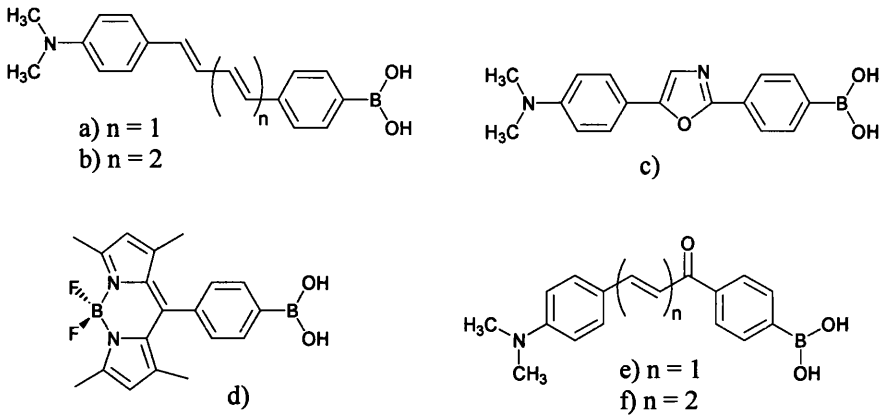

Figure 16: Examples of ICT sensors by Lakowicz et al.

The combination of an electron withdrawing and/or donating group and a boronic acid group, both directly linked to the fluorophore, lead to the formation of an excited state charge transfer. The neutral form of the boronic acid acts as an electron-withdrawing moiety, however, its anionic form acts as an electron-donating moiety. Upon complexation with saccharides, the boronic acid changes from its neutral to anionic form and this causes a change in the charge transfer properties of the fluorophore. For example, the diphenylbutadiene boronic acid (16a) showed a larger spectral shift than the diphenylhexatriene boronic acid (16b). Both are donor-acceptor systems and illustrate that charge transfer can be applied to long wavelength probes compared to the stilbene probes (14a). Lifetime measurements of both compounds have also shown some change, which could possibly be explained by the formation of a TICT state.

The diphenyloxazole substituted with a dimethylamino (electron-donating) and a boronic acid (electron-withdrawing) group (Figure16c) is another example of ICT which displays fluorescence changes upon addition of saccharides. The ICT state is between the boronic acid group (electron-withdrawing) and the *N,N*-dimethylamino group (electron-donating). This family of fluorophore are well known to display a high

fluorescence quantum yield, long wavelength emission, good photostability and are also known to be very sensitive to small perturbations in the charge transfer nature of the excited state. Upon addition of saccharides, large intensity changes and a blue shift (30 nm) is observed.

The chalcone derivatives (Figure 16e and f) have an electron-donating group (dimethylamino) and two electron-withdrawing groups (carboxyl and boronic acid group). They also have the advantage of having long wavelength emissions. In these particular cases, the charge transfer occurs between the dimethylamino group (electron-donating group) and the carbonyl group (electron-withdrawing group). As the boronic acid is in resonance with the carboxyl group the change in the electronic properties of the boron group, both when free and when complexed with sugar, lead to a variation in the electron density of the benzophenone moiety and in the charge transfer properties of the excited state of the fluorophore. When the boron group is in its anionic form, the boronate increases the electron density on the carboxyl group and then reduces the ICT from the dimethylamino group, which is thought to be the origin of the spectral changes observed.

The BODIPY system displays only a small fluorescence change in both absorption and emission spectra. Although the BODIPY system did not work well, more investigations are required for further use of this fluorophore. The BODIPY chromophore presents many advantages as a fluorescence probe: high fluorescence quantum yield, good photostability, narrow emission band and their building block synthesis allows modifications in order to obtain probes with long wavelength fluorophores typically between 500 and 700 nm. This range of long wavelength is highly desirable for fluorescent probes for glucose for the transdermal monitoring and /or measurement of glucose in whole blood.

Recently Wang has published work on a ICT sensor shown in Figure 17.[45] This system is based on the early system with an additional electron-donating group, directly attached to the fluorophore.

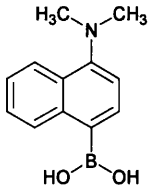

Figure 17: Last reported ICT sensor.

The dimethylamino group acts as an electron-donating group while the boronic acid acts as an electron-withdrawing group in the ICT process. Upon complexation with saccharide, the boron will form the boronate anion and thus switch off the ICT process. This system shows a large fluorescence increase upon addition of saccharides.

Photoinduced Electron Transfer (PET)

Photoinduced electron transfer (PET) has been widely studied.[5, 6, 46, 47] Many different types of PET systems are described in the literature,[25] only saccharide sensors will be discussed in this part.

Saccharide PET sensors can be described as a fluorophore and a receptor linked together by a short spacer[6, 25, 48] as seen in Figure 18.

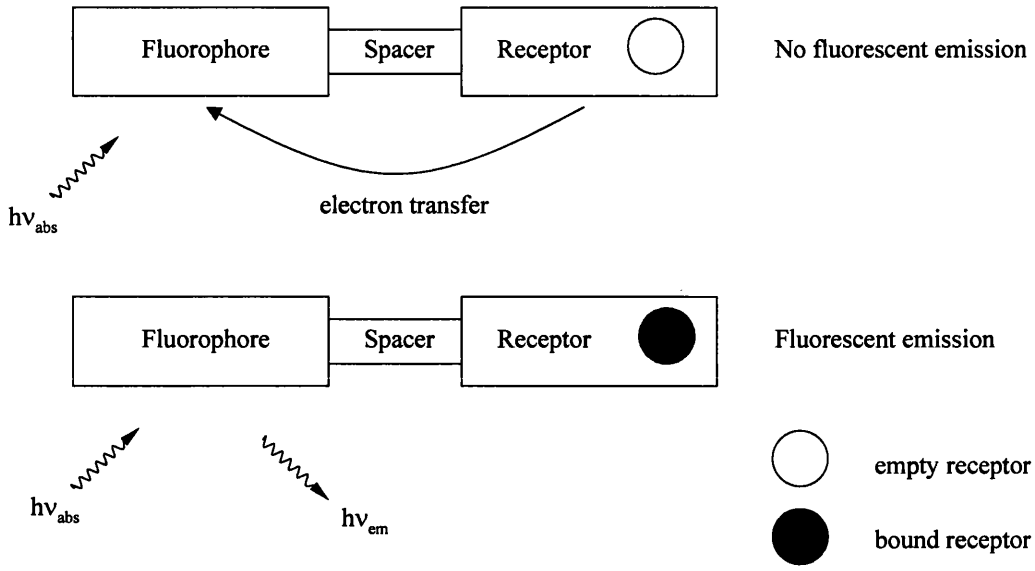

Figure 18: Schematic diagram of an "Off-On" fluorescent PET sensor.[25]

A fluorophore is a molecule, which is able to fluoresce such as anthracene, pyrene or naphthalene. The change in redox potential of the receptor upon guest binding can alter the PET process and generate changes in the fluorescence allowing switching "On" and "Off".[6]

The fluorescence can be "switched Off" by the PET process. The PET process, in turn, can be suppressed by the entry of a substrate into the receptor, which is then able to " switch On" the fluorescence. This is a so called "Off-On" system.

Saccharide sensors designed to work at neutral pH were based on boronic acids with neighbouring amine group participation.[30] The proximity of the boronic acid and the neighbouring amine also provides an electron-rich center for the PET system.[6, 25] Since it is only weakly bound to boron, the amine electron lone pair is largely free to engage in PET activity with the fluorophore nearby in neutral solution. When a saccharide binds to the receptor, the increased acidity of the boronic acid moiety strengthens the boron-nitrogen bond. Thus, the PET activity ceases and the fluorescence is switched "On".[6, 25]

Figure 19, depicts the way an"Off-On" boronic acid PET sensor work.

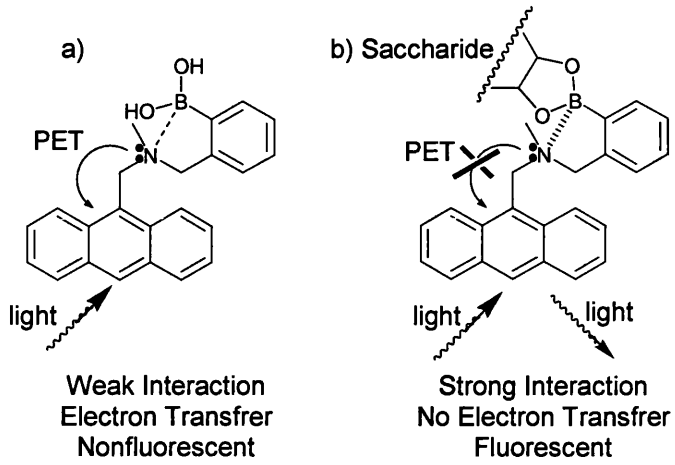

Figure 19: Example of an "Off-On" Boronic Acid PET Sensor
a) unbound and b) bound with saccharide.

A view in terms of the frontier molecular orbital energies is given in Figure 20.

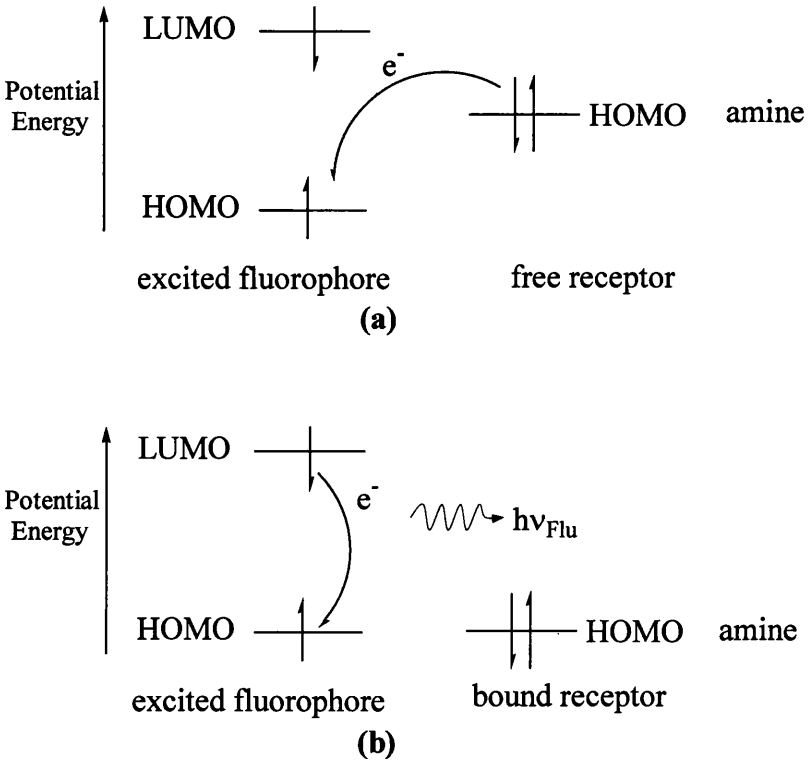

Figure 20: Frontier orbital energy diagram of a PET process in a "spaced fluorophore-receptor" system (a) free receptor and (b) bound receptor.[25]

When the receptor is free (Figure 20a) PET occurs from the amine HOMO to the fluorophore HOMO i.e. to the lower energy level. Since the electron in the excited state cannot return to this lower energy level due to the Pauli exclusion principle, then fluorescence is inhibited. However, when the receptor is bound to its target (Figure 20b), the Lewis acid-base interaction between the boronic acid and the amine is strengthened, lowering the energy of the receptor HOMO. PET, therefore, is disfavoured leading to fluorescence recovery.

The first example of a boronic acid PET sensor[46] for saccharides (Figure 21a) was discovered by the Shinkai group in 1994 and it is the first in a series of such sensors and shows the expected selectivity (D-fructose).[46, 49, 50]

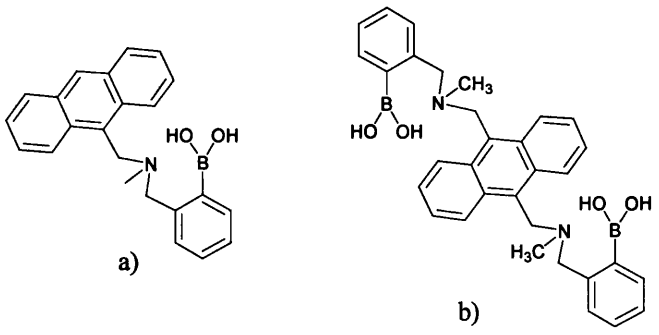

Figure 21: First PET and D-glucose PET sensors

Then, the first glucose PET sensor (figure 21b) was synthesised by the Shinkai group in 1994 by incorporation of a second boronic acid unit.[50]

This sensor is a perfect glucose cleft, with higher "switch On" factor than the first PET sensor (Figure 21a). This sensor (21b) possessed two different ways of binding. This resulted in the formation of two different complexes[49] 2:1 and 1:1 (Figure 22). The 1:1 rigid cyclic complex is specifically formed with D-glucose, therefore the system is D-glucose selective.

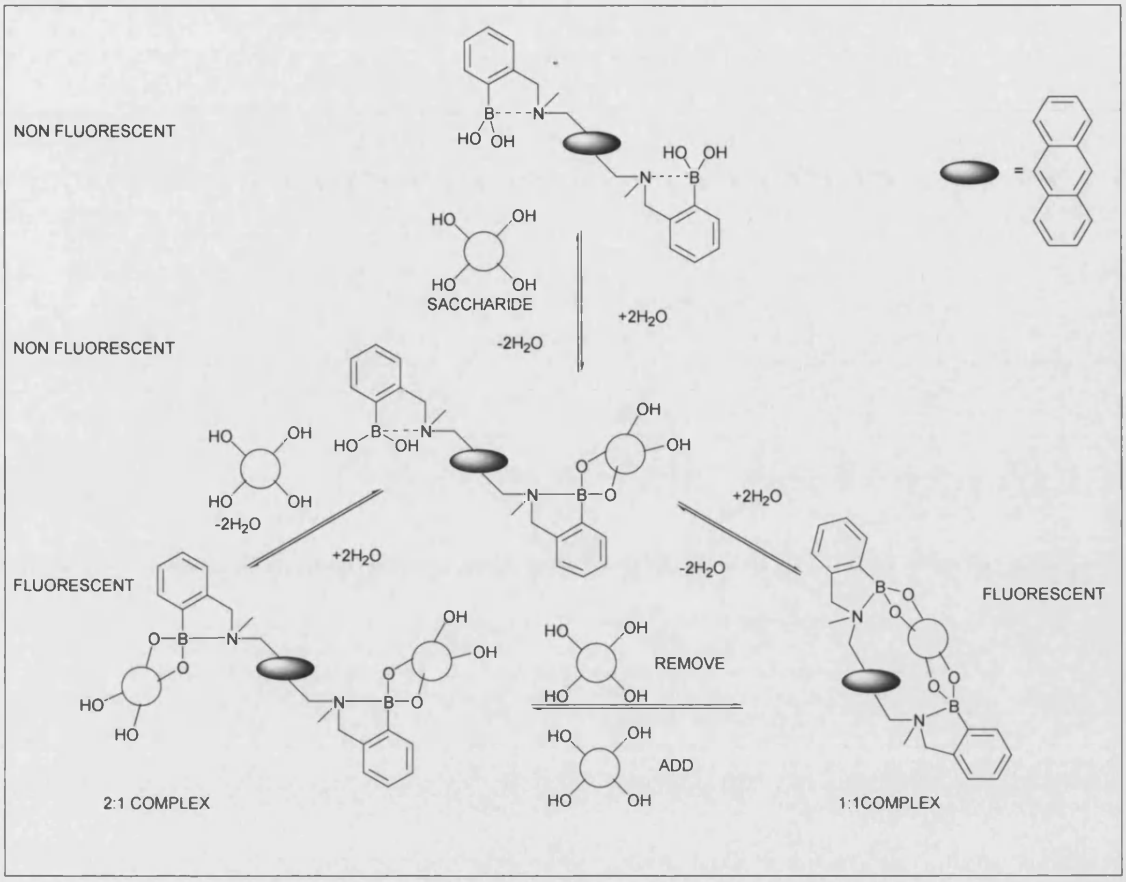

Figure 22: Formation of 2:1 and 1:1 complexes.[49]

Since this discovery, several diboronic acid systems have been synthesised, showing selectivity for a variety of saccharides, including a two-dimentional PET sensor (Figure 23a).[51] Variation in the length of the spacer allows the investigation of disaccharides (Figure 23b).[52] When the length of the spacer is six carbons, the sensor is selective for D-melibiose and D-lactulose. The reducing sugar in both cases can isomerise between the pyranose and furanose conformations. This ability to discriminate for the terminal saccharide of an oligosaccharide will be a useful tool in the glycobiology for future applications.

Tuning the selectivity is possible by changing the fluorophore (Figure 23c).[53] By reducing the size of the hydrophobic π-surface, the saccharide selectivity is switched from D-glucose (Figure 23 c_{i-iii}) to D-galactose (Figure 23c_{iv-v})

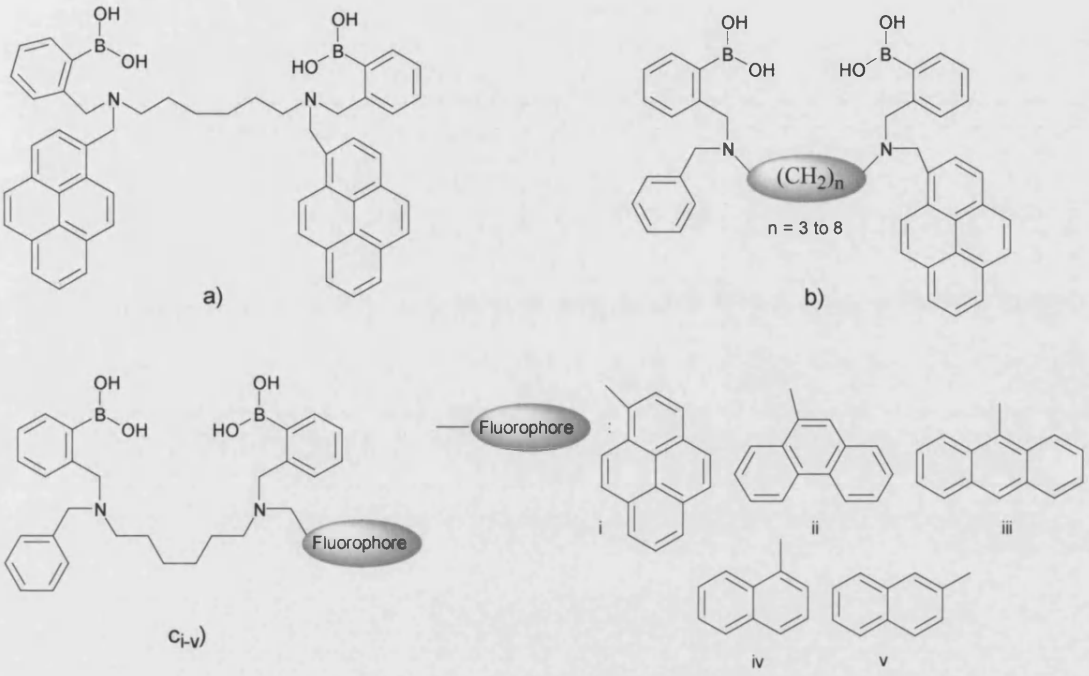

Figure 23: Examples of PET sensors: a) Two-dimensional PET sensor; b) Tuning length of spacer influence disaccharide recognition and selectivity; c) Tuning fluorophore switch selectivity from D-glucose to D-glactose.

Further, more elaborate systems (Figure 24a) can undergo some energy transfer (ET) between two different fluorophores contained within the same molecule.[54] In this system, upon saccharide binding and when phenanthrene was excited at 299 nm (figure 24b), no emission from phenanthrene was observed. Instead, due to overlap between the emission band of phenanthrene (369 nm) and the excitation band of pyrene (342 nm) an energy transfer from phenanthrene to pyrene occurred. Thus, only the emission from the pyrene was detected at *ca.* 417 nm. This system demonstrates an ET from a donor to an acceptor group.

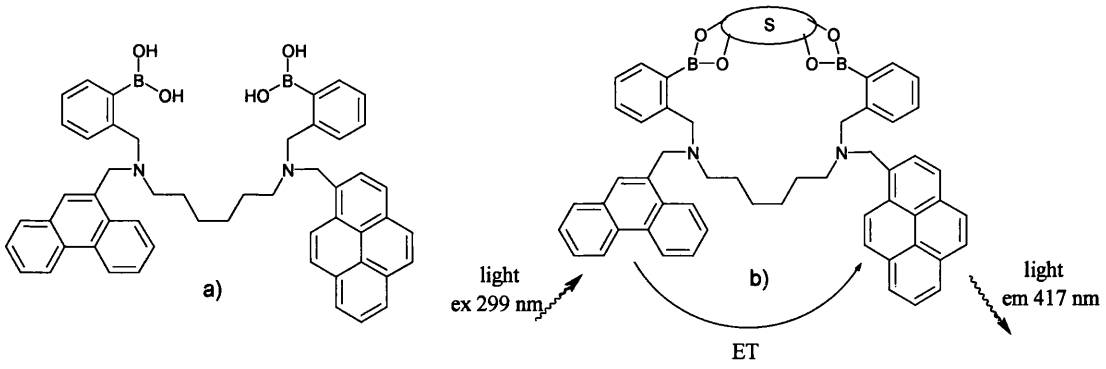

Figure 24: a) First intramolecular ET sensor; b) how it works.

Boronic acid PET sensors have also been used in combination with other binding sites; some examples are presented in Figure 25.

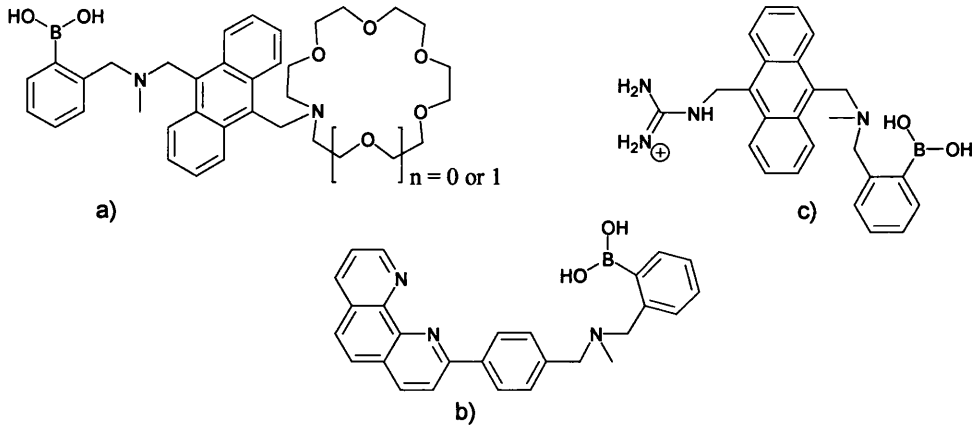

Figure 25: Examples of other PET sensors: a) D-glucosamine PET sensor; b) D-glucuronic acid and sialic acid PET sensor; c) D-glucurate PET sensor.

Cooper and James have developed a D-glucosamine selective sensor (figure 25a) based on boronic acid and aza crown ether. [47, 55] The D-glucosamine hydroxyl groups are recognised by the boronic acid moieties whilst the glucosamine ammonium group is detected by the aza crown ether. Shinkai *et al.* have developed a D-glucuronic acid and sialic acid selective sensor (Figure 25b) based on cooperative binding between a boronic acid receptor and a metal chelate.[56, 57] The boronic acid moiety binds the hydroxyl groups whereas a zinc (II)-carboxylate coordinates on the other side of the

sensor. It has been demonstrated that the Zn (II) is necessary to enhance the fluorescence for the detection of uronic acids and sialic acids, however Zn (II) did not affect the saccharide recognition.

Recently, a D-glucarate system has been reported by Wang based on boronic acid and a guanidinium receptor (Figure 25c).[58] The guanidinium receptor recognised the carboxylate group whilst the boronic acid moiety realised a diol complexation.

Other boronic acid sensors can be found in the literature, based on calixarenes, dendrimers or porphyrin.[23]

For a complete and more detailed review, see the plethora of reviews recently published on PET and boronic acid sensors by different groups. [1, 24, 25, 27, 40, 45]

Molecular logic gates

Molecular logic gates follow the Boolean logic operations. These rely on the binary "yes-no", "1-0" or "true-false" concept.

The simplest logic gate is the 1-input YES operation, where for 1-input there is an output 1. This can be summarized in a truth table (Figure 26).

Input	Output
1	1
0	0

Figure 26: Truth Table for YES logic operation

Many different types of logic gates are described in the literature. Only the OR and AND will be discussed here.[25, 59, 60]

OR logic gate

The OR gate provides an ouput 1 when any combination of its input are present. The molecule produces an output each time one or more input are present. In other words an OR logic gates do not have chemoselectivity. Figure 27, shows the truth table and an example of OR logic gate.

Input	Input	Output
0	0	0
0	1	1
1	0	1
1	1	1

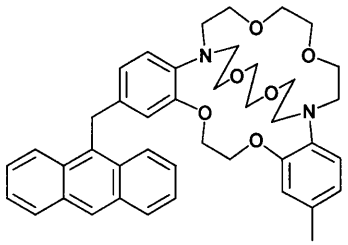

Figure 27: Truth Table and example for OR logic gate for potassium and rubidium ions.

This sensor has poor selectivity for cations and can bind either potassium or rubidium ions. This shows a cation-induced enhancement of the fluorescence by suppression of PET. [61]

AND logic gate

The AND gate provides a positive ouput only if both of its input are present. A truth table and examples of AND logic gate are given in Figure 28.

De Silva and co-workers were the first to design a molecular AND logic gate in 1993.[62] This molecule required both Na^+ and H^+ input, to produce a fluorescence output.

An example of an AND logic gate with a boronic acid receptor, is the D-glucosamine PET sensor systhesised by Cooper and James (mentioned earlier, Figure 25a). This sensor can also be classified as AND logic gate. Enhanced fluorescence is only observed when the D-glucosamine is bound *via* the hydroxyl groups to the boronic acid moiety and *via* the ammonium group to the aza crown ether.

Input	Input	Output
0	0	0
0	1	0
1	0	0
1	1	1

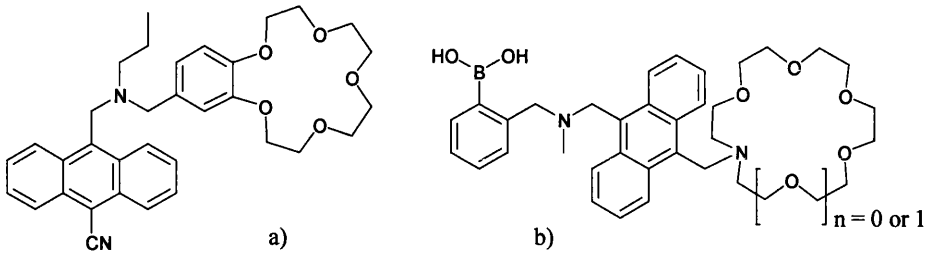

Figure 28: Truth Table and examples for AND logic gate: a) de Silva first molecular AND logic gate; b) D-glucosamine PET sensor.

Other examples of logic gates are present in the literature, as well as complicated logic gates, which are working with ICT systems (see below for one example).[60] This molecule can recognize Ca^{2+} and H^{+}.

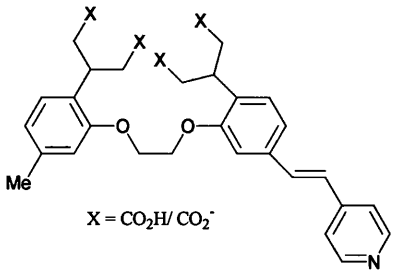

1.5 Anion Sensors

1.5.1 Context of Research

In the last twenty years, a wide range of sensors for anions have emerged and present various affinity and selectivity towards anions, such as fluorides, chlorides, phosphates, and carboxylates.

The design of anion sensors is particularly challenging. Anions are larger than isoelectronic cations and therefore have a lower charge to radius ratio. This means that electrostatic binding interactions are less effective than they would be for smaller cation. Anions may be sensitive to pH thus receptors must function in the pH window of the target anion. Moreover, anionic species have a wide range of geometries and therefore required a higher degree of design to be complementary with the anionic guest. The solvent effect is also important and therefore should be chosen to facilitate effective anion recognition. Finally the hydrophobicity of the anion can also influence the selectivity of the receptor. For example hydrophobic anions bind more strongly to a hydrophobic binding site. Different types of noncovalent interactions are used to complex the anionic guest. These include electrostatic interactions, hydrogen bonding, hydrophobicity, coordination to a metal ion and combinations of these interactions.

Recently, increasing attention has focused on anion recognition.[63, 64] Of particular interest are "colorimetric anion sensors", species that allow the so-called "naked-eye" detection of anion without the use of any instrumentation.

Sessler and co-workers have tried a large variety of commercially available compounds such as 1,2-, 1,4-, 1,5-, 1,8-, 2,6-diaminoanthraquinone, alixarin complexone, 4-nitroaniline.... for the detection of anions.[65] The colour of a solution of 1,2-diaminoanthraquinone in dichloromethane is yellow, the colour of the solution changes

to dark purple, red, reddish orange, purple upon addition of fluoride, chloride, bromide and phosphate respectively.

An alternative method, is using the competition of a colour indicator and the analyte for the binding pocket. The indicator is displaced, from the binding pocket upon addition of the analyte causing a signal modulation, see below.

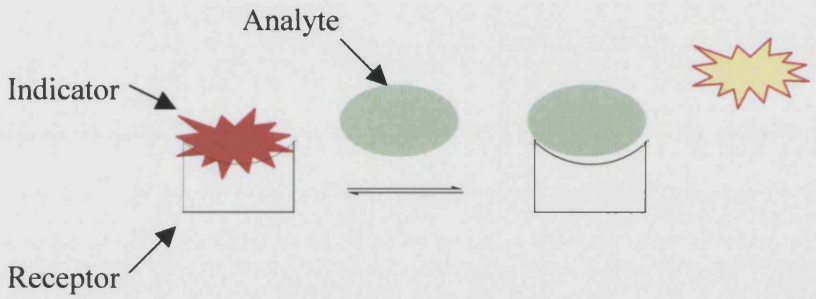

Indicator displacement

Anslyn and co-workers have reported the detection of citrate in beverge (orange juice, tonic water, coca-cola…) using 5-carboxyfluorescein (fluorescence probe),[66] tartrate in wine using the alixarin complexone (colorimetric indicator),[67] gallic acid for the aging of the scotch using pyrocatechol violet (colorimetric indicator),[68] glucose-6-phosphate using 5-carboxyfluorescein and inositol-1,4,5-triphosphate (IP_3) using 5-carboxyfluorescein.[69]

Czarnik and co-workers have reported a sensor for phosphate, sulphate or carboxylate based on anthrylpolyamine, which worked on fluorescence change upon binding with the substrate.[70]

For detailed discussion, read the recent review on "35 years of synthetic anion receptor chemistry 1968-2003". [71]

1.5.2 Fluoride Sensors

Fluoride is present in biological fluids and tissues and especially in bone and tooth. The typical levels of fluoride in blood are in the range of 20-60 μg l^{-1} using a fluoride ion-selective electrode.[72, 73] Fluoride is of particularly interested among the biologically important anions mostly because of its role in prevention off dental carries.[74] Fluoride has also been extensively explored for treatment of osteoporosis.[74] Fluoride is easily absorbed but it is excreted slowly from the body. Recently there has been concern about overexposure to fluoride, which can cause fluorisis, a type of toxicity that can cause increasing bone density. Monitoring fluoride concentration of water supplies and of groundwater contamination from industrial plants are also of interest. Fluoride is also released during the hydrolysis of some chemical weapons such as sarin and determination of the fluoride concentration can be used to quantify the nerve agent.[75, 76]

Fluoride concentrations are currently determined using electrodes prepared from LaF_3.[77] However, optical chemosensors would be of great advantage for direct visualization of intracellular fluoride.

Many fluoride sensors have been developed over recent years. Sessler and co-workers, have designed octamethyl calix[4]pyrrole as an anion recognition element. The first generation of sensor has an anthracene moiety as a fluorescent signaling unit (Figure 29a).[78]

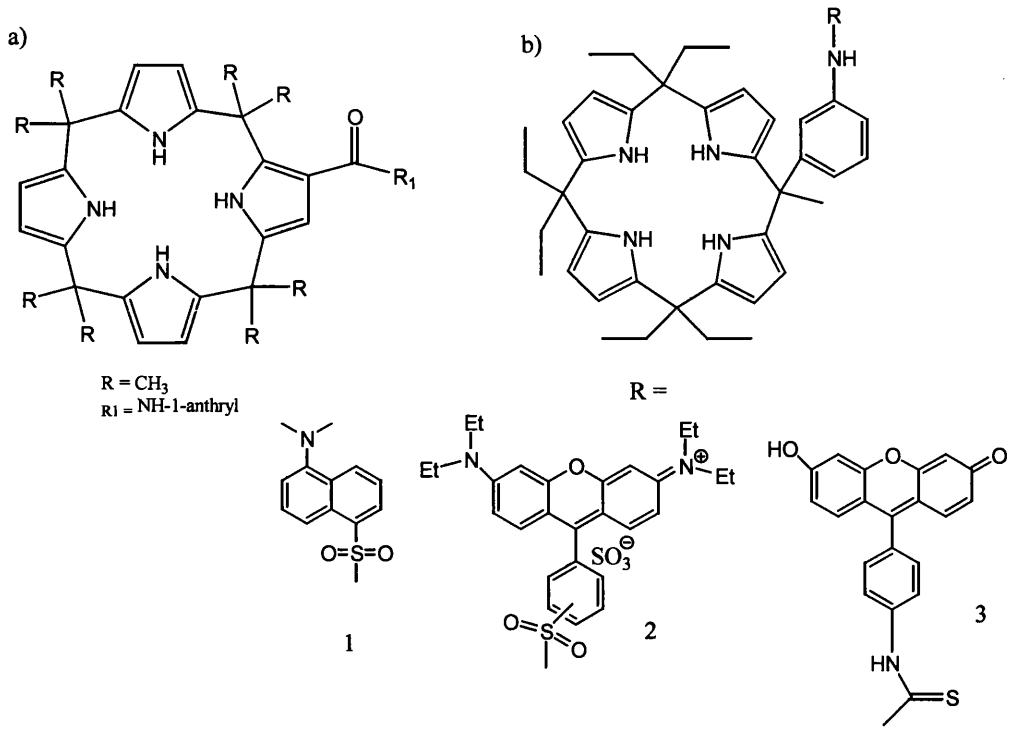

Figure 29: Examples of calix[4]pyrrole anion sensors: a) first generation; b) second generation

Upon addition of fluoride, the fluorescence of the sensor is quenched. The main drawback of the first generation was low selectivity ratio phosphate to chloride The second generation of calixpyrroles, by Sessler and co-workers displayed greater affinity than the first generation and a more efficient fluorescence response.[79] These second generation of calixpyrroles contained a rigid spacer to fix the distance between the quencher (anion) and the signaling moiety. The spacer element is either a sulfonamide or thiourea respectively Figure 29b1, 2 and 3. The linker provides additional hydrogen bond donor sites to act with the calixpyrrole NH protons to enhance the anion binding affinity. The fluorescent unit has also been changed for dansyl, Lissamine-rhodamine B and fluorescein. Anions tested as potential substrates for all three second generation sensors included fluoride, chloride, dihydrogenphosphate ($H_2PO_4^-$) and hydrogen pyrophosphate ($HP_2O_7^{3-}$) as tetrabutylammonium salts (TBA^+). Fluoride anion gave the highest binding affinity.

However, these systems also show high phosphate ($H_2PO_4^-$ or $HP_2O_7^{3-}$)/chloride selectivity.

Kim and Yoon have developed a fluorescent PET chemosensor based on 1,8-bisurea anthracene (Figure 30a).[80] The fluoride binds the four amides by hydrogen bonding and quenches the fluorescence of anthracene. The selectivity for the fluoride is 120 fold compared to chloride ions in an acetonitrile-DMSO mixture (9/1 v/v).

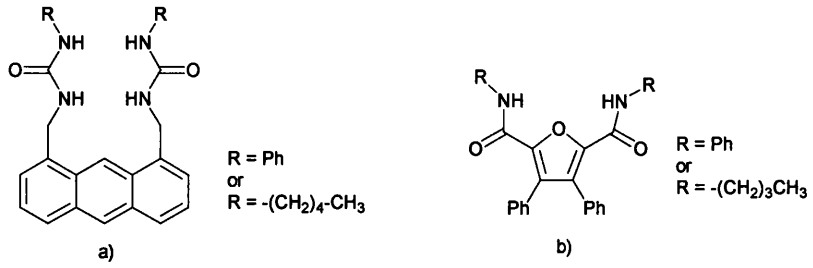

Figure 30: Examples of fluoride sensors: a) Fluorescent PET sensor; b) 2,5-diaminofuran anion receptors

Gale and co-workers have developed 2,5-diaminofuran anion receptors[81](Figure 30b) which are selective for fluoride in DMSO with 0.5% with water.

Yu and co-workers have developed a colorimetric anion sensor (Figure 31).[82] The non-covalent calix[4]pyrrole-chloranil charge transfer complex shows a coloured aggregation which can be used as naked-eye sensor for selective detection of fluoride. The chloranil (absorbtion at 370 nm) in the presence of calix[4]pyrrole shows a change in colour from pale yellow to blue. Upon addition of fluoride and $H_2PO_4^-$, the calix[4]pyrrole-chloranil complex changes from blue to orange-yellow. Interestingly, the F^- and $H_2PO_4^-$ anion-induced colour changes can be reversed by the addition of water (water extracts the F^- and $H_2PO_4^-$).

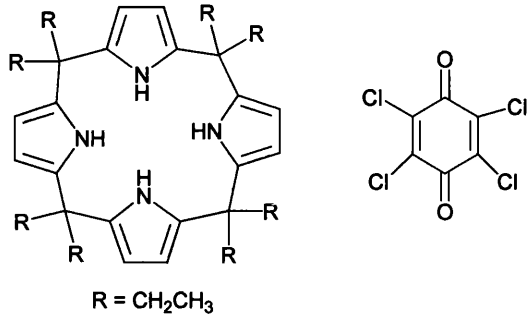

Figure 31: Example of colorimetric anion sensor: calix[4]pyrrole and chloranil

The non-covalent calix[4]pyrrole-chloranil aggregation has shown great potential as a simple colorimetric anion sensor for the facile identification of fluoride and hydrogenphosphate ions in chloroform. The specific phosphate/chloride selectivity is potentially advantageous for biological applications.

1.5.3 Boronic Acid Based Sensors

Boronic acids have been used to detect fluoride. When boronic acid binds to certain anions (fluoride or hydroxides) the sp^2 hybridised trigonal boron atom becomes sp^3 hybridised. [83] The boron atom, which is a "hard acid" strongly, interacts with the fluoride anion, which is a "hard base". This specific boron-fluoride interaction has also been used to facilitate the membrane transport of saccharides.[84]

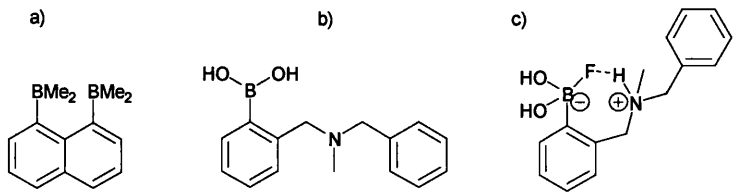

Figure 32: Selected examples of boron containing fluoride sensors.

Katz was the first one to study boron centered fluoride receptors. [85] The 1,8-naphthalenediylbis(dimethylborane) (Figure 32a) traps fluoride and hydroxides ions between the two electron-accepting boron atoms but does not complex with chlorides.[86]

In 1998 Cooper and James developed a fluorescent sensor for fluoride using boronic acid (Figure 32b). The system is based on the Lewis acid-base interaction between boron and fluoride. The system was designed to increased the strength of the fluoride binding compared to phenylboronic acid by an additional hydrogen bond site, which is available when the amine is partially protonated at pH 5.5 (pK_a of tertiary amine). The single fluoride adduct of sensor 32b is selectively stabilised by the additional hydrogen bonding (Figure32c). This system worked using PET, which is suppressed upon addition of fluoride, the observed fluorescence is quenched when fluoride is added.

James and Ward developed a colorimetric fluoride sensor. [87, 88] When the azo dye (Figure 33a) is titrated with potassium fluoride in methanol, the colour of the solution changes from orange (450 nm) to claret (563 nm). The same colour change is observed for the pH titration of this compound. The colour change is associated with the formation of a tetrahedral boronate anion. Therefore, the addition of potassium fluoride to a solution of the azo dye must also produce a tetrahedral boronate anion. This sensor

exists in two forms shown in Figure 33b. The B-N bond of the orange coloured species is broken by the addition of fluoride to give the claret coloured species. The stability constant for the fluoride was determined as 130 M^{-1} in methanol.

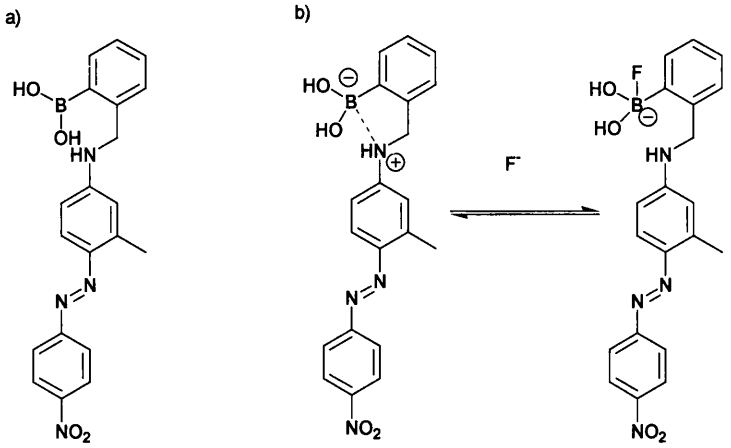

Figure 33: a) A colorimetric fluoride sensor b) fluoride binding to the sensors

DiCesare and Lakowicz have recently prepared a series of ICT fluorescent sensors for fluorides.[89] All of the molecules have also been tested for ICT fluorescent sensors for saccharides (see section 1.4.3).[38, 41]

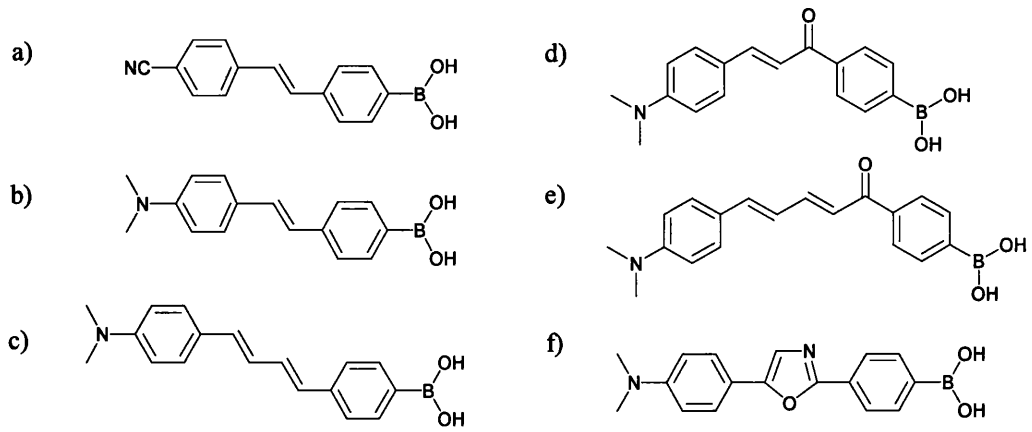

Figure 34: ICT sensors for fluoride.

All sensors use the ICT mechanism and combine the boronic acid group with an electron donating (dimethylamino) or electro withdrawing group (cyano) groups. The sensor Figure 34a, displays ICT when the anionic form of the boronic acid is induced upon addition of fluoride and thus cause the change observed in the spectra (fluorescence quenching). Upon addition of fluoride, the sensors 34a, forms a trifluoro tetrahedral boronate.

The sensors in Figure 34b and c, display an ICT, when they are in their neutral form. Upon addition of fluoride, the anionic form of the boronic acid is obtained and the ICT mechanism is removed. For these two sensors, it is important to note that the stability constant is 10-fold smaller in comparison with sensor 34a (containing the electron withdrawing group). The sensor in Figure 34f, shows a loss of ICT in the presence of fluoride, a large intensity change (14-fold) and at a long wavelength. Surprisingly, the stability constant of this sensor is a better than the stilbene derivatives (34a, b, c). The sensors in Figure 34d and e present ICT mechanism involving the *N,N*-dimethylamino group (donor) and the carbonyl (acceptor) group. The boronic acid is in resonance with the carbonyl group. In the presence of fluoride, the boronic acid changes from its neutral form to its anionic form, becoming an electron-donating group to the carbonyl group. The increase in the electronic density on the carbonyl decreases the ICT, an increase in fluorescence. The intensity changes are higher in comparison with stilbene and diphenylbutadiene derivatives (Figure 34 a-c). For all these sensors no effect is observed upon addition of chloride or bromide.

The ICT mechanism has been shown to be a useful tool in the development of fluorescence probes for fluoride detection.

Finally, Shinkai and co-workers have used ferroceneboronic acid in fluoride recognition.[90] The boronic acid, which is the fluoride binding site, is directly attached to the redox-active ferrocene moiety (Figure 35a). The fluoride binding event occurring at the boronic acid site can be read out through the shift in the redox potentials of the ferrocene moiety. Selectivity for the fluoride has been established in the presence of other halides and common anion such as thiocyanate, phosphate, and sulfate.

The sensor was further developed (Figure 35b) by adding an intramolecular tertiary amine. The sensor binds fluoride and saccharides at neutral pH.[91, 92]

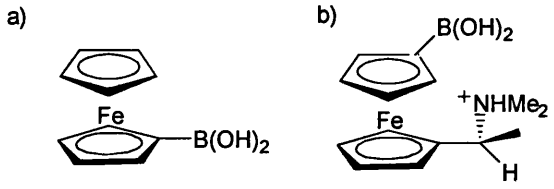

Figure 35: Electrochemical fluoride sensors.

1.6 Objectives

The main drawback in the development of fluorescence ICT sensors for saccharides or fluorides, so far, was the insensitivity of such systems. The B-N bond has been successfully used in the development of fluorescent PET sensors for saccharides. The interaction of the neighbouring amine with the boronic acid is strengthened on saccharide binding (PET). This concept (B-N bond) was already used on the work performed on ICT colour sensors[88] for saccharides and has given interesting results.

All this led us to design and investigate the field of ICT[¶] fluorescent sensors for saccharides. The main idea was to synthesise a simple system and to explore its potential.

[¶] The work performed on fluorescent ICT by Lakowicz and co-workers was realised during the same period of time as the one done for this thesis.

Chapter 2

Results & Discussion

"In the field of observation, chance favours only the prepared mind."

Louis Pasteur (1822-1895)

2.1 Aims of the Project

As part of a research program aimed at developing fluorescent sensors for molecular recognition of neutral molecules; a number of boronic acid fluorescent sensors with the amine group directly attached to the chromophore (no spacer to link the receptor and the fluorophore unit) were synthesised in order to assess their potential as sensors for saccharides and fluoride anion recognition.

In order to explore the potential of these systems, three different series were considered: with one boronic acid unit, *monoboronic acid series*, two boronic acid units, *diboronic acid series*, a boronic acid and a crown ether unit, *crown ether series*.

All the sensors of the monoboronic acid series are presented in Figure 36. The first sensor synthesised was sensor **1**. Then, positional isomers **2** and **3**, model compound **4** and sensor **9**, derivatives with the introduction of different functionalised groups (**5, 6, 7** and **8**) and changes in fluorophores (**10, 11** and **12**) were considered as modification of sensor **1** to fully explore this system. The synthesis of these sensors is described in section 2.2.

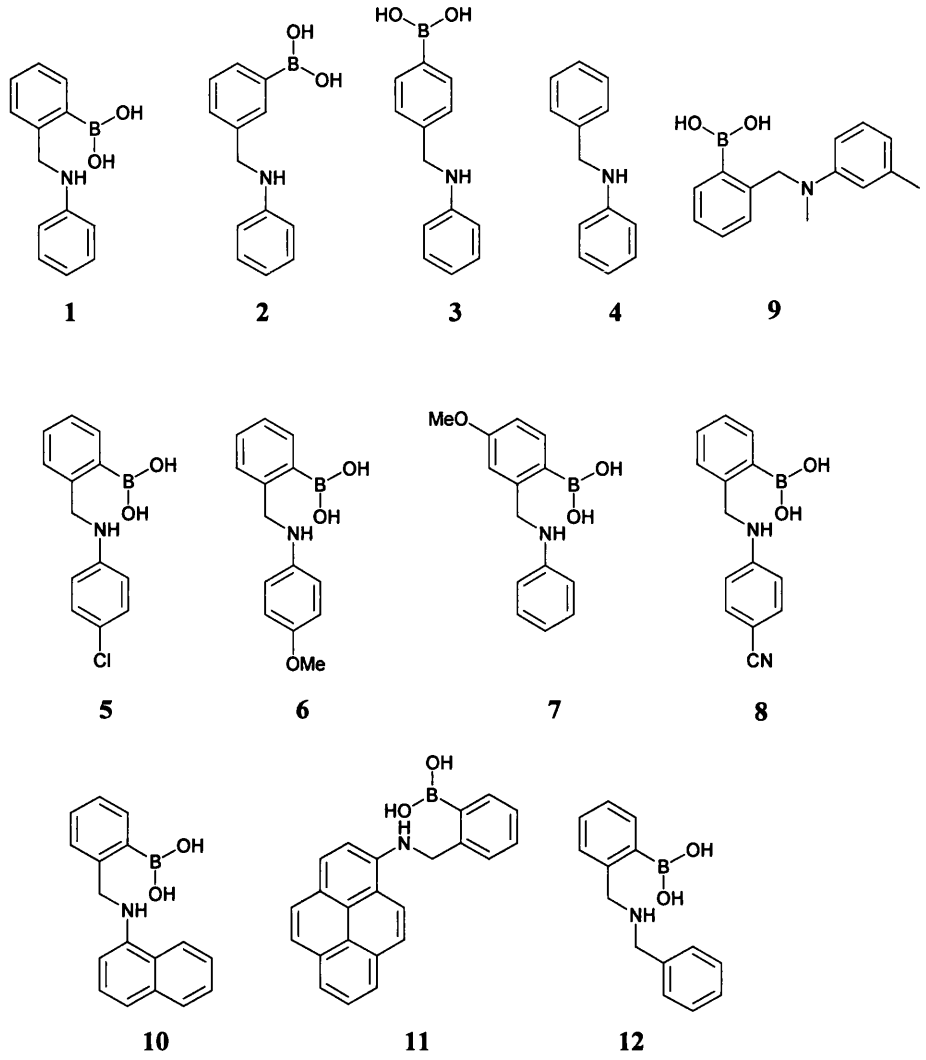

Figure 36: *Monoboronic acid sensors series*

The diboronic acid sensors can be split into two different series based on the diamine used. Sensors **13**, **15** and **17** with the diamine in *meta* position and sensors **14**, **16** and **18** with a diamine in *para* position with respect to the methylene unit. For each group three different boronic acids were used 2-formylphenylboronic acid, 3-formylphenylboronic acid and 4-formylphenylboronic acid to afford in total 6 diboronic acid sensors, presented in Figure 37. Their syntheses are described in section 2.2.

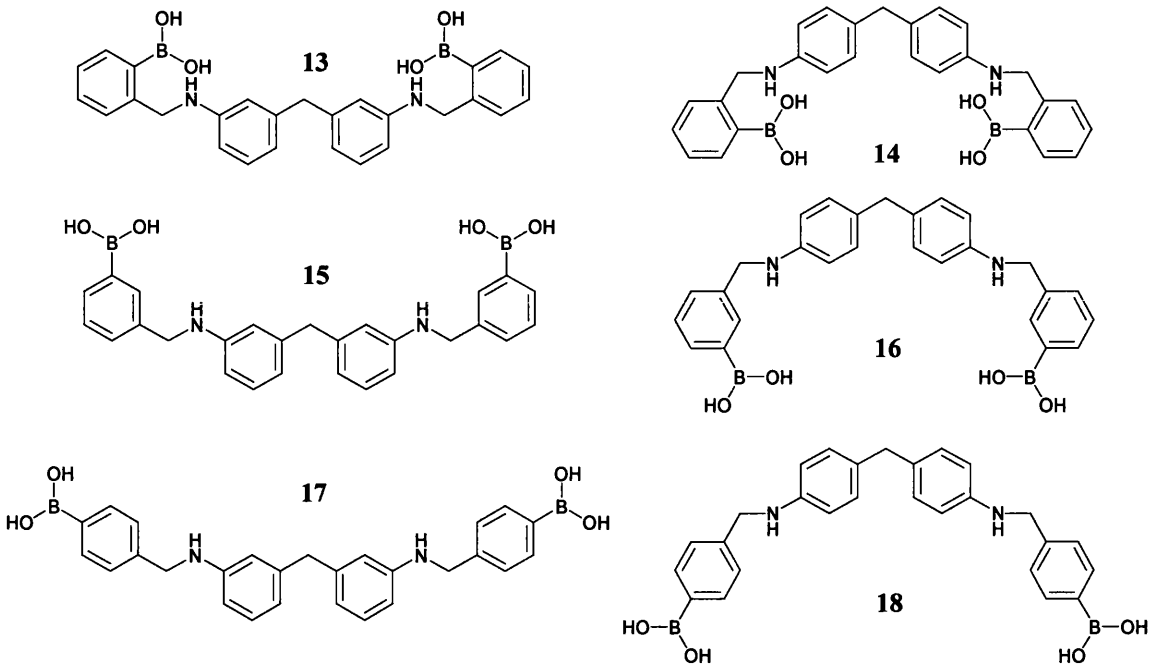

Figure 37: *Diboronic acid sensors series.*

For the Crown Ether series, each sensor contains a 15-crown-5 unit and the positions of the boronic acid is systematically varied through *ortho*, *meta* or *para*, leading to sensors **19**, **20** and **21** respectively and shown in Figure 38. The synthesis is described in section 2.2.

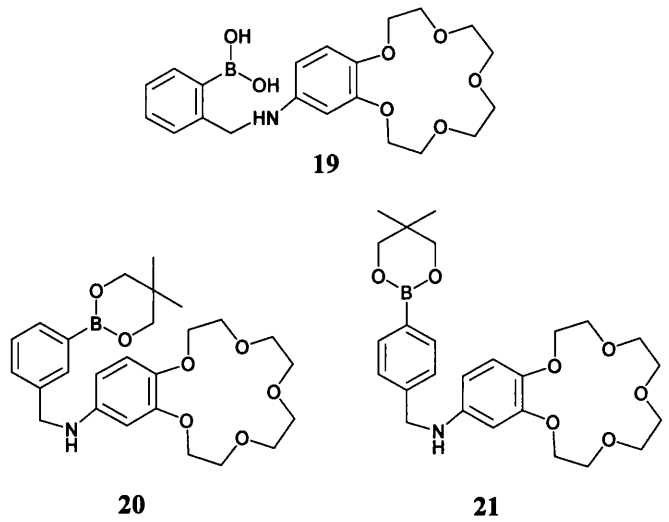

Figure 38: *Crown ether sensors series.*

A saccharide-boronic acid complex was investigated. This study was undertaken to help understand the recognition event, occuring in solution by making a X-ray crystal of a sacharide-boronic acid complex. The sysnthesis is described in section 2.2.

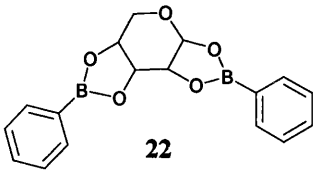

22

Finally, following successful preparation, the sensors' interaction with saccharides and fluoride, were investigated using fluorescence spectroscopy (described in sections 2.3 and 2.4 respectively).

2.2 Synthesis of Boronic Acid Fluorescent Sensors

2.2.1 Monoboronic Acid Sensors 1, 2, 3

Sensor **1**, was prepared as outlined in Scheme 5. The synthesis is facile and requires minimal purification. In this pathway, there are two steps: the first step involved the formation of the imine and the second step is the reduction of this imine by an excess of sodium borohydride.

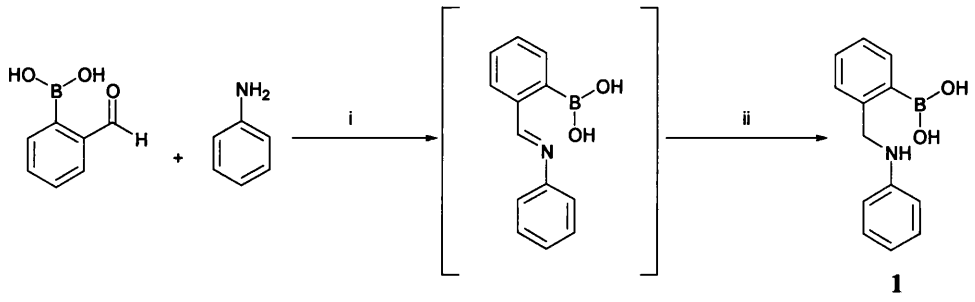

Scheme 5:Reagents and conditions: i) EtOH/Toluene (90:10) reflux in *Dean and Stark trap*, 16h; ii) $NaBH_4$ (5eq), rt, 2.5h, 54% (two steps).

The condensation of the aniline with the commercially available 2-formylbenzeneboronic acid was performed by heating at reflux in a mixture of ethanol/toluene, with azeotropic removal of the water using a *Dean and Stark trap*. The reaction was complete after 16 hours. Then the reduction of the imine intermediate was performed *in situ* by adding an excess of sodium borohydride (5 eq) to the solution. Purification of the crude reaction mixture was achieved by precipitation from chloroform/*n*-hexane to afford the desired sensor **1** as a cream powder in 54% yield. The one pot reaction procedure has been the preferred strategy due to its easier purification by precipitation of the product and the resulting improvement of the yield.

Crystals suitable for X-ray analysis were also obtained. The structure of **1** is shown in Figure 39.

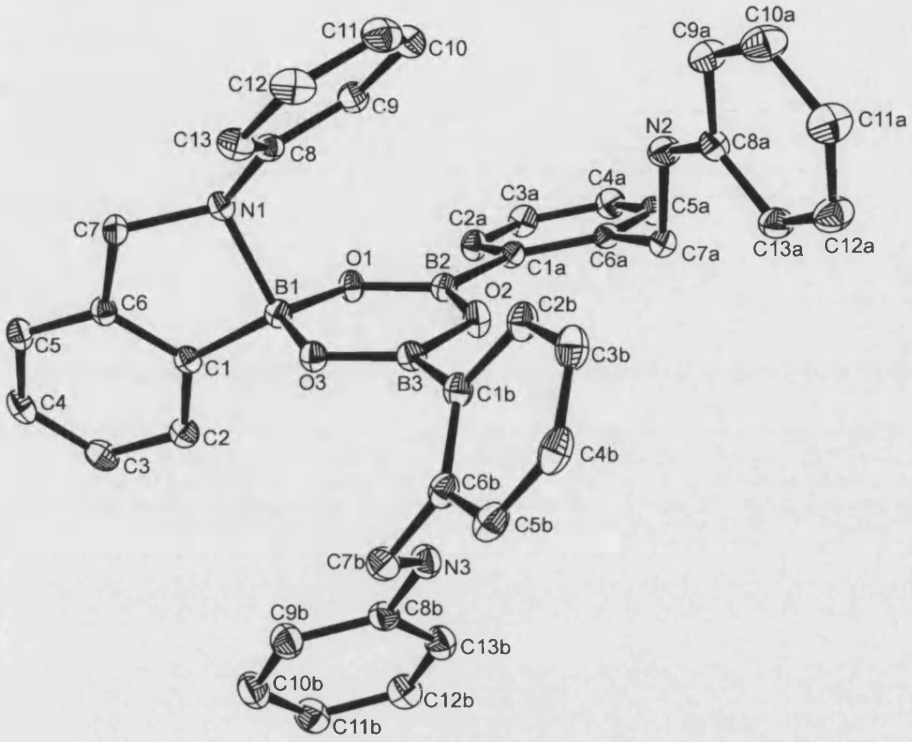

Figure 39: Crystal structure of compound **1**,showing the labelling scheme used. Ellipsoids are illustrated at the 30% probability level. Hydrogen atoms are omitted for clarity.

The data associated with the X-ray analysis are given in the Appendix 1. From the crystal structure it is clear that the boronic acid forms a cyclic trimeric anhydride, where only one of the units contains a B-N bond (B(1) and N (1)), the length of the BN bond is 1.747 (2) Å. This is similar to those found in similar cyclic boroxins by Norrild and co-workers.[93] In the literature a strong B-N bond is within the range 1.5 to 1.8 Å.[94]

All the sensors, and indeed all the compounds described within the Results & Discussion section, have been fully analysed and characterised (see the Experimental section for full details). There are two points to note concerning the analysis. Firstly,

elemental analysis of boronic acids has long been known to give poor correlations between calculated and found compositions.[95] This is usually attributed to the formation of highly stable boron nitride derivatives in the combustion process. Also, free boronic acids can readily and spontaneously form cyclic trimeric anhydrides, boroxines, at room temperature (Scheme 6).[6] Although some boron containing compounds did give a good match between calculated and found composition, this was not always the case. This was not viewed as evidence of impurity, but due to the inherent problems of this technique towards boronic acids. For compounds where elemental analysis proved inconclusive, high-resolution mass spectrometry was performed instead.

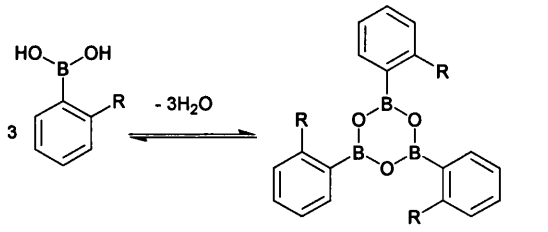

Scheme 6: Formation of boroxines from boronic acids.

The second issue concerns the mass spectra of boronic acid compound obtained using the technique of fast atom bombardment (FAB) mass spectrometry. FAB requires the use of a matrix, usually *m*-nitrobenzylalcohol, to mobilise the sample. Boronic acids readily bind to one or two hydroxyl groups of *m*-nitrobenzylalcohol molecules to form adducts (Scheme 7) that are predominantly observed by FAB over the free boronic acid.

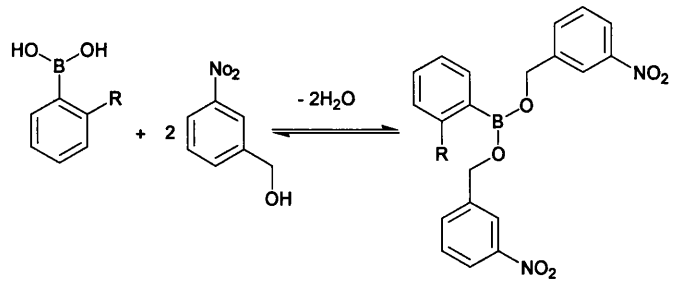

Scheme 7: *m*-nitrobenzylalcohol adduct with boronic acid observed by FAB mass spectrometry.

The preparation of sensors **2** and **3** are presented in Scheme 8. Sensors **2** and **3** are both synthesised according to the same method. These two sensors are positional isomers of sensor **1**. The condensation of the aniline with the commercially available 3-formylbenzeneboronic acid, or 4-formylbenzeneboronic acid, in methanol at room temperature overnight afforded after reduction of the imine by an excess of sodium borohydride (5 eq), sensors **2** and **3** respectively in 45% yield after purification by precipitation from chloroform/*n*-hexane.

Two methods have been used to synthesise all the sensors based on the fluorophore directly attached to the boronic acid. The difference between the methods is the choice of solvent. The method using methanol and room temperature is the first one, which is tried. When the reaction does not go to completion, the solvent is changed for a mixture of ethanol and toluene (90/10) and heated under reflux.

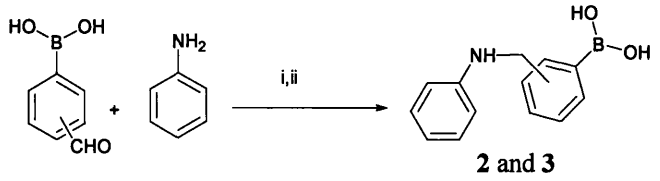

2 and **3**

Scheme 8: Reagents and conditions: i) MeOH, rt, overnight; ii) $NaBH_4$ (5 eq), rt, 1-1.5h, **2** and **3** 45% (two steps).

2.2.2 Model Compound 4 and Sensor 9

The synthesis of compound **4** is shown in Scheme 9. The aniline was condensed with the commercially available benzaldehyde in refluxing toluene to produce the imine. The latter, was then reduced in the presence of an excess of sodium borohydride (5 eq) in methanol to afford the desired compound **4** in 98% yield, no further purification was required.

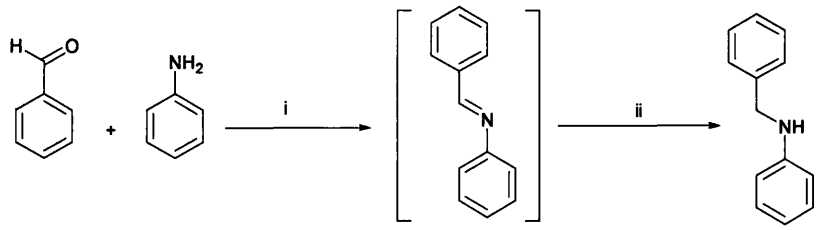

4

Scheme 9: Reagents and conditions: i) Toluene, reflux in *Dean and Stark trap*, 16h; ii) MeOH, $NaBH_4$ (5eq), rt, 2h, 98% (two steps).

Sensor **9**, has been previously prepared by Christopher Ward,[96] but was not investigated as a fluorescent probe. The synthesis of this sensor is outlined in Scheme 10.

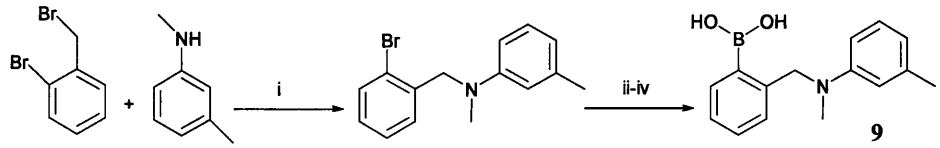

Scheme 10: Reagents and conditions: i) K_2CO_3, acetonitrile, reflux, 4h, under argon; ii) *n*-BuLi, THF, -78°C, 1 h, under argon; iii) $B(OCH_3)_3$, THF, -78°C, under argon; iv) H_3O^+, 1h; 25% yield.

2.2.3 Small Group of Sensors 5, 6, 7 and 8

Scheme 11 shows the two-steps synthetic route used to prepare a small group of fluorescent sensors. This group is based on sensor **1** with modifications of either the aniline ring (incorporation of an electron-withdrawing or -donating group) or modification of the boronic acid ring by addition of electron-donating group.

The syntheses were straightforward and followed the same method as that used to prepare sensor **1** with different aniline derivatives (chloro and cyano-aniline, for the withdrawing functionality; methoxy-aniline for the electron-donating functionality and finally a methoxy group on the boronic acid ring for an electron-donating functionality on the boronic acid ring).

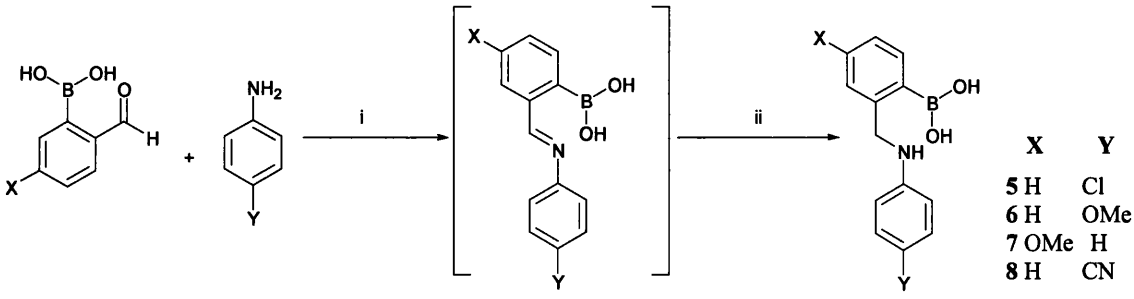

Scheme 11: Reagents and conditions: i) EtOH/Toluene (90:10) reflux in *Dean and Stark trap*, overnight; ii) $NaBH_4$ (5eq), rt, 1.5 to 2.5h, **5** 31%, **6** 56%, **7** and **8** 34% (two steps).

The condensation of the aniline derivatives with the commercially available 2-formylbenzeneboronic acid, in a mixture of ethanol/toluene (90/10) heated at reflux overnight, afforded after reduction of the imine by an excess of sodium borohydride (5 eq), sensors **5-8** respectively after purification.

The purification method varied from one sensor to another according to the nature of the product. Sensors **5** and **7** were obtained after a precipitation from chloroform/*n*-hexane with a yield of 31% (white powder) and 34% (yellow solid) respectively.

Sensor **6** was obtained as a pale brown foam with 56% yield and did not require any further purification.

Sensor **8**, was obtained after purification by a basic-acidic extraction. The crude was dissolved in water and some aqueous NaOH solution was added to reach pH 14, a chloroform extraction removed the starting material, 4-aminobenzonitrile. Then the pH was brought back to 6 to allow the extraction of the desired product with chloroform. After drying and evaporation of the solvent, sensor **8** was afforded as a white powder with 34% yield. This technique has allowed us to obtain the purified desired product and a very useful method for compounds where the classical precipitation method is not successful.

2.2.4 Modification of the Fluorophore: Sensors 10, 11 and 12

The sensors synthesised to date contain exclusively a benzene ring attached to the amine. Modifications of the size of the fluorophore have also been investigated. Replacement of the aniline ring by benzyl ring, naphthalene ring or pyrene ring have been attempted. Modifying the size of the aromatic ring allows increased electronic conjugation and should shift the emission fluorescence to longer wavelength.

Sensor **12** was prepared accordingly to the classical route used to synthesise sensor **1**, using benzylamine instead of aniline. The preparation is outlined in Scheme 12. Sensor **12** was obtained as a white powder with 37% yield.

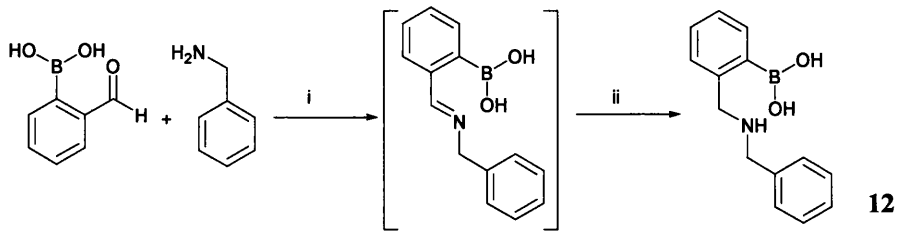

12

Scheme 12: Reagents and conditions: i) EtOH/Toluene (90:10) reflux in *Dean and Stark trap*, overnight; ii) $NaBH_4$ (5eq), rt, overnight, **12** 37% (two steps).

Sensor **10**, was synthesised by Christopher Ward,[96] but has not been investigated as a fluorescent probe. The synthesis of this sensor is outline in Scheme 13.

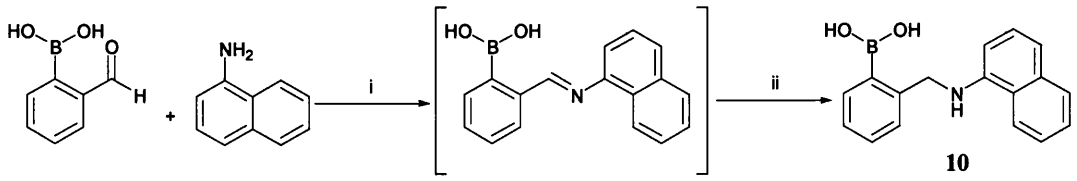

10

Scheme 13: Reagents and conditions: i) MeOH, rt, 1 h; ii) $NaBH_4$ (2eq), rt, 1h, **10** 68% (two steps).

Sensor **11**, was synthesised in two-steps after deprotection of the amine salt (Scheme 14). The reaction was carried out under a nitrogen atmosphere; free 1-pyrenemethylamine and 2-formylphenylboronic acid were dissolved in a mixture of THF/MeOH and stirred at reflux overnight. The imine formed was then reduced *in situ* by addition of an excess of sodium borohydride (3 eq) at room temperature.

Purification by precipitation from chloroform/*n*-hexane afforded sensor **11** as an olive green powder with 47% yield.

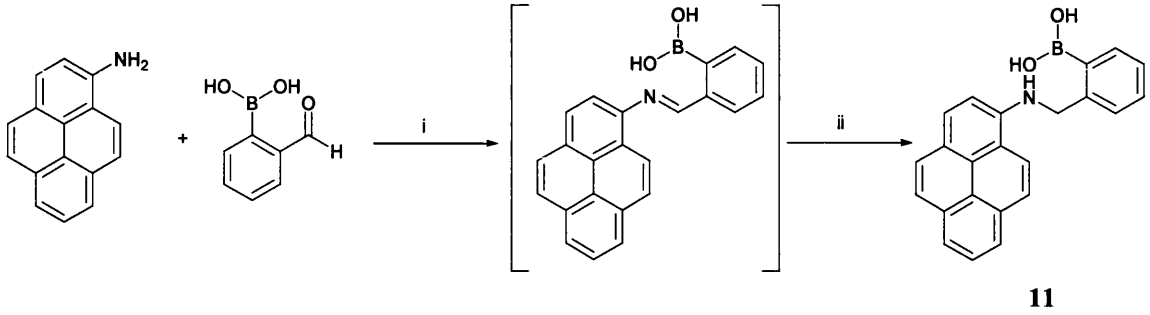

11

Scheme 14: Reagents and conditions: i) THF/MeOH (50:50) reflux in *Dean and Stark trap* under nitrogen atmosphere, overnight; ii) $NaBH_4$ (5eq), rt, 1h, **11** 47% (two steps).

2.2.5 Diboronic Acid Series, Sensors 13, 14, 15, 16, 17, and 18

The diboronic acid series was designed to provide a more efficient molecular cleft for monosaccharides. Commercially available 3,3'-methylenedianiline and 4,4'-methylenedianiline (Figure 40) were chosen as possible starting points for the synthesis of the diboronic acid series. The difference in spacing of the two amine groups in the two molecules was predicted to produce a change in the selectivity of the diboronic acids towards monosaccharides.

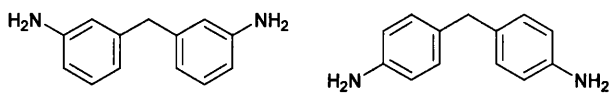

3,3'-methylenedianiline 4,4'-methylenedianiline

Figure 40: Diamines suitable for use in the synthsesis of diboronic acid series

The diboronic acids can be divided into two series, according to the amine used, the 3,3'-methylenedianiline (sensors **13**, **15**, **17**) or 4,4'-methylenedianiline (sensors **14**, **16**, **18**).

Each series contains three different sensors, each one made with one of the three boronic acid units: 2-formylphenylboronic acid, 3-formylphenylboronic acid, 4-formylphenylboronic acid. A total of six boronic acid sensors were prepared (Figure 41).

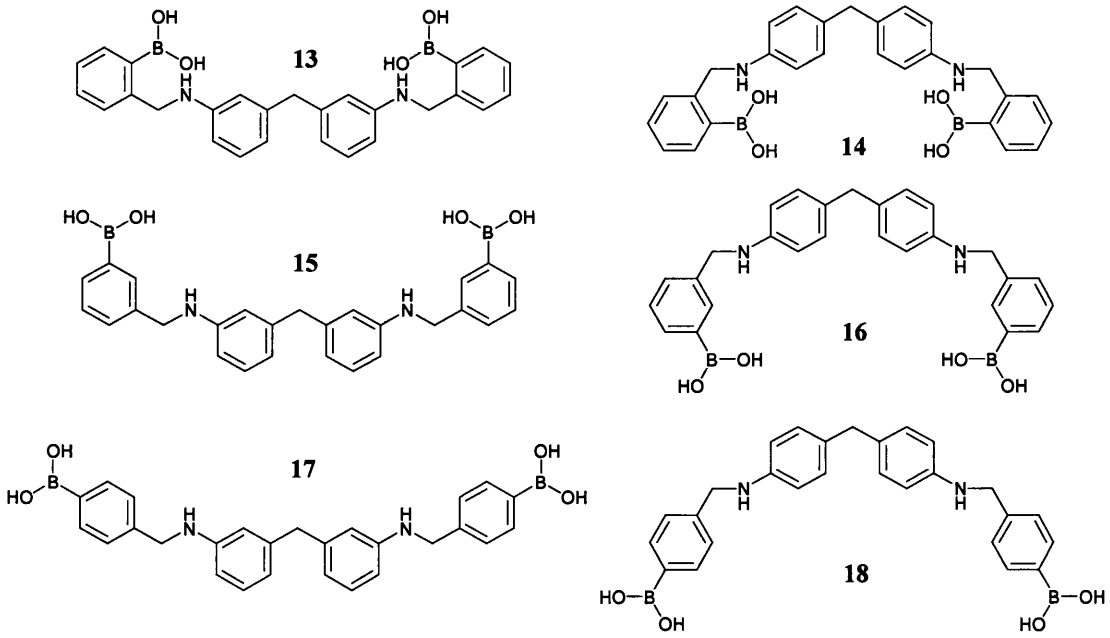

Figure 41: *Diboronic acid series, meta CH_2-bridged, (sensors **13**, **15**, **17**) and para CH_2-bridged, (sensors **14**, **16**, **18**).*

The diboronic acid sensors were synthesised using a one-pot reaction procedure as described in Scheme 15 and 16. Both diboronic acid series, were prepared according to a general method. The 3,3'-methylenedianiline or 4,4'-methylenedianiline was condensed with commercially available 2-formylphenylboronic acid, 3-formylphenylboronic acid or 4-formylphenylboronic acid (2 eq) in methanol, at room

temperature overnight to form the imine intermediate. This imine was then reduced *in situ*, in the presence of an excess of sodium borohydride (5 eq) leading to the desired sensors.

This method worked well in general, however, in the case of sensor **15**, this method failed due to incomplete reaction. The reaction was then repeated with heating at reflux in EtOH/toluene (90/10) overnight. The reduction of the imine was carried out *in situ*, in the presence of an excess of sodium borohydride to provide the desired sensor **15** by precipitation from chloroform with 37% yield.

Sensors **13** and **14** were purified successfully by precipitation from chloroform/*n*-hexane with 56% and 29% yield respectively. Purification of all the others sensors was achieved by precipitation in water by adjusting the pH from pH 14 to pH 8-9 by addition of HCl (1M) to afford sensors **16**, **17**, **18** with 74%, 44% and 62% yield respectively.

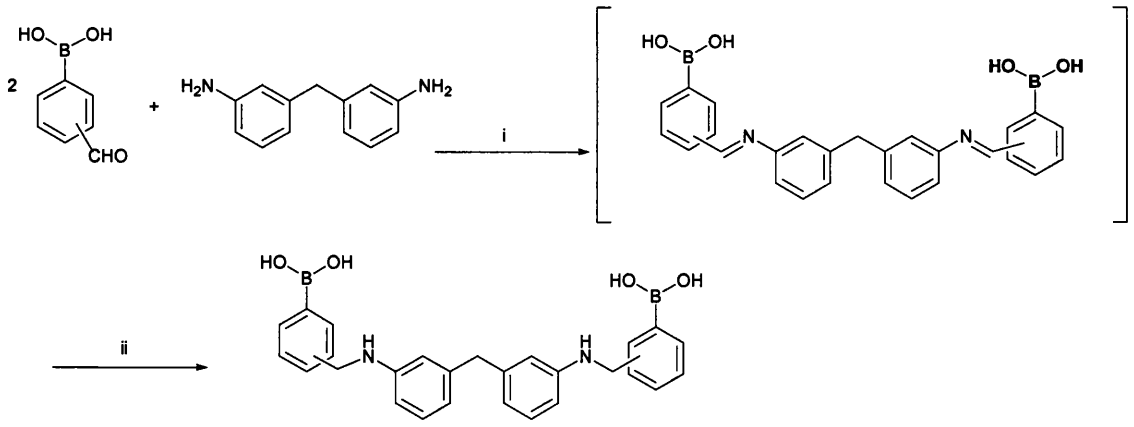

Scheme 15: Reagents and conditions: (i) EtOH/$PhCH_3$ (90/10), reflux in *Dean and Stark trap*, overnight; (ii) $NaBH_4$, **15** 37% (two steps) and (i) MeOH, rt; (ii) MeOH, $NaBH_4$, **13** 56% (two steps) and **17** 44% (two steps) respectively.

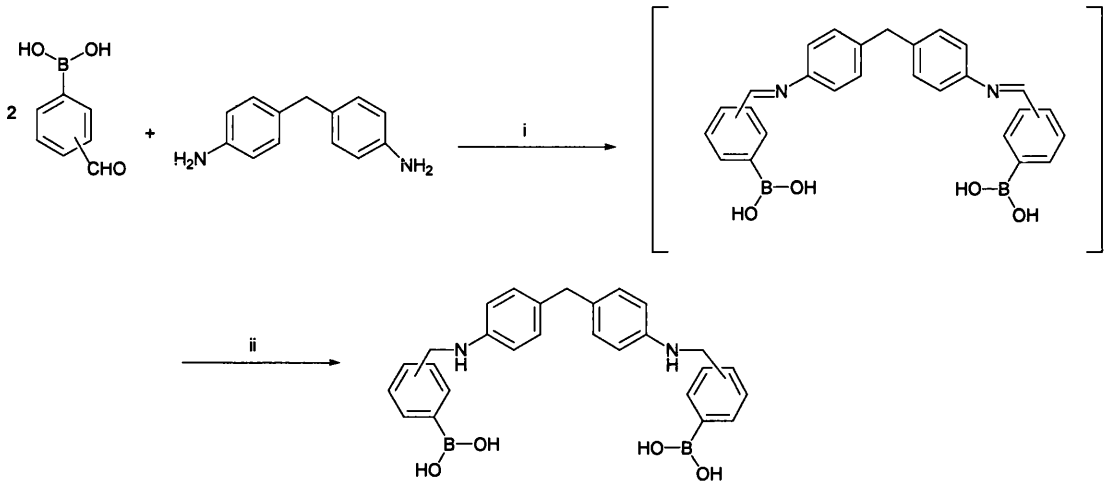

Scheme 16: Reagents and conditions: (i) MeOH, rt; (ii) MeOH, $NaBH_4$, **14** 29% (two steps), **16** 74% (two steps) and **18** 62% (two steps).

2.2.6 The Crown Ether Series, Sensors 19, 20, and 21

For the Crown Ether Series, a benzocrown ether unit, was chosen for the extension of the system to possible logic gates. The benzocrown ether unit acts as a suitable receptor for cations such as ammonium, sodium or potassium. Whereas, the boronic acid unit acts as a receptor for saccharides (diols in general) or fluoride, as discussed in the introduction. Each sensor contains a 15-crown-5 unit and the positions of the boronic acid varies from *ortho*, *meta* or *para*, leading to sensors **19**, **20** and **21** respectively.

For the purpose of the synthesis, sensors **20** and **21** were synthesised with a boronic acid group protected by 2,2'-dimethyl-1,3-propanediol. The protecting group remained in the final sensors. Under fluorescent measurement conditions, the protecting group at the concentration of 10^{-6} M is labile. Whereas sensor **19,** was synthesised as free boronic acid. The syntheses are outlined in Scheme 17 and 18.

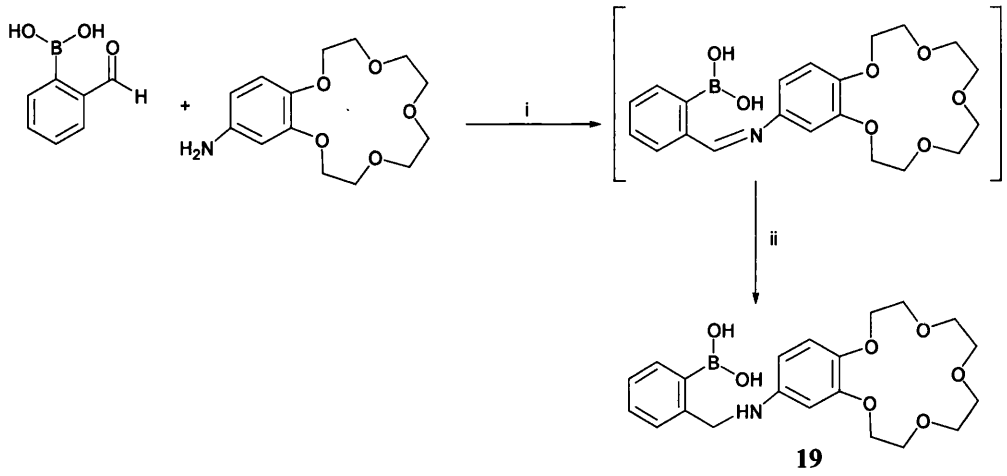

19

Scheme 17: Reagents and conditions: (i) THF/MeOH (50 / 50), rt, overnight; (ii) $NaBH_4$, rt, 4h; **19** 28% (two steps).

Sensor **19**, was synthesised in a one-pot reaction as described above in Scheme 13. The 2-formylboronic acid as a solution in THF/MeOH was added to a solution of 4-amino-benzo-15-crown-5 in the same mixture of solvents. The reaction was stirred overnight at room temperature leading to the imine, which was then reduced *in situ*, using an excess of sodium borohydride (5 eq) affording the desired sensor **19** in 28% yield after purification by a basic-acidic extraction similar to that used for the purification of sensor **8**.

Sensors **20** and **21** required the protection of the boronic acid prior to reaction with the amine. The protection of the boronic acids was achieved quantitatively by refluxing the 3-formylphenylboronic acid or 4-formylphenylboronic acid with 2,2'-dimethyl-1,3-propanediol in toluene. These reactions went to completion and did not require any further purification. Sensors **20** and **21** were synthesised using the one pot reaction method previously described for sensor **19**. The major difference is that the

boronic acids used are protected. Sensors **20** and **21** were obtained in 59% yield (as an apricot oil) and in 42% yield (as a white foam) respectively without any further purification.

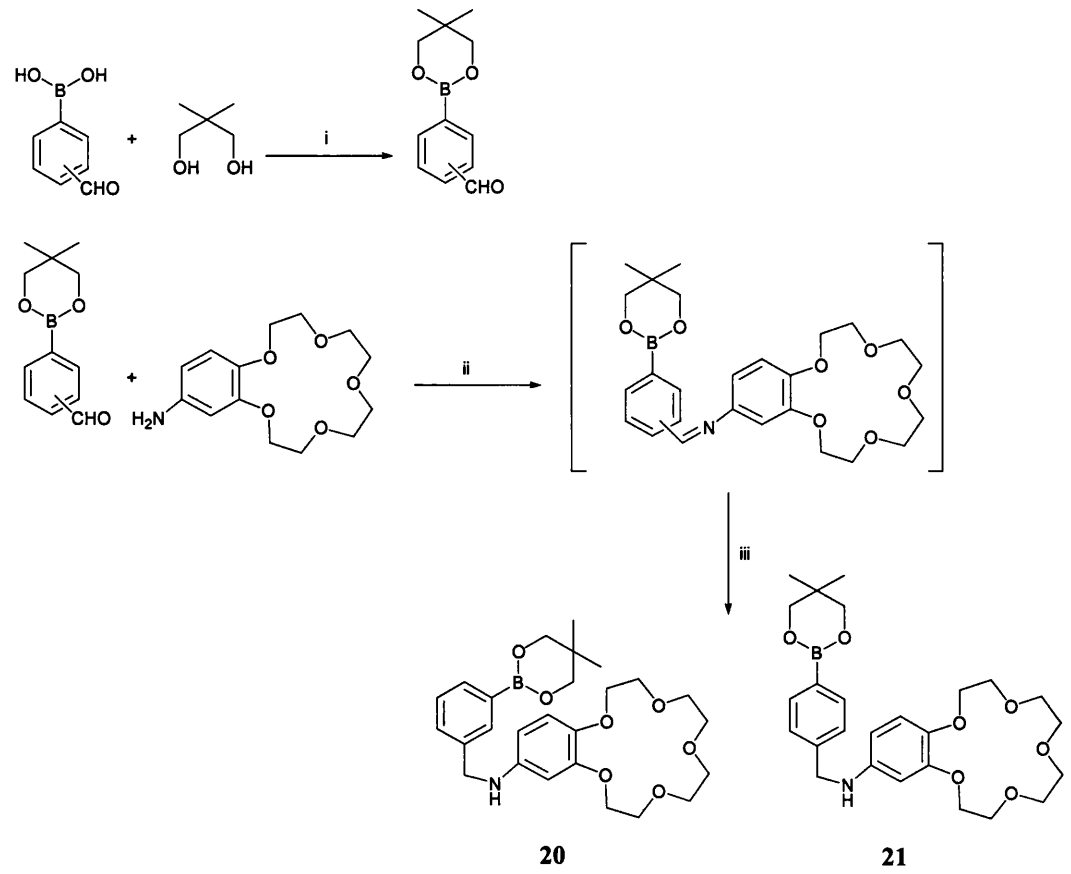

Scheme 18: Reagents and conditions: (i) Toluene, reflux, 2h, 100% conversion (ii) THF/MeOH (50 / 50), rt, overnight; (iii) $NaBH_4$, rt, 3h; **20** and **21** 59% and 42% (two steps) respectively.

2.2.7 Arabinose-Phenylboronic Acid Complex, Compound 22

The preparation of the arabinose-phenylboronic acid complex, is very straightforward (Scheme 19). The purpose was to study a saccharide-boronic acid complex by X-ray as there are few to date of such complexes in the literature.[97]

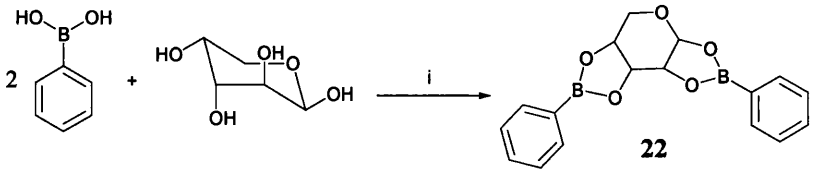

Scheme 19: Reagents and conditions: (i) Toluene, reflux, 2h.

Two equivalents of phenylboronic acid were heated under reflux in a *Dean and Stark trap*, in toluene with *β*-D-arabinose for 2 hours, leading to compound **22** as a white crystal. Crystals suitable for X-ray analysis were obtained after crystallisation from toluene/*n*-hexane. The crystal structure is presented in Figure 42. The data associated with the X-ray analysis are given in the Appendix 2. The X-ray structure shows that the arabinose's ring present an envelope shape. Both cycles including a boron atom are planars. Boron atoms present high sp^2 charater.

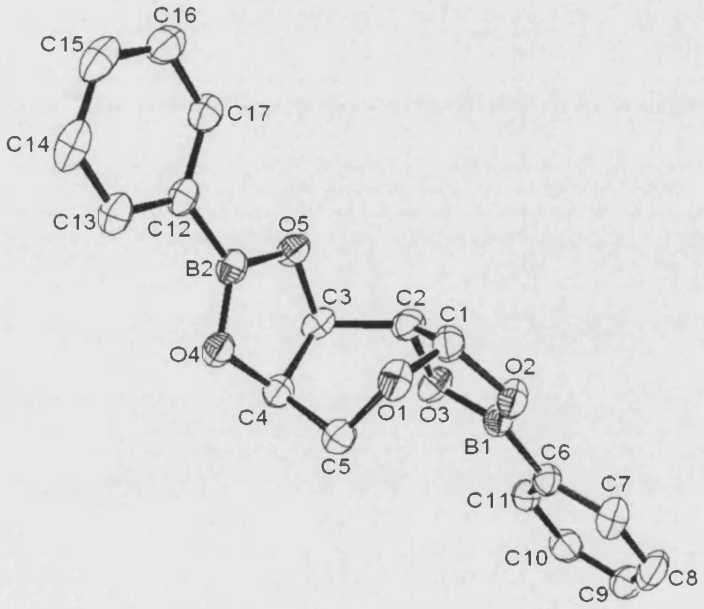

Figure 42: Crystal structure of compound **22**, showing the labelling scheme used.

2.3 Interaction of Boronic Acid Sensors with Saccharides

All the sensors described in synthesis are investigated through fluorescence spectroscopy to evaluate their binding behaviour towards saccharides. The aim is to discover "good" fluorescent sensors, which possess high selectivity, sensitivity and a large signal response upon molecular recognition.

2.3.1 Monoboronic Acid Series

*Evaluation of Sensor **1***

Sensor **1** was the first sensor to be synthesised and also to be investigated. pH-evaluation, molecular recognition, photophysical properties were investigated and are presented in this section.

*pH-titration of **1***

The aim of the first pH-titration was to determine if the system works at neutral pH and the pK_a of sensor **1** with and without saccharide. The pH-titration was performed in an osmotic buffer (33.3% methanol aqueous solution with NaCl 0.05 mol.dm^{-3}). The excitation wavelength chosen was 244 nm. The fluorescence intensity *versus* pH profiles of sensor **1** (1.0×10^{-5} mol.dm^{-3}) in the absence and presence of D-fructose (0.05 mol.dm^{-3}) are shown in Figure 43.

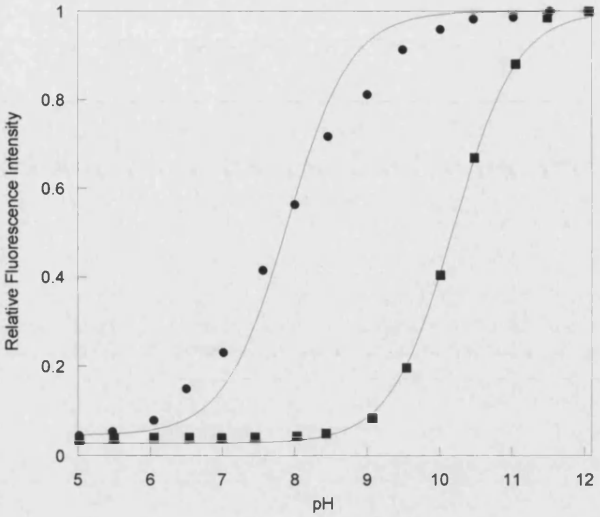

Figure 43: Fluorescence intensity *versus* pH profile of **1** at 25°C; [**1**] = 1.0 x 10^{-5} mol.dm^{-3}, 33.3wt% methanolic aqueous solution in the presence of [NaCl] = 0.05 mol.dm^{-3}, (■) in the absence of D-fructose, (●) in the presence of D-fructose (0.05 mol.dm^{-3}). λ_{ex} 244 nm, λ_{em} 360 nm.

The sodium chloride present in the osmotic buffer acts as an ionic buffer because of the small amounts of the sodium chloride formed on adjustment of the pH with the minimum volumes of sodium hydroxide and hydrochloric acid solutions. Because the titrations are carried out in a methanol-water mixture rather than simply water, the concept of pH is not strictly applicable to this situation.[98]

However, De Ligny and Renhbach have shown that for solution in 50% methanol the pH is only changed by 0.1 of a pH unit compared to a 100% water solution.[99] At percentages lower than 84% methanol, the error does not exceed 0.2 pH units, but for the higher percentages it dramatically increases and for absolute methanol it is equal to 2 pH units.

The pK_a values of sensor **1** were calculated using the equation 1:[47]

$$I_F = (I_{Fmin} + I_{Fmax} \text{ x } K \times [H^+])/(1+K \times [H^+])$$

Equation 1

The pK_a of sensor **1** was 10.20 ± 0.01 (0.99) and 7.96 ± 0.06 (0.99) in the absence and presence of D-fructose (0.05 mol.dm^{-3}) respectively.[100] The observed shift in pK_a to lower values on saccharide binding is in agreement with previous work.[5, 6, 21, 23] This shift results from the reduction of the boron-oxygen bond angle due to saccharide binding (Scheme 2b) which increases the acidity of the boron center.[6]

It was decided that further measurements would be carried out using a buffered pH of 8.21. pH 8.21 was chosen to give a large fluorescence change with and without saccharide. The second pH-titration experiment was carried out on sensor **1** with λ_{ex} 274 nm and with a new osmotic buffer (52.1% methanol aqueous solution with NaCl 0.05 mol.dm^{-3}) to investigate a change of excitation wavelength. The fluorescence intensity *versus* pH profiles of sensor **1** (1.0 x 10^{-5} mol.dm^{-3}) in the absence and presence of D-fructose (0.05 mol.dm^{-3}) are shown in Figure 44.

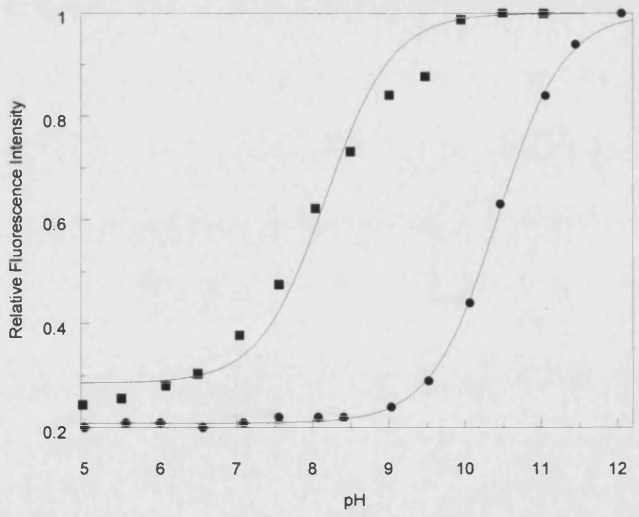

Figure 44: Fluorescence intensity *versus* pH profile of **1** at 25°C; [**1**] = 1.0 x 10^{-5} mol.dm^{-3}, 52.1wt% methanolic aqueous solution in the presence of [NaCl] = 0.05 mol.dm^{-3}, (●) in the absence of D-fructose, (■) in the presence of D-fructose (0.05 mol.dm^{-3}). λ_{ex} 274 nm, λ_{em} 361 nm and 355 nm respectively.

The pK_a of sensor **1** was respectively 10.42 ± 0.01 (0.99) (without) and 8.17 ± 0.09 (0.98) (with D-fructose).

No real changes of pK_a were observed when the excitation wavelength and the osmotic buffer was changed. The pK_a values for the different wavelengths are presented in Table 2.

Table 2: Summary of p*Ka* values.

Sensor **1**	Ex 244 nm	Ex 274 nm
pKa without D-fructose	10.20 ± 0.01	10.42 ± 0.01
pKa with D-fructose	7.96 ± 0.06	8.17 ± 0.09

*Saccharide binding at 274 nm and 244 nm of **1***

All saccharide binding studies were carried out in a pH 8.21 buffer (52.1wt% methanol in water with KCl, 0.01000 mol.dm^{-3}; KH_2PO_4, 0.002752 mol.dm^{-3}; Na_2HPO_4, 0.002757 mol.dm^{-3}).[101] This pH 8.21 buffer was chosen in accordance with the previous results, to allow us to observe a maximum change in fluorescence from unbound species to bound species and facilitate the solubility of the sensor.

The first saccharide titrations of **1** were performed in pH 8.21 buffer at 274 nm excitation wavelength (longer excitation wavelength so lower energy), with 4 different monosaccharides, (D-fructose, D-glucose, D-galactose and D-mannose) and sensor concentration (2.0×10^{-5} mol.dm^{-3}). The fluorescence spectra of **1** in the presence of D-fructose (0-0.1 mol.dm^{-3}) are shown in Figure 45.

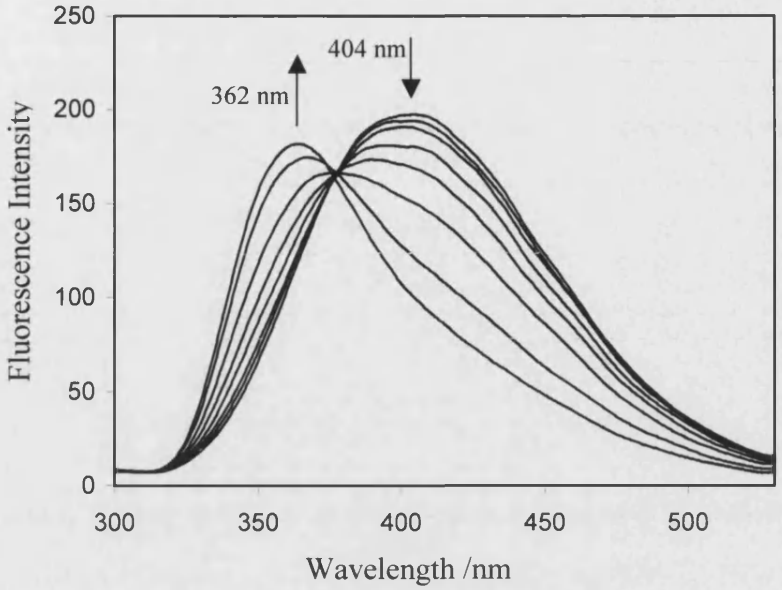

Figure 45: Fluorescence spectra change of **1** (2.0×10^{-5} mol.dm^{-3}) with different concentration of D-fructose (0-0.1 mol.dm^{-3}) in pH 8.21 buffer. λ_{ex} 274 nm

The fluorescence intensity of **1** decreased and wavelength maximum shifted from 404 to 362 nm with increasing saccharide concentration, an isostilbic point was observed at 377 nm. The observation of an isostilbic[§] point indicates that fluorescence sensor **1** changes from a single unbound species to a single saccharide bound species.[100] The stability constants (K) of sensor **1** were calculated by fitting the emission intensity at 360 nm *versus* concentration of saccharide. The curves are shown in Figure 46 and the calculated values are given in Table 3. The stability constants[¶] (K) were calculated using equation 2.[47]

$$I_F = (I_{Fmin} + I_{Fmax} \times K \times [\text{saccharide}])/(1 + K \times [\text{saccharide}])$$

Equation 2

[§] Isostilbic is the equivalent term of isosbestic commonly used for the fluorescence emission.
[¶] Each time stability constant is mentioned, it will refer to these observed stability constants.

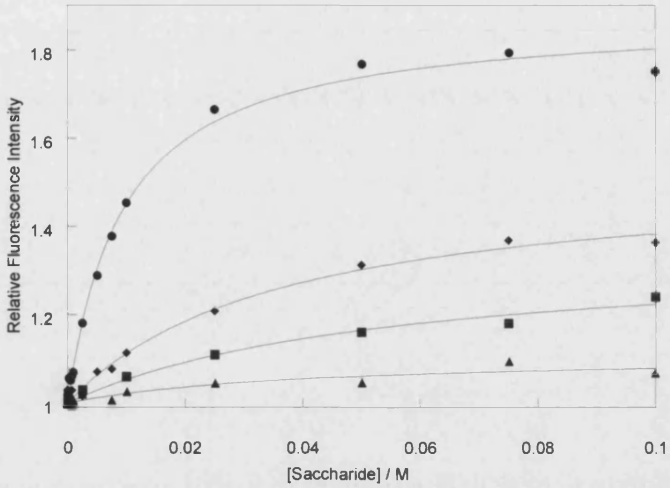

Figure 46: Relative fluorescence intensity *versus* saccharide concentration profile of **1** with (●) D-fructose, (■) D-glucose, (♦) D-galactose, (▲) D-mannose, in pH 8.21 buffer λ_{ex} 274 nm, λ_{em} 360 nm.

Table 3: Stability constant *K* (coefficient of determination; r^2) for saccharide complexes of fluorescence sensor **1** at λ_{ex} 274 nm.

	D-Fructose	D-Glucose	D-Galactose	D-Mannose
K $mol^{-1}.dm^3$	106 ± 7.0 (0.99)	18 ± 6.0 (0.98)	27 ± 4.0 (0.99)	— **

** small fluorescence changes

The observed order of stability constants (*K*) with D-fructose > D-galactose > D-glucose, is the expected order for all monoboronic acids.[5, 6, 21, 23]

The second saccharide tritrations with sensor **1** were performed at the excitation wavelength 244 nm (shorter wavelength, so higher energy with respect to 274 nm). The same conditions as in the first saccharide titrations were used: pH 8.21 buffer (52.1wt% methanol in water with KCl, 0.01000 $mol.dm^{-3}$; KH_2PO_4, 0.002752 $mol.dm^{-3}$; Na_2HPO_4, 0.002757 $mol.dm^{-3}$),[101] 4 different monosaccharides (D-fructose, D-glucose, D-galactose and D-mannose) with the same sensor concentrations.

Figure 47 represents the fluorescence spectra of sensor **1** in the presence of D-fructose (0-0.1 mol.dm^{-3}).

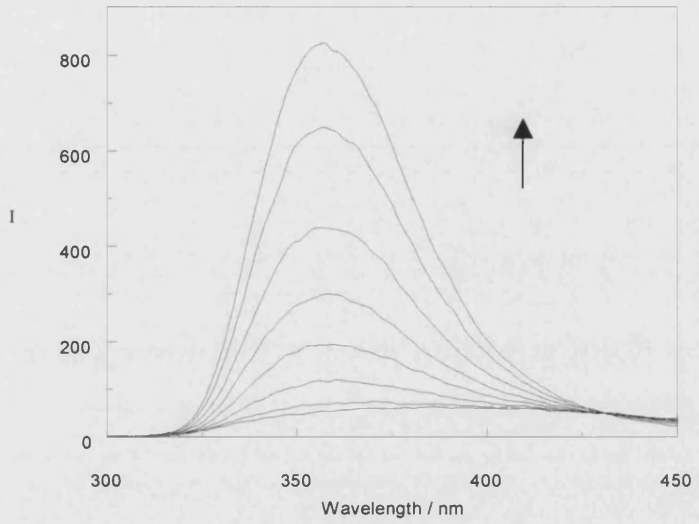

Figure 47: Fluorescence spectra change of **1** (2.0×10^{-5} mol.dm^{-3}) with different concentration of D-fructose (0-0.1 mol.dm^{-3}) in a pH 8.21 buffer, λ_{ex} 244 nm.

The maximum fluorescence intensity was observed at 357 nm. A large fluorescence intensity enhancement (fifteen fold) was noticed in this spectrum. This implies that sensor **1** was more sensitive at this excitation wavelength.

A fluorescence intensity shift and an isostilbic point were not observed in this spectrum. At this excitation wavelength, only the bound species was observed. The stability constants (*K*) of fluorescence sensor **1** (Table 4) were calculated by fitting the emission at their maximum, λ_{em} 357 nm *versus* concentration of saccharide (Figure 48).

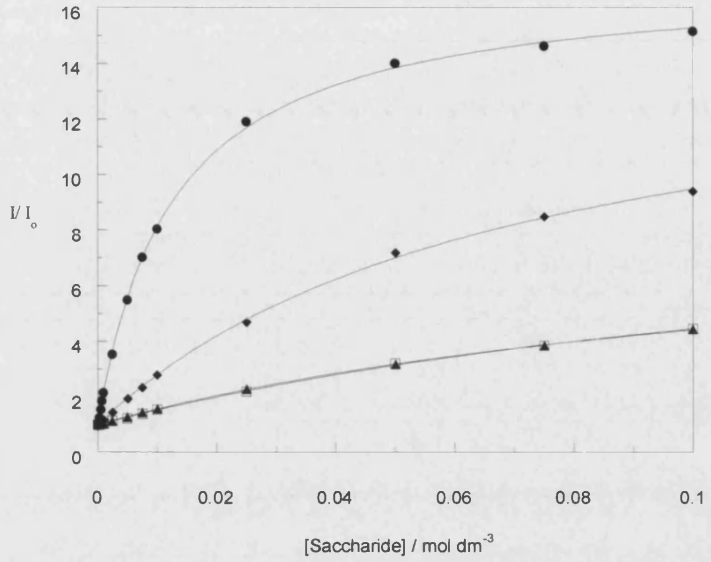

Figure 48. Relative fluorescence intensity *versus* saccharide concentration profile of **1** with (●) D-fructose, (□) D-glucose, (♦) D-galactose, (▲) D-mannose, in a pH 8.21 buffer. λ_{ex} 244 nm, λ_{em} 357 nm.

Table 4. Stability constant *K* (coefficient of determination; r^2) for saccharide complexes of fluorescence sensor 1 at λ_{ex} 244 nm.

	D-Fructose	D-Glucose	D-Galactose	D-Mannose
K mol^{-1}.dm^3	79 ± 1.7 (0.99)	6.4 ± 0.4 (0.99)	14 ± 0.6 (0.99)	7.8 ± 0.3 (0.99)

The observed order of the stability constants (*K*) is found as follow, D-fructose > D-galactose > D-mannose > D-glucose. This result is comparable to the one obtained at 274 nm (except that at 244 nm we were able to calculate the stability constant with D-mannose) and in accordance with the expected order of all the monoboronic acids.[5, 6, 21, 23]

UV-Vis behaviour and fluorescence excitation of ***1***

To understand the result of the two saccharide binding studies, a D-fructose titration was undertaken by UV-Vis spectroscopy.

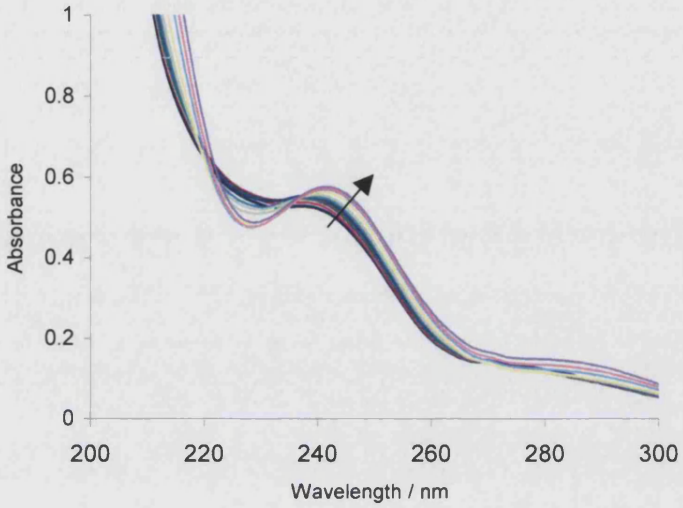

Figure 49: Absorption spectra changes of sensor **1** (5.0×10^{-5} mol.dm^{-3}) with increasing concentration of D-Fructose (0-0.1 mol.dm^{-3}) in a pH 8.21 buffer.

The absorption spectra of sensor **1** on addition of different concentrations of D-fructose show (Figure 49) a very small change in absorbance at 274 nm, where both bound and unbound species were present. However a small but significant shift can be observed around 244 nm, due to the bound species only. Investigation of sensor **1** was pursued further. The excitation spectra were recorded during a D-fructose titration (Figure 50).

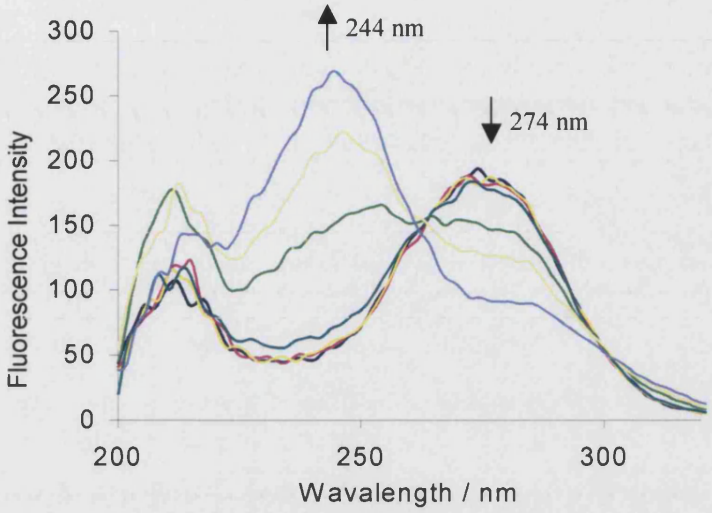

Figure 50: Fluorescence excitation change of sensor **1** (2.0×10^{-5} mol.dm^{-3}) with increasing D-fructose concentration, in a pH 8.21 buffer, λ_{em} 393 nm.

The excitation wavelength maximum shifted from 274 nm to 244 nm. Moreover an isostilbic point in the excitation spectra, was also found at 263 nm.

Here, the excitation spectra and the absorbance spectra are complementary. Usually the absorbance spectrum is used to find the isosbestic point for excitation. The absorbance spectrum is the mirror of the fluorescence excitation spectrum.

Sensor **1** had unusual behaviour and to fully study it, a saccharide binding study has also been undertaken at the excitation wavelength 263 nm (isostilbic point in the excitation spectra).

*Saccharide binding study at 263 nm of **1***

To further explore the behaviour of sensor **1**, the saccharide binding studies at 263 nm (isostilbic point) were then performed. The saccharide titrations were carried out in the same conditions (pH 8.21 buffer, sensor concentration, 4 different saccharides) as previously mentioned, except that the excitation wavelength was 263 nm.

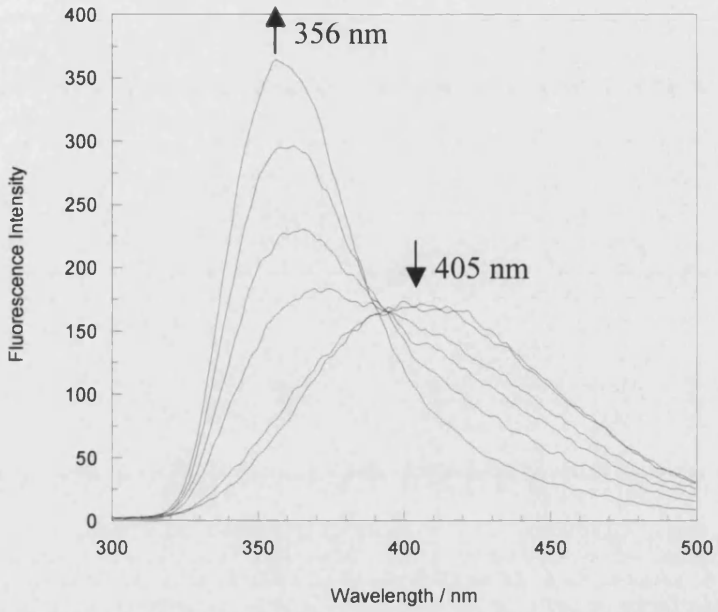

Figure 51: Fluorescence spectra change of **1** (2.0×10^{-5} mol.dm^{-3}) with different concentrations of D-fructose (0-0.1 mol.dm^{-3}) in pH 8.21 buffer, λ_{ex} 263 nm.

The fluorescence intensity shifted from 405 nm to 356 nm with increasing the saccharide concentration and an isostilbic point was observed at 391 nm (Figure 51). The enhancement of the fluorescence intensity at 356 nm was more important than the one observed when excited at 274 nm because at the excitation wavelength 263 nm, both species, bound and unbound, were excited at the same time.

The curves and the stability constants values (*K*) are shown in Figure 52 and Table 5 respectively.

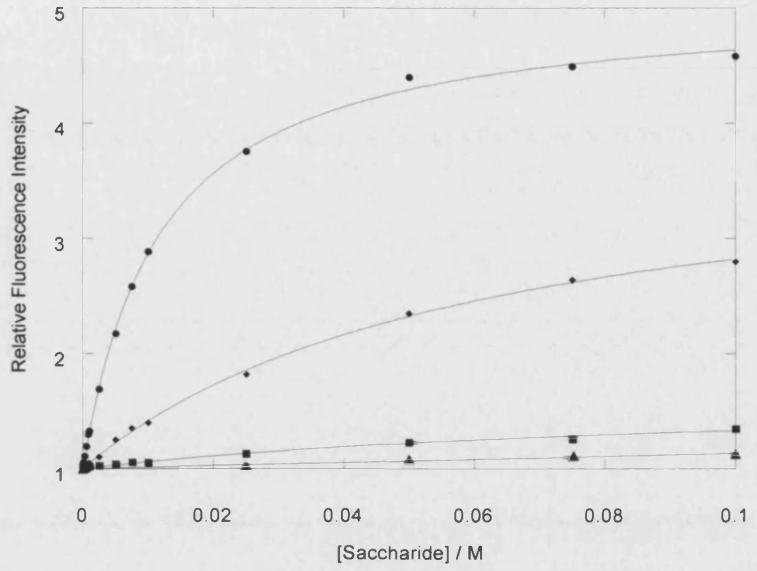

Figure 52: Relative fluorescence intensity *versus* saccharide concentration profile of **1** with (●) D-fructose, (■) D-glucose, (♦) D-galactose, (▲) D-mannose, pH 8.21 buffer, λ_{ex} 263 nm, maximum of λ_{em} for each spectrum 360-372 nm.

Table 5: Stability constant *K* (coefficient of determination; r^2) for saccharides complexes of fluorescence sensor **1** at λ_{ex} 263 nm.

	D-Fructose	D-Glucose	D-Galactose	D-Mannose
K $mol^{-1}.dm^3$	85 ± 2.7 (0.99)	10 ± 2.6 (0.99)	16 ± 1.2 (0.99)	—— **

** small fluorescence changes

The stability order found was D-fructose > D-galactose > D-glucose. This is in accordance with the literature work[5, 6, 21, 23] and also our two previous experiments on this sensor.

Summary

A summary of the stability constants (K) values is presented in Table 6.

Table 6: Stability constant K (coefficient of determination; r^2) for saccharides complexes of fluorescence sensor 1 at different excitation wavelengths.

Saccharides	**1** (ex 244 nm) K $mol^{-1}.dm^3$	**1** (ex 263 nm) K $mol^{-1}.dm^3$	**1** (ex 274 nm) K $mol^{-1}.dm^3$
D-Fructose	79 ± 1.7 (0.99)	85 ± 2.7 (0.99)	106 ± 7.0 (0.99)
D-Glucose	6.4 ± 0.4 (0.99)	10 ± 2.6 (0.99)	19 ± 6.0 (0.98)
D-Galactose	14 ± 0.6 (0.99)	16 ± 1.2 (0.99)	27 ± 4.0 (0.99)
D-Mannose	7.8 ± 0.3 (0.99)	— **	— **

** small fluorescence changes

Similar results were found at 244 nm, 263 nm and 274 nm, however the one obtained at 244 nm is probably closer to the true value. Excitation wavelength at 263 nm or 274 nm leads us to observe two different species: unbound and bound one at λ_{em} 404 nm and 360 nm respectively. Excitation at 244 nm, allows the observation of only one species, the bound one at λ_{em} 360 nm (Figure 53).

To explore further the system and to understand the mechanism of fluorescence of sensor **1**, the model compound **4** and sensor **1** were also studied in methanol. The effect of the saccharide binding can be reproduced in methanol by addition of a drop of base (NaOH aqueous 3 M). Compound **4** shows only one fluorescence emission at 342 nm (when excited at 244 nm or 274 nm). However, when sensor **1** is excited at 274 nm, a band at 393 nm is observed. After addition of a drop of NaOH (3 M), the band shifted to 360 nm. By addition of base, the conditions obtained in methanolic aqueous buffer upon saccharide binding were reproduced. Moreover, the spectra obtained for sensor **1** with base are similar to those obtained with model compound **4**. The above results indicate that the B-N bond in sensor **1** is broken on addition of saccharide (cf addition of base to sensor **1** in methanol).

The methanol study was performed to allow comparison with ^{11}B-NMR experiments, unfortunately, these NMR-experiments were inconclusive. Further study on the effect of the B-N interaction is presented in the section concerning sensors **2** and **3**, since both of these sensors do not contain any B-N bond.

Without saccharide, when the excitation used is 244 nm, the fluorescence observed is a "weak" fluorescence (nearly flat baseline) because no bound species are present. With the addition of saccharide, the fluorescence intensity increases due to the formation of bound species (Figure 53).

In the other cases, with excitation at 274 nm or 263 nm the fluorescence shifted from 404 nm to 360 nm, from unbound to bound species. This could explain why two emission wavelength maxima were observed in the spectra. At the beginning of the experiment, without any saccharide, only the fluorescence of the unbound species is observed at λ_{em} 404 nm. This unbound species contains a B-N bond. When the saccharide is added to the solution, a new signal appeared at λ_{em} 360 nm, corresponding to the other fluorescence species, the bound one. On addition of saccharide the B-N bond is broken to form the boronate-saccharide complex, bound species, which emits at 360 nm (Figure 53).

In the spectra recorded with either λ_{ex} 274 or 263 nm the value obtained at λ_{em} 360 nm without saccharide came from the decrease of fluorescence of the unbound species and not the bound one. So the fluorescence values obtained at λ_{em} 360 nm came from two fluorescent species. This is why the fluorescent values obtained after excitation at 244 nm and used to calculate the stability constants, are closer to the true values.

In conclusion, the fluorescence spectra at different excitation wavelengths 244 nm and 263 or 274 nm allow us to observe two fluorescent events.

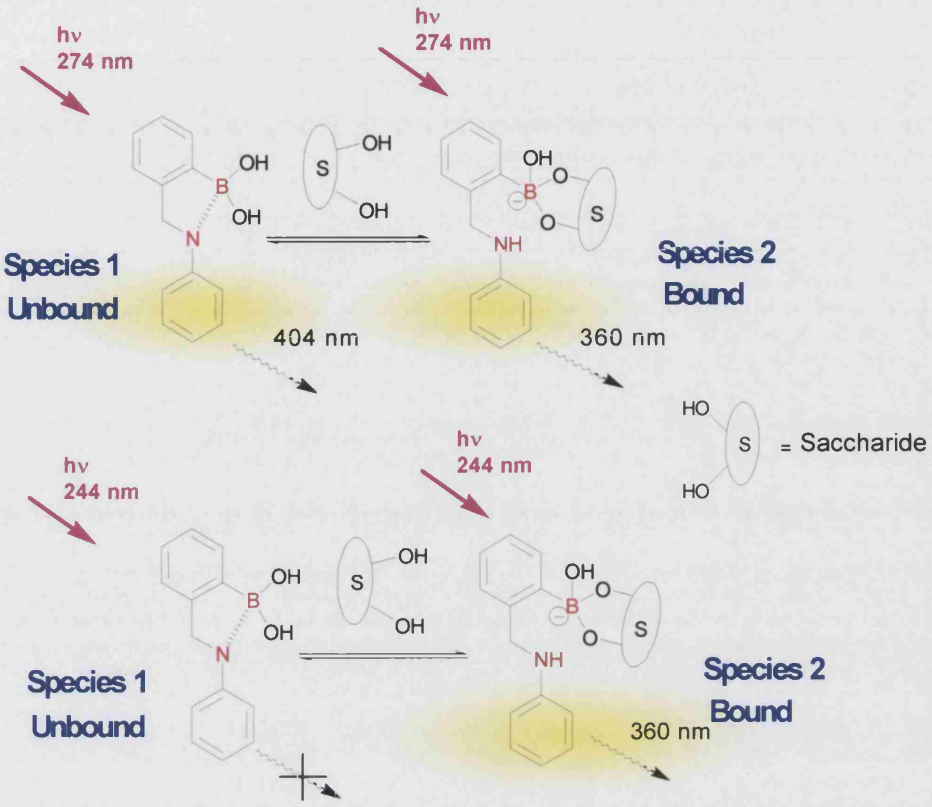

Figure 53: Proposed fluorescent species.

At this point, the effect of some factors, which might influence the results of the fluorescence measurement presented previously, have been considered: the effect of the buffer, the effect of predominant form of the sugar for the binding event (due to mutarotation in aqueous solution) and the effect of species present in the buffer (like anions or conjugated buffer bases).

Firstly the effect of the buffer was investigated. The saccharide titrations with sensor **1** were performed in phosphate buffer, in HEPES (0.1 M, MeOH/water 50% v/v) buffer and just in an ionic buffer (MeOH/water 50% v/v with 0.5 M of NaCl). The results are presented in Figure 54 and the stability constants values (*K*) are shown in Table 7.

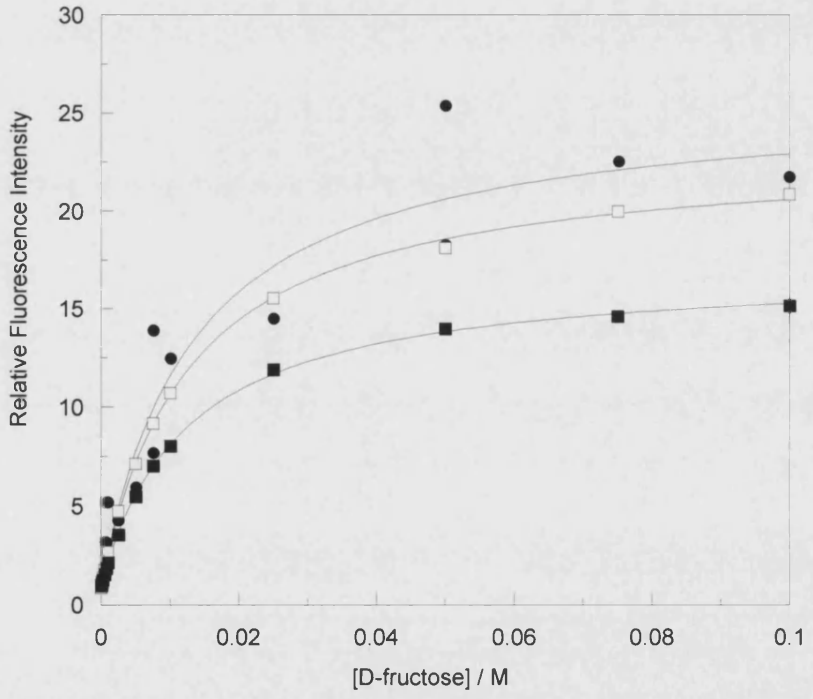

Figure 54: Relative fluorescence intensity *versus* saccharide concentration profile of **1** with (●) ionic buffer, (□) HEPES (0.1 M, MeOH/ water 50% v/v) buffer, (■) phosphate buffer, pH 8.21 buffer, λ_{ex} 244 nm, λ_{em} 360 nm.

Table 7: Stability constant K (coefficient of determination; r^2) for D-fructose complexes of fluorescence sensor **1** at λ_{ex} 244 nm, comparison of buffers.

Buffers	**1** (ex 244 nm) K $mol^{-1}.dm^3$
Phosphate	79 ± 1.7 (0.99)
HEPES	77 ± 1.9 (0.99)
Ionic	74 ± 17.1 (0.95)

No significant changes can be observed from the results shown in Table 7. The similar stability constants are obtained. However, the three curves do not overlay, this is due to the day-to-day variations in "intensity" that make the maximum fluorescence response different for the three experiments. The stability constant determined for the ionic media, do not have a good fit, because keeping a constant pH was harder than in the two other buffers (phosphate and HEPES). Phosphate buffer, HEPES buffer and ionic buffer are all behaving the same like an unbuffered system. In conclusion, the phosphate buffer used, previously in the James group, is essentially behaving as an unbuffered system and will remain the chosen system.

Secondly, the effect of the predominant form of the sugar has been investigated. Saccharides are well known to mutarotate on dissolution in water leading to the preferred stable form of the sugar in water. This is known as mutarotation that means that an equilibrium mixture contains the saccharide with different ring sizes and anomeric configurations. Each saccharide varies according to its more stable forms. For D-fructose, the composition in aqueous solution at equilibrium is, 65% β-pyranose, 25% β-furanose, 6.5% α-furanose, 2.5% α-pyranose and 0.8% acylic carbonyl form.[102] All these possible forms are in a continuous equilibrium in aqueous solution. The different forms of the D-fructose will have different affinities since the diol-sub-structure vary. When one of these is bound, the equilibrium will shift to produce a new distribution that preserves the same proportions of the unbound sugar. Usually this shift involves only a

small amount of the total sugar. NMR studies have shown that this is fast in homogeneous solutions. [6, 5, 22, 103, 104, 105, 49]

Is this equilibrium obtained very quickly when starting from solid and did it modify or reduce the efficiency of the binding with boronic acid? To answer this question, a solution of D-fructose in water (2 M) has been made and kept for a few days before been used. So all the D-fructose should be at the equilibrium and in the major stable form, *β*-pyranose. This solution was then used to titrate D-fructose (from 0-0.1 M using volume) into a solution of sensor **1** in phosphate buffer. At the same time, the experiment has been repeated for sensor **1** with D-fructose added as a solid. The results of these two experiments are presented in Figure 55, and *K* values are calculated and given in Table 8.

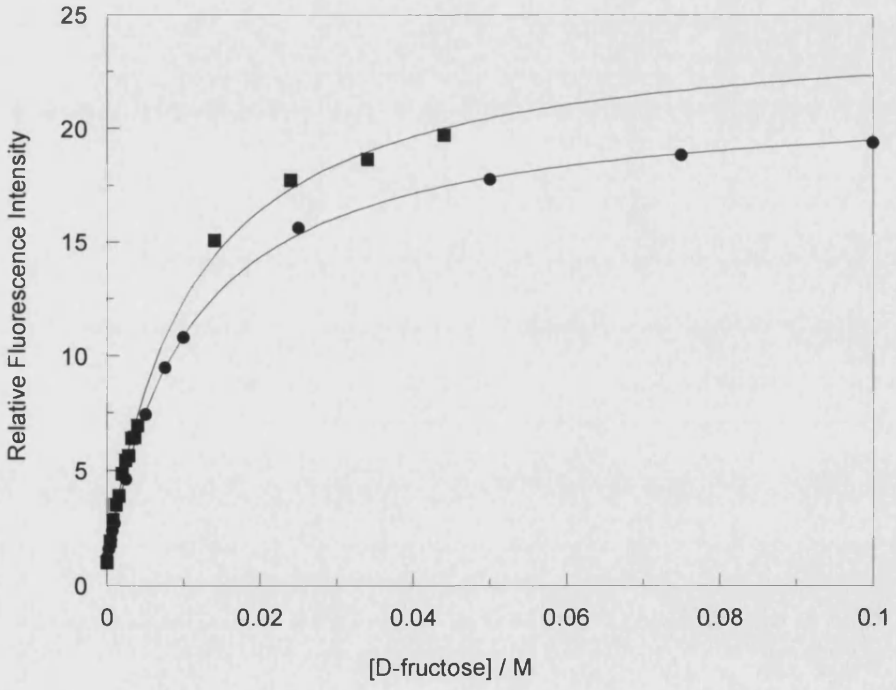

Figure 55: Relative fluorescence intensity *versus* saccharide concentration profile of **1** with (●) D-fructose as a solid, (■) D-fructose solution, pH 8.21 buffer, λ_{ex} 244 nm, λ_{em} 358 nm.

Table 8: Stability constant *K* (coefficient of determination; r^2) and enhancement factor for D-fructose complexes of fluorescence sensor **1** at λ_{ex} 244 nm, comparison of D-fructose solution or solid.

	1 D-fructose (solid)	**1** D-fructose (solution)
K mol^{-1}.dm^3	93 ± 1.7 (0.99)	93 ± 4.5 (0.99)

From this result, no changes in recognition are observable and the mutarotation is fast enough even if solid D-fructose is used. In conclusion, the addition of solid D-fructose is not a problem, and all the future experiments were carried out using solid D-fructose.

Finally, the effect of the association of the boronic acids with the buffer conjugate bases (phosphate, citrate and imidazole depending of the chosen buffer) has been investigated.[106]

It is well known since Lorand and Edward[21] that boronic acid in aqueous solution forms a boronate anion plus a proton by reacting with water molecules. Thereby the boronate anion can react with a diol leading to the formation of the diol boronate complex.

By investigating the association of the boronic acid and the buffered conjugate base present in the media using pH titration technique, two others complexes have been discovered: the binary and ternary complexes. This technique can detect all the complexes formed and not only the one, which fluoresce.

The binary complex is defined as a complex formed between the boronate and Lewis bases (X) noted as boronate-X. The ternary species is a complex between boronate-X and saccharide noted boronate-X-Saccharide. In most of the cases ternary species, which were until recently unknown, can be dominant species in solution under some conditions (acidic and/or stoichiometric). These ternary complexes reduce the concentration of free boronate and free boronic acid leading to a decrease in the

measured apparent formation constants. An example of these complexes is presented in Figure 56 and calculated by the program Hyperquad.

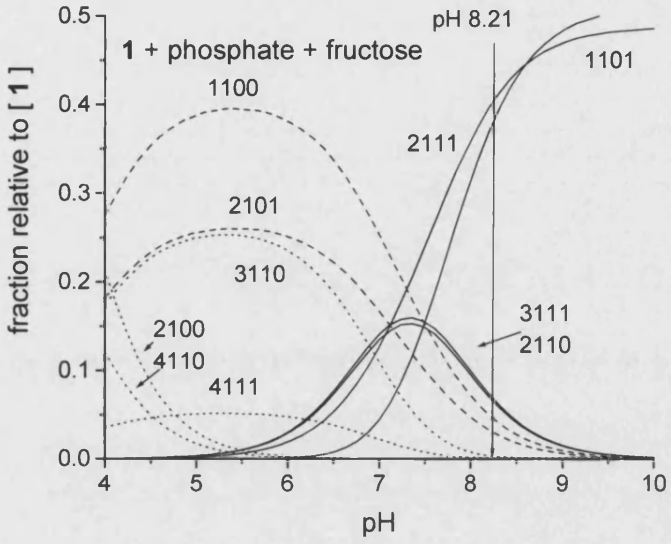

Figure 56: Different complexes formed calculated at [**1**] = 2×10^{-5} M, pH 8.21, phosphate buffer. [D-fructose] = 0.01 M.[106]

In this experiment, the phosphate complexes are expected to behave like the "hydroxo" complexes i.e. B-OPO_3 is just like B-OH, so the only signal detected is from the "free" boronic acid.

The species stoichiometries are H + boronate + phosphate + sugar. D-Fructose in this scheme is a deprotonated reactant, so the normal form is 1001. Little B-N interaction is present, so the acyclic version is the way to formulate species abundant between pH 4 and 7. The species to consider at pH 8.21 are:

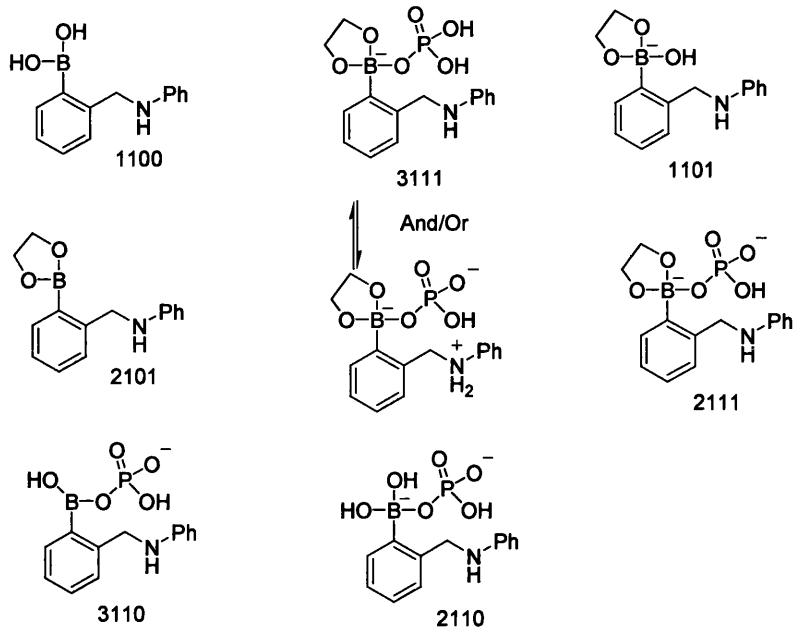

Without any D-fructose at pH 8.21 the species are the ones shown above where the fourth integer is zero plus the following, which are too low abundance when there is excess of D-fructose. They are about equal abundance.

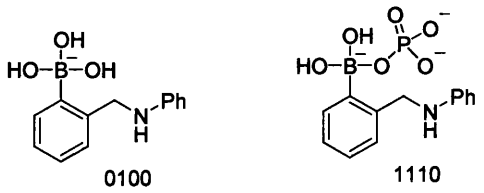

So in fluorescence titration, species start with a 0100/1100/1110/2110 mixture and form a 1101/2111/3111 mixture. The change in intensity is due solely to the decrease in the amount of 1100 on addition of D-fructose.

In conclusion, the ternary complexes form when the phosphate buffer is used. However, the apparent constants we determine are suitable for evaluating these systems, since the competing complex with the buffer does not overwhelm the system.

*Evaluation of Sensors **2** and **3***

From the investigation on sensor **1**, the species emitting at 360 nm, do not contain a B-N bond, but still showed some fluorescence enhancement. So sensor **2** and **3** were designed since there is no possibility of B-N bond formation as they are isomers of position *meta* and *para* respectively, of sensor **1**.

pH-evaluation and molecular recognition were investigated and are presented in this section.

*pH-titration of **2** and **3***

The pH-tritrations were performed in an osmotic buffer (52.1% methanol aqueous solution with NaCl 0.05 mol.dm^{-3}) which are presented in figures 57 and 58 for **2** and **3** respectively and the pK_a values are given in Table 9.

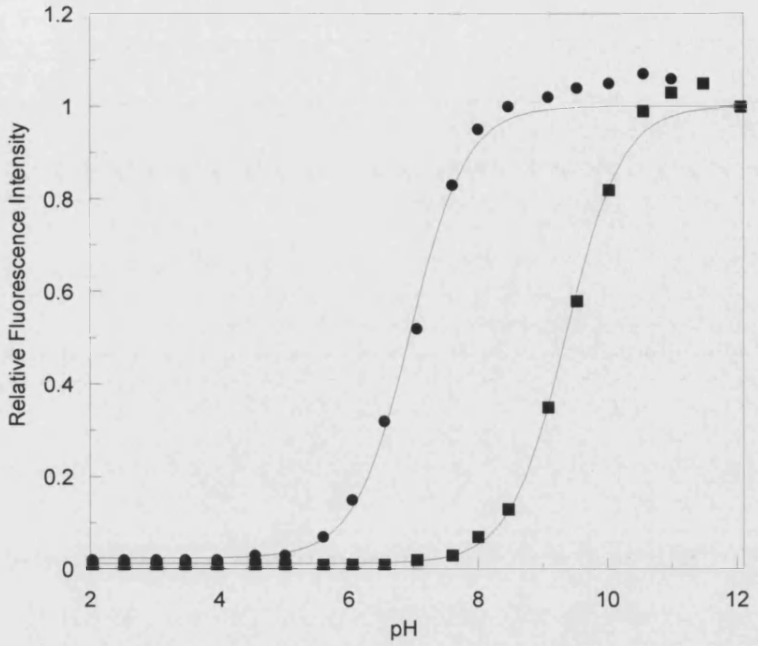

Figure 57: Fluorescence intensity *versus* pH profile of **2** at 25°C; [**2**] = 1.0 **x** 10^{-5} mol.dm^{-3}, 52.1wt% methanolic aqueous solution in the presence of [NaCl] = 0.05 mol.dm^{-3}, (■) in the absence of D-fructose, (●) in the presence of D-fructose (0.05 mol.dm^{-3}). λ_{ex} 240 nm, λ_{em} 350 nm.

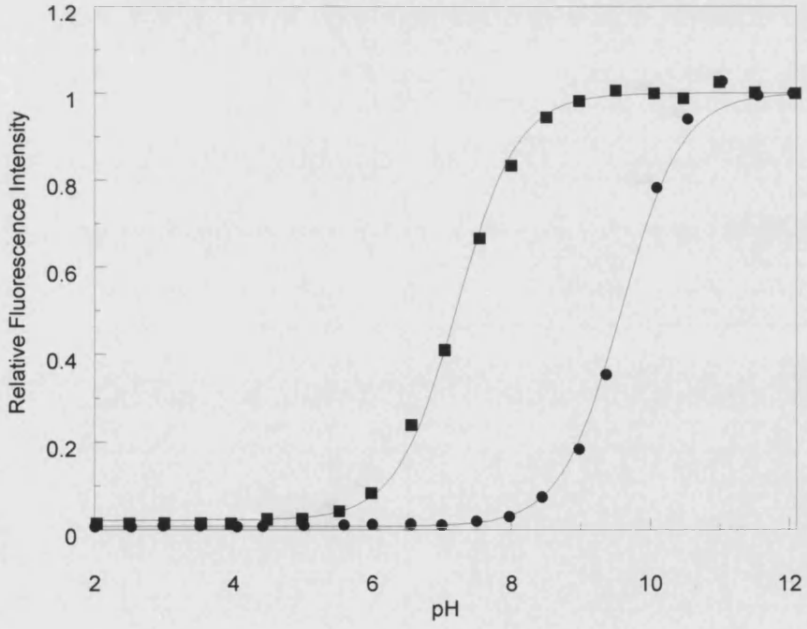

Figure 58: Relative fluorescence intensity *versus* pH profile of **3** at 25°C; [**3**] = 1.0 **x** 10^{-5} mol.dm^{-3}, 52.1wt% methanolic aqueous solution in the presence of [NaCl] = 0.05 mol.dm^{-3}, (●) in the absence of D-fructose, (■) in the presence of D-fructose (0.05 mol.dm^{-3}). λ_{ex} 244 nm, λ_{em} 350 nm.

Table 9: Summary of pK_a values for sensors **1**, **2** and **3**.

	1	**2**	**3**
pK_a without D-fructose	10.20 ± 0.01	9.30 ± 0.03	9.58 ± 0.02
pK_a with D-fructose	7.96 ± 0.06	6.95 ± 0.04	7.22 ± 0.02

The pK_a of sensors **2** and **3** were: 9.30 ± 0.03 (0.99) and 9.58 ± 0.02 (0.99) respectively and in the presence of D-fructose 6.95 ± 0.04 (0.99) and 7.22 ± 0.02 (0.99) respectively. The observed change in pK_a to lower values on saccharides binding is on agreement with previous work.

A pH 8.21 phosphate buffer will be used to perform the molecular recognition experiments.

*Saccharide binding at 244 nm of **2** and **3***

The fluorescence titration of **2** and **3** were performed in pH 8.21 phosphate buffer at 240 nm and 244 nm excitation wavelength respectively (no emission was observed on excitation at 274 nm), with 4 different monosaccharides, (D-fructose, D-glucose, D-galactose and D-mannose) and sensor concentration (1.0×10^{-5} mol.dm^{-3}). The fluorescence spectra of **2** and **3** in the presence of D-fructose (0-0.1 mol.dm^{-3}) are presented in Figure 59 and 60.

The maximum emission is observed at 350 nm for both sensors **2** and **3**. The fluorescence enhancement on addition of D-fructose is respectively eighteen and twenty-five fold for sensors **2** and **3**. The fluorescence enhancements for four sugars are shown in figure 61 and 62 for sensors **2** and **3** respectively. The stability constants are calculated from the curves and given in Table 10.

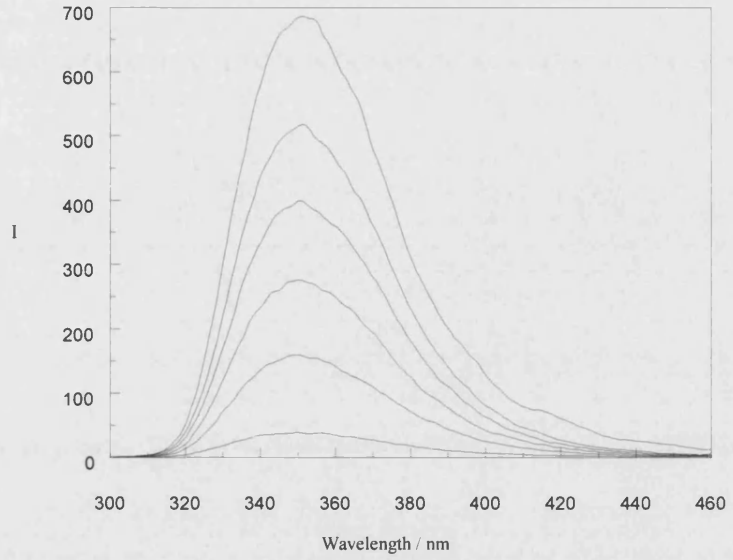

Figure 59: Fluorescence spectra change of **2** (1.0×10^{-5} mol.dm^{-3}) with different concentration of D-fructose (0-0.1 mol.dm^{-3}) in a pH 8.21 buffer. λ_{ex} 240 nm.

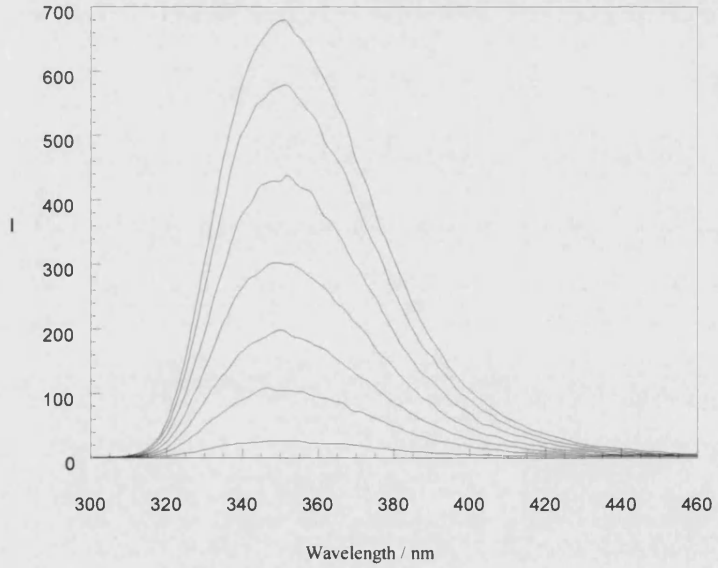

Figure 60: Fluorescence spectra change of **3** (1.0×10^{-5} mol.dm^{-3}) with different concentration of D-fructose (0-0.1 mol.dm^{-3}) in a pH 8.21 buffer, λ_{ex} 244 nm.

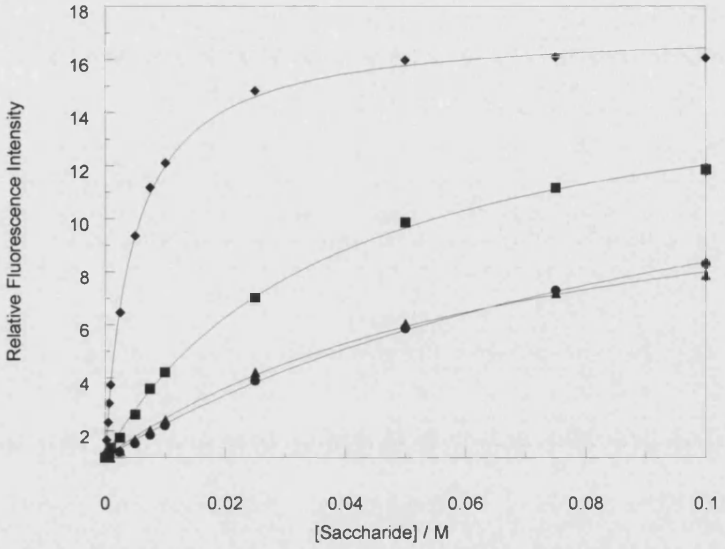

Figure 61: Relative fluorescence intensity *versus* saccharide concentration profile of **2** with (♦) D-fructose, (●) D-glucose, (■) D-galactose, (▲) D-mannose. The measurement conditions are the same as those in Figure 24. λ_{ex} 240 nm, λ_{em} 350 nm.

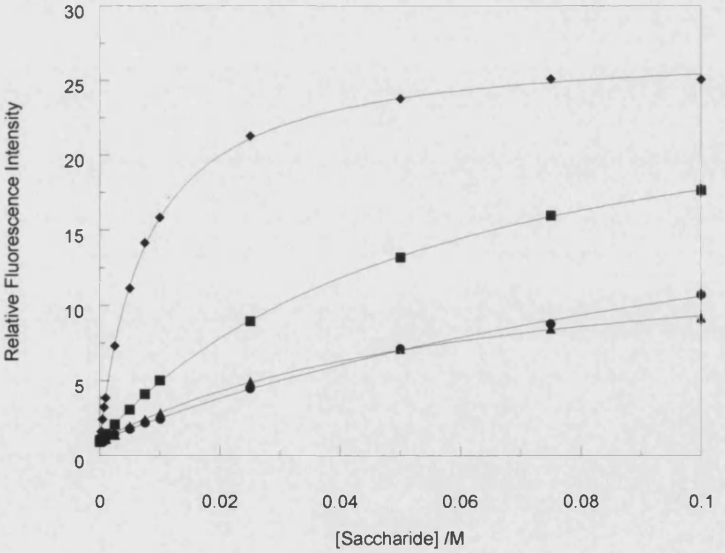

Figure 62: Relative fluorescence intensity *versus* saccharide concentration profile of **3** with (♦) D-fructose, (●) D-glucose, (■) D-galactose, (▲) D-mannose. The measurement conditions are the same as those in Figure 25. λ_{ex} 244 nm, λ_{em} 350 nm.

Table 10: Stability constant K (coefficient of determination; r^2) for saccharide complexes of fluorescent sensors **2** and **3**, in pH 8.21 buffer at λex 244 nm (sensor **3**) and 240 nm (sensor **2**).

Saccharides	**2** K $mol^{-1}.dm^3$	**3** K $mol^{-1}.dm^3$
D-Fructose	212 ± 6.9 (0.99)	129 ± 2.6 (0.99)
D-Glucose	8.7 ± 1.0 (0.99)	6.7 ± 0.5 (0.99)
D-Galactose	27 ± 1.3 (0.99)	18 ± 0.3 (0.99)
D-Mannose	14 ± 1.4 (0.99)	16 ± 0.8 (0.99)

Sensor **2** has the highest stability constant. However sensor **3** showed the highest fluorescence enhancement. The selectivity order for the different sugars stayed unchanged as D-fructose > D-Galactose > D-Mannose > D-Glucose. Upon saccharide binding with sensors **2** and **3,** the fluorescence is only observed if the fluorophore is excited at 240 and 244 nm respectively. This observation fits the earlier explanation for sensor **1** (Figure 53).

*Comparison between Sensors **1, 2** and **3***

Sensors **1, 2** and **3** showed similar fluorescence behaviour if excited at 244 nm (sensors **1** and **3**) and 240 nm (for sensor **2**). This fluorescence property has been assigned to the detection of the bound species only. However, sensor **1** also showed another fluorescence band as previously mentioned, i.e. a second band at a longer wavelength. The unbound species, containing a B-N bond, gradually disappears on addition of saccharides. This B-N bond has been broken upon formation of the boronate-saccharide complex. In the literature, the dual fluorescence of aniline fluorophores has been associated with Twist Internal Charge Transfer (TICT) state. Dual fluorescence produced two bands in the spectra, one "normal", due to the Locally Excited (LE) state and the other one referred to as the "anomalous" band due to a twist

in the molecule (TICT state). Examples of this phenomenon are described by Lippert *et al.* on aniline derivative moiety, then later by Rettig *et al.*, and Grabowski *et al.*[31]

The first compound to display dual fluorescence was *p-N,N*-dimethylaminobenzonitrile (figure 63 a) (conjugation in the system is present or not). The twist is around the carbon nitrogen bond of the dimethylamino group (Figure 63).

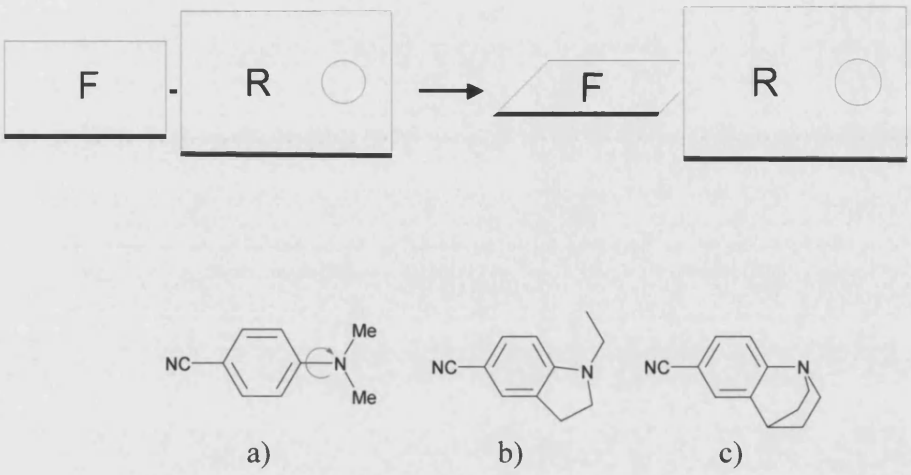

Figure 63: Change in geometrical arrangement of flurophore (F) and receptor (R). Examples of molecules to study TICT state. [31]

Grabowski *et al.*, have reported derivatives of the Lippert compound.[31] The bridged nitrile (figure 63 b), for example did not exhibit the anomalous band (TICT state) but showed the normal, short wavelength band (LE state) in the fluorescence spectra (the lone pair of the nitrogen is in conjugaison with the π system). However, the fully perpendicular benzoquinoline (the lone pair is perpendicular to the π system) (figure 63 c), showed the anomalous band (TICT state) but lacked the normal band (LE state) in the fluorescence spectra. These systems have clearly demonstrated that the possibility for reaching an orthogonal conformation of the dimethylamino group (figure 63 a) is a "*sine qua non*" condition for observing a band due to TICT state.

The different fluorescent properties of the unbound species and bound species of sensor **1** can also be ascribed to Locally Excited and Twisted Internal Charge transfer states of the aniline fluorophore. [31, 107, 108, 109] The bound species shows only, a "normal" short wavelength band at 362 nm due to the Locally Excited (LE) state because the nitrogen lone pair is free to conjugate with the π-system. Whereas the unbound species (which contained a B-N bond) shows the "anomalous" band associated with the TICT state, since the nitrogen lone pair is coordinated with the boron and perpendicular to the π-system. Sensors **2** and **3** (when excited at 240 and 244 nm respectively), display a single band at 350 nm similar to the one observed at 362 nm with sensor **1** (when excited at 244 nm). Also no fluorescence was observed when they are excited 274 nm. Therefore, sensors **2** and **3** only display a LE state.[110]

It has been reported that the "anomalous" band (TICT state) is shifted to longer wavelength (red shifted) by increasing the solvent polarity.[31] The fluorescence of sensor **1** was investigated upon increasing the solvent polarity (from 100% methanol to 100% water), see Table 11. The "anomalous" band shifted from 396 to 430 nm.

Table 11: Investigation of TICT state

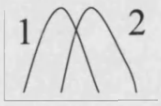

Sovent system	Peak 1	Peak 2
100% H_2O	360 nm	430 nm
90% H_2O - 10% MeOH	360 nm	420 nm
75% H_2O - 25% MeOH	360 nm	412 nm
50% H_2O - 50% MeOH	360 nm	404 nm
100% MeOH	360 nm	396 nm

For sensors **1** (λex 244 nm), **2** (λex 240 nm) and **3** (λex 244 nm) the fluorescence is enhanced by a factor of 15, 18 and 25 fold upon addition of D-fructose respectively. The large fluorescence enhancements can be attributed to the fluorescence recovery of the aniline fluorophore. With these systems in the absence of saccharides, the normal fluorescence of the LE state of the aniline donor is quenched by energy transfer to the phenylboronic acid acceptor. When saccharides are added, a negatively charged boronate anion is formed and under these conditions, energy transfer from aniline donor is unfavourable and fluorescence recovery of LE state of aniline donor is observed.

Quantum yield measurements were performed to confirm this hypothesis. Prior to quantum yield measurements, the Beer-Lambert Law was checked for different concentrations of all sensors for which the quantum yield is reported and no aggregation was observed. The quantum yields Φ were measured in 100% HPLC grade methanol for all the sensors and aniline used as reference. The absorbance and fluorescence were recorded for each sensor at its maximal fluorescence excitation wavelength, see Table 12.

Table 12: Absorbance, quantum yields and excitation wavelength used for sensors **1**, **2** and **3**.

Sensors	λ max	Abs	Φ^a	Φ^b
1	244 nm	0.25404	0.0074	0.0082
2	240 nm	0.27236	0.0085	0.0087
3	244 nm	0.31695	0.0069	0.0070

[a] (weight curves method for determining the area under the curves)
[b] (kaleidagraph for determining the area under the curves)
Aniline Φ = 0.09 (in methanol) [111]

The areas under the fluorescence spectra were calculated either using the weight curves method or KaleidaGraph version 3.51 for PC, publish by Synergy Software and

developed by Abelbeck Software, 2457 Perikiomen Avenue, Reading, PA19606. The quantum yield of sensors **1**, **2** and **3** were then calculated by comparison with aniline as standard using the following equation:[112]

$$\Phi_s = \Phi_{an} \times (FA_s / FA_{an}) \times (A_{an} / A_s)$$

Φ is quantum yield; FA is the area under the curve of the fluorescence peak; A is the absorbance of each sensor at 244 nm (for **1** and **3**) and 240 nm for **2**. *s* and *an* are the abbreviation for sensors (**1**, **2**, **3**) and the aniline reference respectively. Φ =0.09 (in methanol) [111] is used as the reference quantum yield of aniline in methanol.

The quantum yield for sensors **1**, **2** and **3** are presented in Table 12. Both methods gave similar results. The quantum yield of sensors **1**, **2** and **3** are 0.0082, 0.0087 and 0.0070 (in methanol) respectively. For each sensor, the values of the quantum yield are very low compared to the aniline standard reference, which implies that in the absence of saccharide the fluorescence of aniline moiety is quenched. Recovery of the fluorescence signal is observed when saccharides are added, this is shown by the large fluorescence enhancement factor 15, 18 and 25 fold for sensors **1**, **2** and **3** respectively.

In conclusion all three sensors displayed a large fluorescence enhancement on saccharide binding and this can be correlated to a LE state and ascribed to fluorescence recovery of the aniline fluorophore. A long wavelength band is observed for sensor **1** and is correlated with a TICT state of the species containing a B-N bond.

Evaluation of Sensor ***9***

Sensor **9**, is an interesting compound since it contains a methyl and not just a hydrogen on the nitrogen atom. Investigating the fluorescence of this sensor, is important to elucidate if the effect of the methyl on the nitrogen affected the fluorescent properties, and the formation of the B-N bond.

pH-titration of ***9***

The pH-tritration was performed in an osmotic buffer (52.1% methanol aqueous solution with NaCl 0.05 mol.dm^{-3}). The curves are shown in figures 64 and the p*K*a values are for sensors **9** are 10.75 ± 0.02 (0.99) and 8.88 ± 0.11 (0.92) in the absence and in the presence of D-fructose respectively.

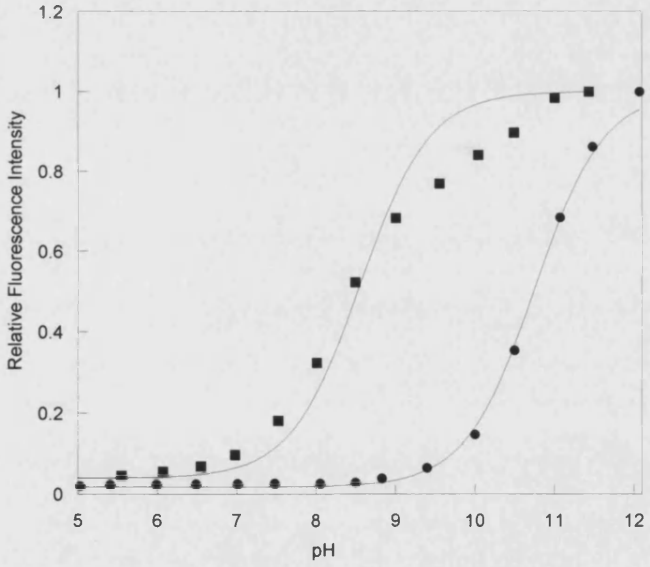

Figure 64: Relative fluorescence intensity *versus* pH profile of **9** at 25°C; [**9**] = 1.0 × 10^{-5} mol.dm^{-3}, 52.1wt% methanolic aqueous solution in the presence of [NaCl] = 0.05 mol.dm^{-3}, (●) in the absence of D-fructose, (■) in the presence of D-fructose (0.05 mol.dm^{-3}). λ_{ex} 252 nm, λ_{em} 360 nm.

Saccharide binding at 252 nm of **9**

The fluorescence spectra of sensor **9** showed two bands (anomalous and normal band) at the beginning of the fluorescence experiment, but on addition of saccharide, only one maximum is detected at 357 nm. Nevertheless, sensor **9** did not emit any fluorescence if a longer wavelength excitation is used, similar to sensors **2** and **3**.

The fluorescence titrations of **9** (2.2×10^{-5} mol.dm^{-3}) were performed in pH 8.21 phosphate buffer at 252 nm excitation wavelength, with 4 different monosaccharides (D-fructose, D-glucose, D-galactose and D-mannose). The maximum fluorescence was observed at 357 nm. The fluorescence enhancement on addition of D-fructose is fifteen fold. This is equivalent to the enhancement factor of sensor **1**. The stability constants (*K*) of fluorescence sensor **9** (Table 13) were calculated by fitting the emission at their maximum, λ_{em} 357 nm *versus* concentration of saccharide (Figure 65).

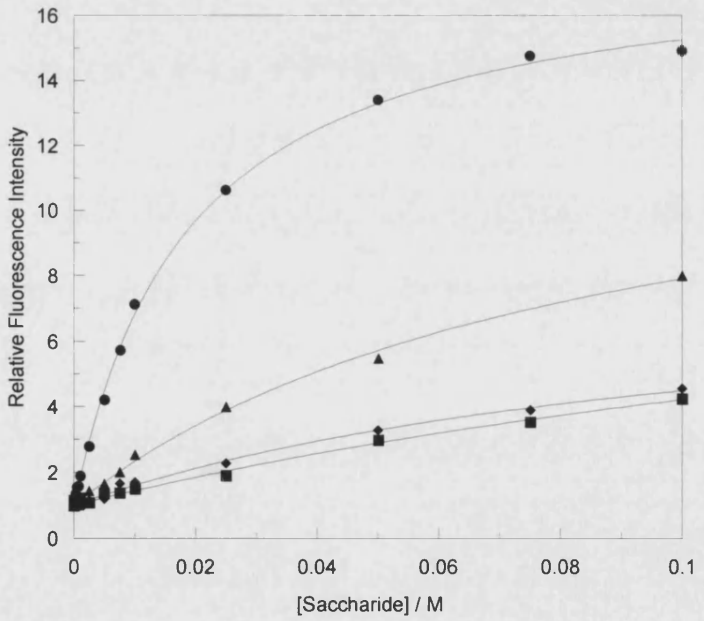

Figure 65: Relative fluorescence intensity *versus* saccharide concentration profile of **9** with (●) D-fructose, (■) D-glucose, (♦) D-galactose, (▲) D-mannose, pH 8.21 buffer, λ_{ex} 252 nm, λ_{em} for each spectrum 357 nm.

Table 13: Stability constant K (coefficient of determination; r^2) for saccharide complexes of fluorescence sensor **9** at λ_{ex} 252 nm.

	D-Fructose	D-Glucose	D-Galactose	D-Mannose
K $mol^{-1}.dm^3$	52 ± 2.2 (0.99)	4.4 ± 1.4 (0.99)	12 ± 1.2 (0.99)	9.0 ± 1.5 (0.99)

The selectivity order for the different sugars are D-fructose > D-Galactose > D-Mannose > D-Glucose. This is in accordance with the literature.[5, 6, 21, 23]

The quantum yields for sensor **9** were measured and are given in Table 14.

Table 14: Absorbance, quantum yields and excitation wavelength used for sensors **9.**

Sensors	λ max	Abs	Φ^a	Φ^b
9	252 nm	0.25028	0.0038	0.0045

[a] (weight curves method for determining the area under the curves)
[b] (kaleidagraph for determining the area under the curves)

The quantum yield of sensor **9** is lower than sensor **1, 2** and **3.**

*Evaluation of Sensors **5, 6, 7** and **8***

The evaluation of a small group of sensors containing electron withdrawing and donating groups allows us to explore further the fluorescent properties of the system. The effect of an electron-withdrawing group is presented first, followed by the effect of an electron-donating group.

Sensors **5** and **8** are both examples of electron-withdrawing groups. Sensor **8,** which contained a cyano-aniline, was investigated. With sensor **8,** no changes in fluorescence were observed on addition of saccharides. Therefore no further investigations were

carried out on sensor **8**. However, sensor **5**, which contained a chloro-aniline, was investigated. The fluorescence of sensor **5** is quenched on addition of saccharides.

pH-titration of ***5***

The pH-tritration was performed in an osmotic buffer (52.1% methanol aqueous solution with NaCl 0.05 mol.dm^{-3}). p*K*a values are for sensors **5** are 10.47 ± 0.05 (0.99) and 7.82 ± 0.04 (0.99) in the absence and presence of D-fructose respectively.

Saccharide binding at 279 nm of ***5***

The fluorescence titrations of **5** (2.0×10^{-5} mol.dm^{-3}) were performed in pH 8.21 phosphate buffer at 279 nm excitation wavelength, with 4 different monosaccharides (D-fructose, D-glucose, D-galactose and D-mannose). The maximum fluorescence intensity was observed at 400 nm. The fluorescence is quenched on addition of D-fructose (6.7 fold). The bound species is non-fluorescent, so the quenched fluorescence observed is due to the decrease of the unbound species present in the media upon addition of saccharides. The stability constants (*K*) of fluorescence sensor **5** were calculated by fitting the emission at their maximum, λ_{em} 400 nm *versus* concentration of saccharide. The curves are shown in Figure 66 and the calculated values are given in Table 15.

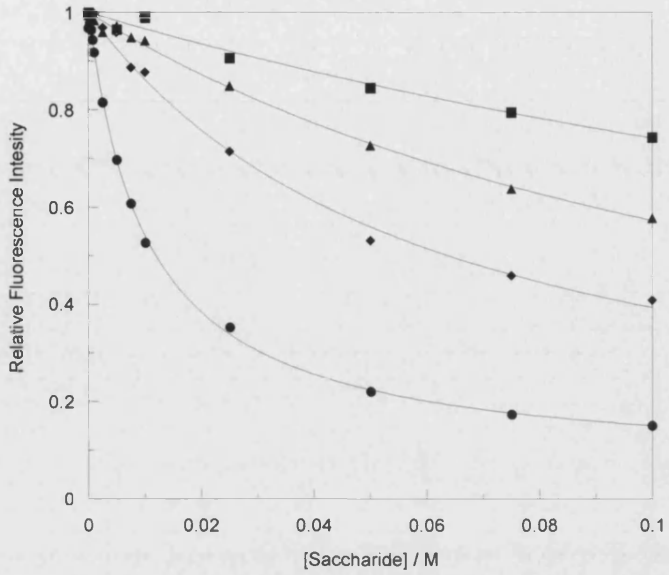

Figure 66: Relative fluorescence intensity *versus* saccharide concentration profile of **5** with (●) D-fructose, (■) D-glucose, (♦) D-galactose, (▲) D-mannose, pH 8.21 buffer, λ_{ex} 279 nm, λ_{em} 400 nm.

Table 15: Stability constant *K* (coefficient of determination; r^2) for saccharide complexes of fluorescence sensor **5** at λ_{ex} 279 nm.

	D-Fructose	D-Glucose	D-Galactose	D-Mannose
K mol^{-1}.dm^3	96 ± 3.8 (0.99)	3.3 ± 3.0 (0.97)	16 ± 2.6 (0.99)	7.0 ± 1.4 (0.99)

The observed order of stability constant (*K*) with D-fructose > D-galactose > D-Mannose > D-glucose, is the expected order for all monoboronic acids.[5, 6, 21, 23]

Sensors **6** and **7** both have electron-donating group, a methoxy group on the aniline ring in sensor **6**, or on the phenylboronic acid ring in sensor **7**. Both sensors display an enhancement of fluorescence upon addition of saccharides.

pH-titration of **6** *and* **7**

The pH-tritration was performed in an osmotic buffer (52.1% methanol aqueous solution with NaCl 0.05 mol.dm^{-3}) in the absence and in the presence of 50 mM of D-fructose. For both compounds, the usual fitting curve, using Kaleidagraph failed, so another program, Scientist, has been used to fit the pK_a values. However this program

cannot be used in the presence of D-fructose, due to large number of species involved. The two pK_a values in the absence of D-fructose for sensors **6** and **7** are 10.85 ± 0.06 (0.90), 4.99 ± 0.42 (0.90) and 10.95 ± 0.03 (0.90), 4.14 ± 0.31 (0.90) respectively.

*Saccharide binding at 240, 286 (**6**) 274 nm (**7**)*

The fluorescence titrations of **6** and **7** were performed in pH 8.21 phosphate buffer at 240 and 286 nm for sensor **6** and 274 nm excitation wavelength for sensor **7**, with 4 different monosaccharides (D-fructose, D-glucose, D-galactose and D-mannose). The concentration used was 4.0×10^{-5} and 2.0×10^{-5} mol.dm^{-3} for sensors **6** and **7** respectively.

The spectra of sensor **6**, when excited at 240 nm does not show any isostilbic point, and shows only the enhancement of fluorescence (4.7 fold) of the bound species upon addition of saccharide, due to LE state. However when sensor **6** is excited at 286 nm, the spectra displays two bands so two species are present, the unbound one and the bound one. The unbound species disappears upon addition of saccharides, the spectra shifted from 430 nm to 378 nm. An isostilbic point is observed at 409 nm upon addition of D-fructose. So sensor **6** behaves similar to sensor **1** with both TICT state and LE state depending excitation wavelength and condition used.

The spectrum of sensor **7**, shows a band where the maximum is shifted from 380 nm to 358 nm when excited at 274 nm. A decrease in fluorescence at 420 nm is observed. An isostibic point is observed at 394 nm for the spectra with addition of D-fructose.

The stability constants (K) of fluorescence sensor **6** and **7** were calculated by fitting the intensity at their emission maximum *versus* concentration of saccharide. The curves are shown in Figure 67, 68, 69 and the calculated values are given in Table 16.

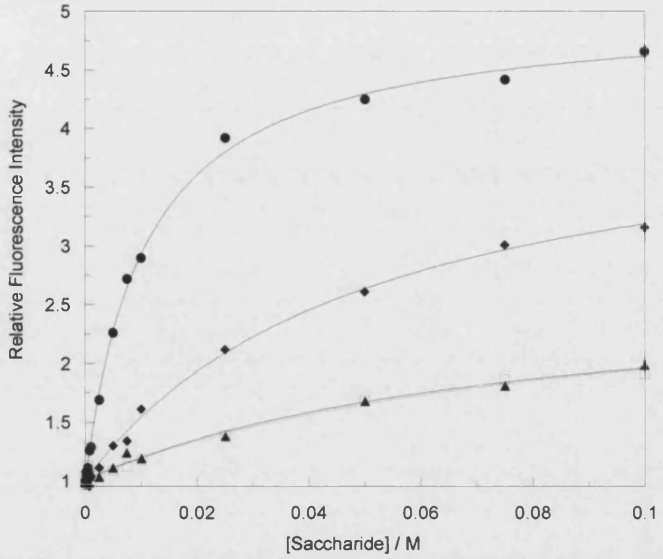

Figure 67: Relative fluorescence intensity *versus* saccharide concentration profile of **6** with (●) D-fructose, (□) D-glucose, (♦) D-galactose, (▲) D-mannose, pH 8.21 buffer, λ_{ex} 240 nm, λ_{em} for each spectrum 370 nm.

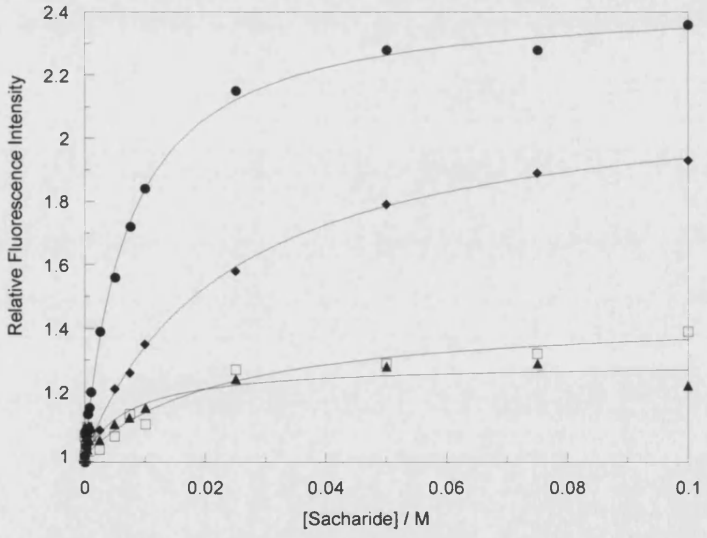

Figure 68: Relative fluorescence intensity *versus* saccharide concentration profile of **6** with (●) D-fructose, (□) D-glucose, (♦) D-galactose, (▲) D-mannose, pH 8.21 buffer, λ_{ex} 286 nm, λ_{em} for each spectrum at their maximum 375-378 nm.

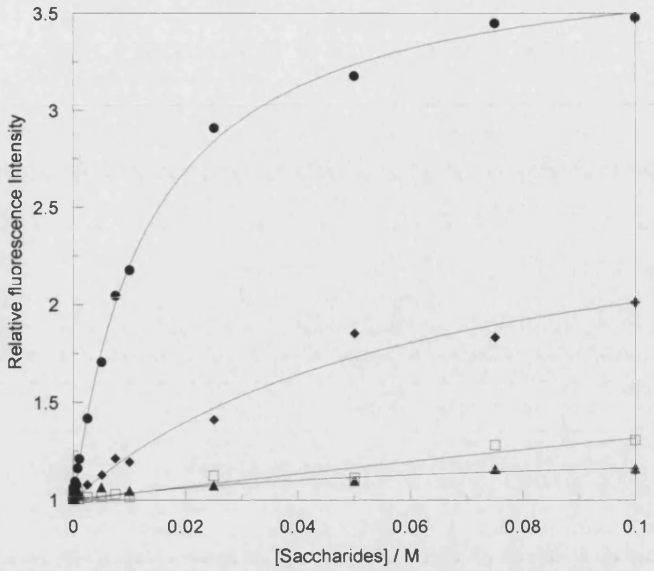

Figure 69: Relative fluorescence intensity *versus* saccharide concentration profile of **7** with (●) D-fructose, (□) D-glucose, (♦) D-galactose, (▲) D-mannose, pH 8.21 buffer, λ_{ex} 274 nm, λ_{em} for each spectrum at their maximum 358-368 nm.

Table 16: Stability constant *K* (coefficient of determination; r^2) for saccharide complexes of fluorescence sensors **6** and **7**.

Saccharides	**6** (ex 240 nm) *K* $mol^{-1}.dm^3$	**6** (ex 286 nm) *K* $mol^{-1}.dm^3$	**7** (ex 274 nm) *K* $mol^{-1}.dm^3$
D-Fructose	93 ± 4.4 (0.99)	138 ± 6.8 (0.99)	73 ± 3.4 (0.99)
D-Glucose	12 ± 3.0 (0.98)	——— *	——— *
D-Galactose	20 ± 2.2 (0.99)	42 ± 5.4 (0.99)	16 ± 4.5 (0.98)
D-Mannose	13 ± 4.0 (0.97)	——— *	——— *

* small fluorescence changes

The observed order of stability constant (*K*) with D-fructose > D-galactose > D-Mannose > D-glucose, is the expected order for all monoboronic acids.[5, 6, 21, 23]

The quantum yields for sensors **5, 6** and **7** were measured and are given in Table 17.

Table 17: Absorbance, quantum yields and excitation wavelength used for sensors **5, 6** and **7.**

Sensors	λ max	Abs	Φ^a	Φ^b
5	279 nm	0.05767	0.1905	0.1921
6	240 nm	0.19543	0.0139	0.0149
7	274 nm	0.08939	0.0297	0.0330

[a] (weight curves method for determining the area under the curves)
[b] (kaleidagraph for determining the area under the curves)

*Comparison between Sensors **1, 5, 6** and **7***

A summary of the stability constants (*K*) values are presented in Table 18.

Table 18: Stability constant *K* (coefficient of determination; r^2) for saccharide complexes of fluorescence sensors **1, 5, 6** and **7.**

Saccharides	**1** (ex 244 nm) *K* $mol^{-1}.dm^3$	**5** (ex 279 nm) *K* $mol^{-1}.dm^3$	**6** (ex 240 nm) *K* $mol^{-1}.dm^3$	**7** (ex 274 nm) *K* $mol^{-1}.dm^3$
D-Fructose	79 ± 1.7 (0.99)	96 ± 3.8 (0.99)	93 ± 4.4 (0.99)	73 ± 3.4 (0.99)
D-Glucose	6.4 ± 0.4 (0.99)	3.3 ± 3.0 (0.97)	12 ± 3.0 (0.98)	——— *
D-Galactose	14 ± 0.6 (0.99)	16 ± 2.6 (0.99)	20 ± 2.2 (0.99)	16 ± 4.5 (0.98)
D-Mannose	7.8 ± 0.3 (0.99)	7.0 ± 1.4 (0.99)	13 ± 4.0 (0.97)	——— *

* small fluorescence changes

Similar results were found for sensor **1** and the sensors **5, 6** and **7**. Generally, sensor **1** has a better stability constant for all the 4 saccharides.

Sensor **5** is the only sensor where the fluorescence is quenched. The decrease of fluorescence observed is due to the decrease of the unbound species (TICT state), as the bound species (LE state) in this case is non-fluorescent.

The two electron-donating group sensors **6** and **7** do not give better results than sensor **1.**

*Evaluation of Sensors **10, 11** and **12***

To further explore the system, the aniline was replace by a benzyl (sensor **12**), a naphthalene (sensor **10**) and a pyrene ring (sensor **11**).

All the three sensors were successfully prepared, however, sensor **12** does not fluoresce, therefore, only sensors **10** and **11** were investigated and are presented in this section.

Both sensors **10** and **11** display stronger fluorescence than sensor **1**.

The fluorescence titration of **10** and **11** were performed in pH 8.21 buffer at 324 nm and 383 nm excitation wavelength respectively, with 4 different monosaccharides, (D-fructose, D-glucose, D-galactose and D-mannose) and sensors concentration (2.0×10^{-6} and 2.5×10^{-7} $mol.dm^{-3}$ for sensors **10** and **11** respectively). The spectra of sensor **10** shifted from 428 nm to 443 nm (15 nm) and increased upon addition of D-fructose. An isostilbic point is observed at 417 nm. The spectra of sensor **11** decreased and shifted from 441 nm to 454 nm (13 nm) upon addition of D-fructose. An isostilbic point is observed at 449 nm. The fluorescence enhancements for four sugars are shown in figure 70 and 71 for sensors **10** and **11** respectively. The stability constants are calculated from the previous curves and given in Table 19.

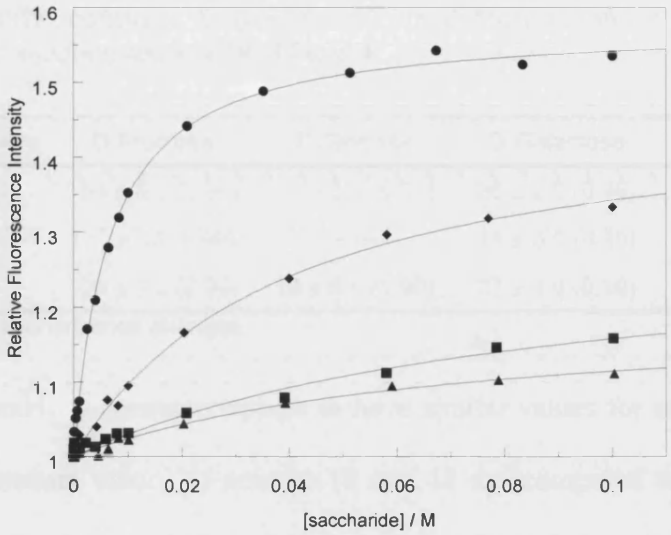

Figure 70: Relative fluorescence intensity *versus* saccharide concentration profile of **10** with (●) D-fructose, (■) D-glucose, (♦) D-galactose, (▲) D-mannose, pH 8.21 buffer, λ_{ex} 324 nm, λ_{em} 443 nm.

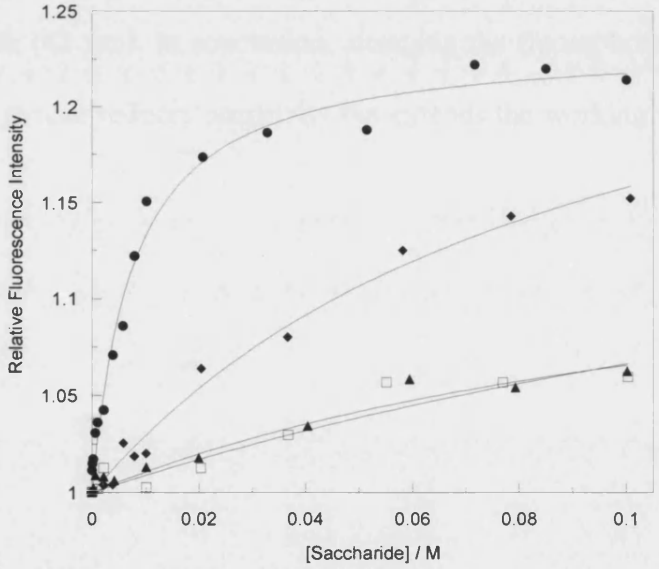

Figure 71: Relative fluorescence intensity *versus* saccharide concentration profile of **11** with (●) D-fructose, (□) D-glucose, (♦) D-galactose, (▲) D-mannose, pH 8.21 buffer, λ_{ex} 383 nm, λ_{em} 460 nm.

Table 19: Stability constant K (coefficient of determination; r^2) for saccharide complexes of fluorescence sensors **10**, **11** and **1**.

	Sensors	D-Fructose	D-Glucose	D-Galactose	D-Mannose
K mol^{-1}.dm^3	**10**	154 ± 8.0 (0.99)	11 ± 3.0 (0.97)	26 ± 2.0 (0.99)	14 ± 3.0 (0.98)
K mol^{-1}.dm^3	**11**	132 ± 15 (0.99)	—— *	11 ± 3.0 (0.99)	8.0 ± 5.0 (0.97)
K mol^{-1}.dm^3	**1**	106 ± 7.0 (0.99)	18 ± 6.0 (0.98)	27 ± 4.0 (0.99)	—— *

* small fluorescence changes

From Table 19, stability constants appear to have similar values for sensors **10** and **11**. If the stability constant values of sensors **10** and **11** are compared to sensor **1** (when excited at 274 nm), the values are in the same order and are close to each other. However, the spectra of sensor **1** shifted from 404 nm to 362 nm (42 nm) and increased upon addition of D-fructose. An isostilbic point is found at 377 nm. Sensors **10** and **11** produce a smaller shift but a higher emission wavelength, due to the two higher wavelength fluorophores used (naphthalene and pyrene). Sensor **1** produces the largest shift in wavelength (42 nm). In conclusion, changing the fluorophore from benzene to naphathalene and pyrene reduces sensitivity but extends the working wavelength of the sensors.

2.3.2 Diboronic Acid Series

Diboronic acid sensors series were designed to provide a more efficient molecular receptor for monosaccharides and especially D-glucose by virtue of having two receptor units (boronic acid units). A total of six diboronic acid sensors were successfully prepared and there can be divided in two series: *meta CH_2-bridged* (sensors **13**, **15**, and **17**) and *para CH_2-bridged series* (sensors **14**, **16**, and **18**). Sensors **13** and **14** are the diboronic acid analogues of sensor **1**. Likewise, sensors **15** and **16**, and sensors **17** and **18** are the diboronic acid analogues of sensors **2** and **3** respectively.

*Evaluation of Sensors **13** and **14***

Sensor **13** and **14** were fully investigated using fluorescence spectroscopy. For all the different experiments presented below, the conditions used have been chosen as follows: methanolic aqueous osmotic buffer (52.1% methanol aqueous solution with NaCl 0.05 mol.dm^{-3}) for the pH-titration and pH 8.21 buffer for the saccharide binding studies (52.1wt% methanol in water with KCl, 0.01000 mol.dm^{-3}; KH_2PO_4, 0.002752 mol.dm^{-3}; Na_2HPO_4, 0.002757 mol.dm^{-3}),[101] 4 different monosaccharides (D-fructose, D-glucose, D-galactose and D-mannose) and the sensor concentrations are (4.2×10^{-5} mol.dm^{-3}) and (4.1×10^{-5} mol.dm^{-3}) for sensors **13** and **14** respectively.

pH-titration of ***13***

The pH-titration was performed in an osmotic buffer (52.1% methanol aqueous solution with NaCl 0.05 mol.dm^{-3}). The excitation wavelength chosen was the longer one, 285 nm.

The pH-titration in the absence and presence of D-fructose (0.05 mol.dm^{-3}) were carried out and the curves are shown in Figure 72.

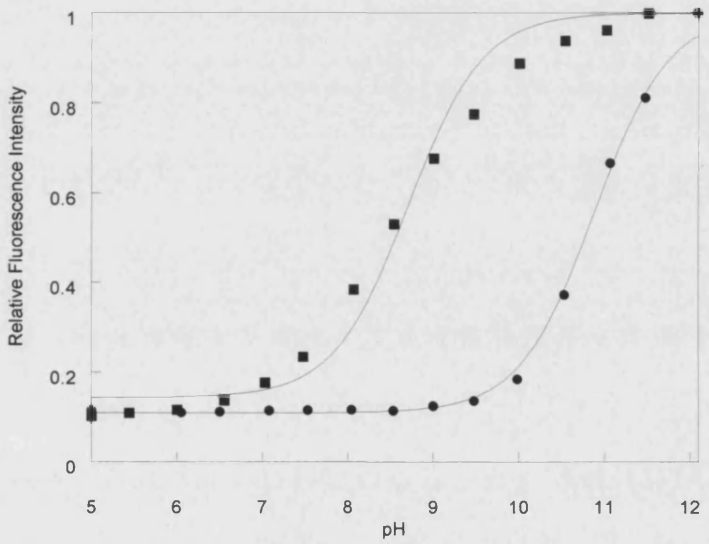

Figure 72: Fluorescence intensity *versus* pH profile of **13** at 25°C; [**13**] = 4.2 x 10^{-5} mol.dm^{-3}, 52.1wt% methanolic aqueous solution in the presence of [NaCl] = 0.05 mol.dm^{-3}, (●) in the absence of D-fructose, (■) in the presence of D-fructose (0.05 mol.dm^{-3}), in osmotic buffer, λ_{ex} 285 nm, λ_{em} 360 nm.

The pK_a of sensor **13** was 10.88 ± 0.02 (0.99) and 8.71 ± 0.08 (0.98) in the absence and in the presence of D-fructose respectively.

The presence of an isostilbic point in the excitation spectra of sensor **1**, lead us to investigate the excitation spectra of sensor **13**. The excitation wavelengths were recorded during a D-fructose titration and 3 different excitation wavelengths were

found: 244 nm, 265 nm (isostilbic point) and 280 nm. The saccharide binding studies were performed at all 3 excitation wavelengths.

*Saccharide binding study of **13***

The saccharide binding studies were performed at 3 different wavelengths as follows 285 nm (longer wavelength), 265 nm (isostilbic point) and 244 nm (shorter wavelength) in pH 8.21 buffer (52.1wt% methanol in water with KCl, 0.01000 mol.dm^{-3}; KH_2PO_4, 0.002752 mol.dm^{-3}; Na_2HPO_4, 0.002757 mol.dm^{-3}).[101]

The binding studies were started with the longer excitation wavelength at 285 nm. The fluorescence spectra changes of sensor **13** in different concentration of D-fructose (0-0.1 mol.dm^{-3}) are presented in Figure 73.

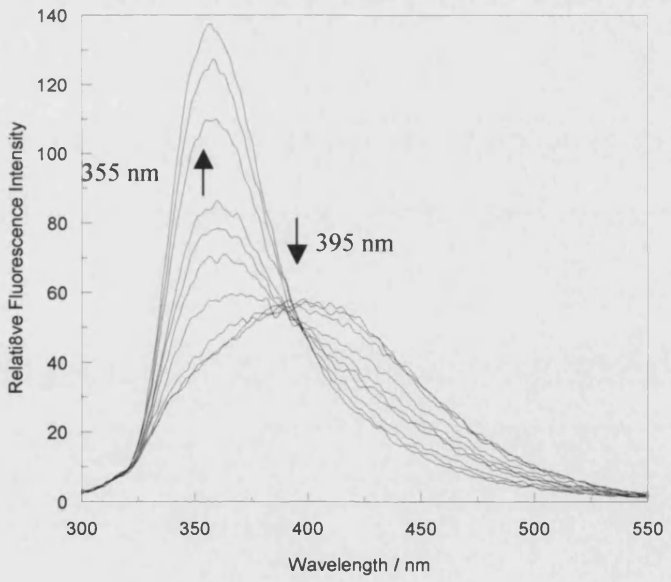

Figure 73: Fluorescence spectra change of **13** (4.2×10^{-5} mol.dm^{-3}) at 25°C with different concentration of D-fructose (0-0.1 mol.dm^{-3}) in pH 8.21 buffer, λ_{ex} 285 nm.

The fluorescence intensity of **13** shifted from 395 nm to 355 nm and increased with the increasing of saccharide concentration, an isosbestic point was observed at 390 mn. This isostilbic point indicates that sensor **13** changes from unbound to bound species. The stability constants (*K*) were calculated from the curves shown in Figure 74 and the calculated values are presented in Table 20.

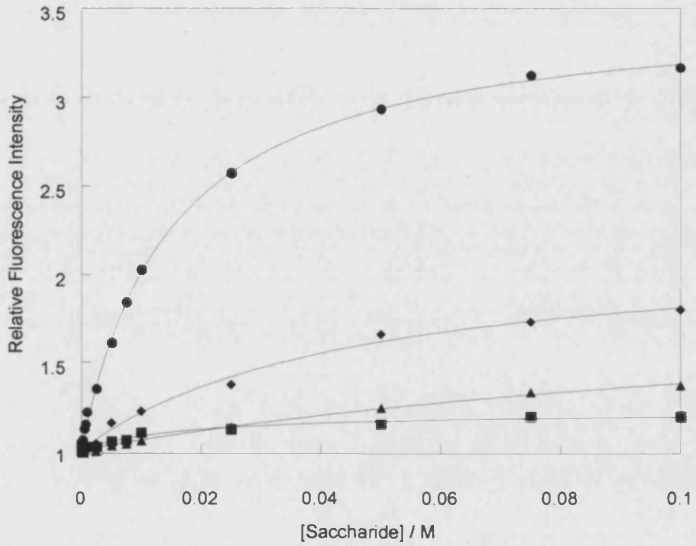

Figure 74: Relative fluorescence intensity *versus* saccharide concentration profile of **13** (4.2×10^{-5} mol.dm^{-3}) with (●) D-fructose, (■) D-glucose, (♦) D-galactose, (▲) D-mannose, in pH 8.21 buffer, λ_{ex} 285 nm, λ_{em} 360 nm.

Table 20: Stability constant *K* (coefficient of determination; r^2) for saccharide complexes of fluorescence sensor **13** at λ_{ex} 285 nm.

	D-Fructose	D-Glucose	D-Galactose	D-Mannose
K mol^{-1}.dm^3	67 ± 2.0 (0.99)	58 ± 13 (0.96)	22 ± 3.0 (0.99)	6.0 ± 2.0 (0.98)

The observed order of stability constants (*K*) was D-fructose > D-glucose > D-galactose > D-mannose. Although this sensor is D-fructose selective, the selectivity for D-glucose has been enhanced compared to sensor **1**.

Saccharide binding experiments were repeated at 265 nm[113] and at 244 nm in the same conditions (pH 8.21 buffer, sensor concentration, 4 different saccharides) as previously mentioned.

The fluorescence spectra of sensor **13** with different concentration of D-fructose (0-0.1 $mol.dm^{-3}$), obtained by excitation at 265 nm, are shown in Figure 75.

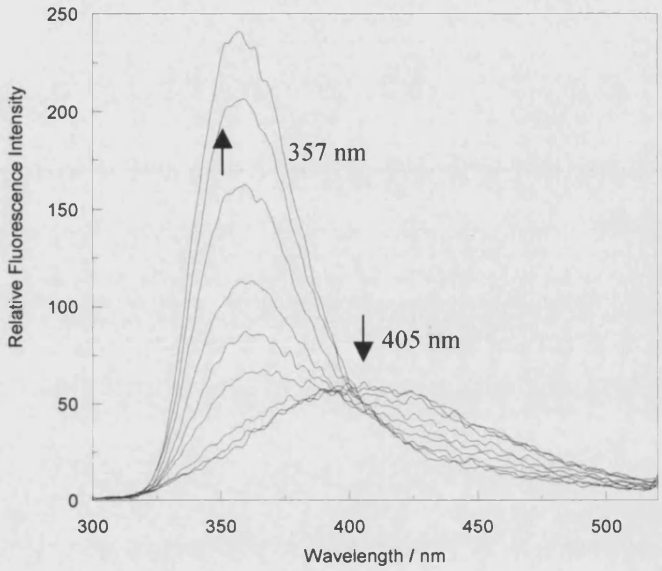

Figure 75: Fluorescence spectra change of **13** (4.2×10^{-5} $mol.dm^{-3}$) at 25°C with different concentration of D-fructose (0-0.1 $mol.dm^{-3}$) in pH 8.21 buffer, λ_{ex} 265 nm.

The fluorescence intensity shifted from 405 nm to 357 nm and increased when the saccharide concentration was increased. An isosbestic point was also observed at 394 nm. As already noticed with sensor **1**, the enhancement of the fluorescence intensity was more important than the one observed at 285 nm.

The stability constants were calculated from the curves shown in Figure 76 and the values are presented in Table 21.

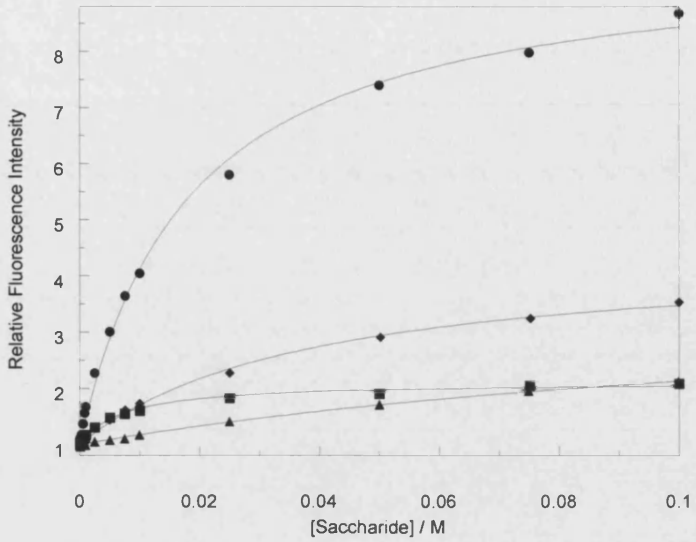

Figure 76: Relative fluorescence intensity *versus* saccharide concentration profile of **13** (4.2×10^{-5} mol.dm^{-3}) with (●) D-fructose, (■) D-glucose, (♦) D-galactose, (▲) D-mannose, in pH 8.21 buffer, λ_{ex} 265 nm, λ_{em} 360 nm.

Table 21: Stability constant K (coefficient of determination; r^2) for saccharide complexes of fluorescence sensor **13** at λ_{ex} 265 nm.

	D-Fructose	D-Glucose	D-Galactose	D-Mannose
K mol^{-1}.dm^3	55 ± 3.7 (0.99)	140 ± 13 (0.99)	26 ± 1.8 (0.99)	6.8 ± 0.9 (0.99)

The order of stability constants (K) was D-glucose > D-fructose >D-galactose > D-mannose, sensor **13** clearly shows a high selectivity for D-glucose.

The study was completed by using an excitation wavelength of 244 nm.

The fluorescence spectra of sensor **13** with different concentration of D-fructose (0-0.1 mol.dm^{-3}) are shown in Figure 77.

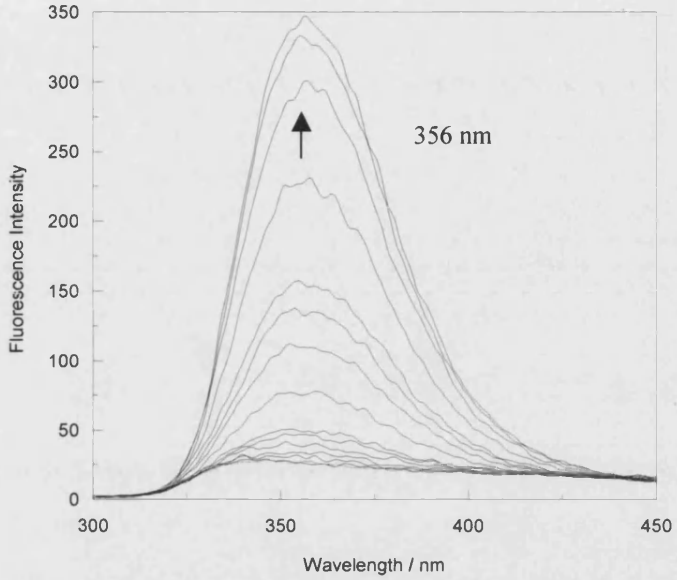

Figure 77: Fluorescence spectra change of **13** (4.2×10^{-5} mol.dm^{-3}) with different concentration of D-fructose (0-0.1 mol.dm^{-3}) in pH 8.21 buffer, λ_{ex} 244 nm.

The fluorescence intensity maximum was observed at 356 nm. A large fluorescence intensity enhancement of thirteen fold was observed.

Neither fluorescence intensity shift nor isostilbic point were observed at this excitation wavelength. At this wavelength, only the bound species was observed.

The stability constants (*K*) of fluorescence sensor **13** were calculated by fitting the intensity at 355 nm *versus* concentration of saccharide. The curves are shown in Figure 78 and the calculated values are given in Table 22.

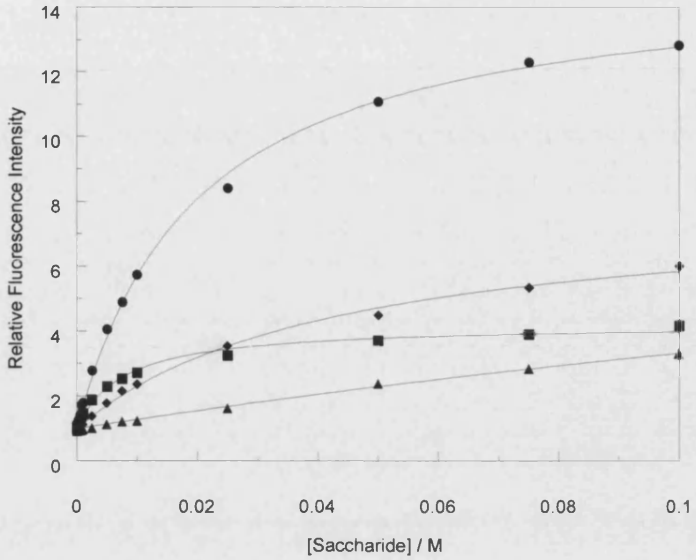

Figure 78: Relative fluorescence intensity *versus* saccharide concentration profile of **13** (4.2×10^{-5} mol.dm^{-3}) with (●) D-fructose, (■) D-glucose, (♦) D-galactose, (▲) D-mannose, in pH 8.21 buffer, λ_{ex} 244 nm, λ_{em} 355 nm.

Table 22: Stability constant K (coefficient of determination; r^2) for saccharide complexes of fluorescence sensor **13** at λ_{ex} 244 nm.

	D-Fructose	D-Glucose	D-Galactose	D-Mannose
K mol^{-1}.dm^3	50 ± 2.3 (0.99)	129 ± 11 (0.99)	23 ± 1.9 (0.99)	2.5 ± 1.0 (0.99)

The observed order of the stability constants (K) was identical with the one found at 265 nm, so D-glucose > D-fructose > D-galactose > D-mannose and sensor **13** clearly shows a high selectivity for D-glucose.

Summary

A summary of the stability constants (K) values are presented in Table 23.

Table 23: Stability constant K (coefficient of determination; r^2) for saccharides complexes of fluorescence sensor **13** at different excitation wavelengths.

Saccharides	K values for different excitation wavelengths		
	244 nm	265 nm	285 nm
D-Glucose	129 ± 11 (0.99)	140 ± 13 (0.99)	58 ± 13 (0.96)
D-Fructose	50 ± 2.3 (0.99)	55 ± 3.7 (0.99)	67 ± 2.0 (0.99)
D-Galactose	23 ± 1.9 (0.99)	26 ± 1.8 (0.99)	22 ± 3.0 (0.99)
D-Mannose	2.5 ± 1.0 (0.99)	6.8 ± 0.9 (0.99)	6.4 ± 2.0 (0.98)

Similar results were found at 265 nm and 244 nm, however the one obtained at 244 nm is probably closer to the true value because only the bound species was observed. All of the discussion for sensor **1** are also valid for sensor **13**. Sensor **13** displays both TICT and LE states like sensor **1**.

pH-titration of ***14***

The pH-titration was performed in an osmotic buffer (52.1% methanol aqueous solution with NaCl 0.05 mol.dm^{-3}). The excitation wavelength chosen was the longer one, 285 nm.

The pH-titration in the absence and presence of D-fructose (0.05 mol.dm^{-3}) were carried out and the curves are shown in Figure 79.

The pK_a of sensor **14** was 10.95 ± 0.05 (0.99) and 8.60 ± 0.05 (0.99) in the absence and in the presence of D-fructose respectively.

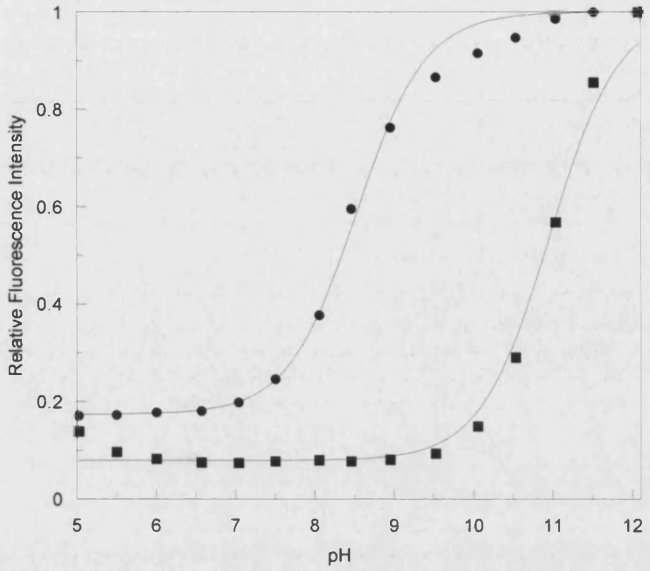

Figure 79: Fluorescence intensity *versus* pH profile of **14** at 25°C; [**14**] = 4.1 x 10^{-5} mol.dm^{-3}, 52.1wt% methanolic aqueous solution in the presence of [NaCl] = 0.05 mol.dm^{-3}, (■) in the absence of D-fructose, (●) in the presence of D-fructose (0.05 mol.dm^{-3}), in osmotic buffer, λ_{ex} 285 nm, λ_{em} 365 nm.

After investigation of the excitation spectra of sensor **14**, two excitation wavelengths were found: 244 nm and 285 nm. The saccharide binding study has been achieved at both excitation wavelengths.

*Saccharide binding study of **14***

The saccharide binding study were performed at the two different wavelengths as follows 285 nm (longer wavelength) and 244 nm (shorter wavelength) in pH 8.21 buffer (52.1wt% methanol in water with KCl, 0.01000 mol.dm^{-3}; KH_2PO_4, 0.002752 mol.dm^{-3}; Na_2HPO_4, 0.002757 mol.dm^{-3}).[101]

The binding studies were started firstly with the longer excitation wavelength at 285 nm then with the shorter excitation wavelength 244 nm. The stability constants (*K*) were

calculated from the curves shown in Figure 80 and 81 and the calculated values were reported in Table 24 and 25 respectively for the excitation at 285 nm and 244nm.

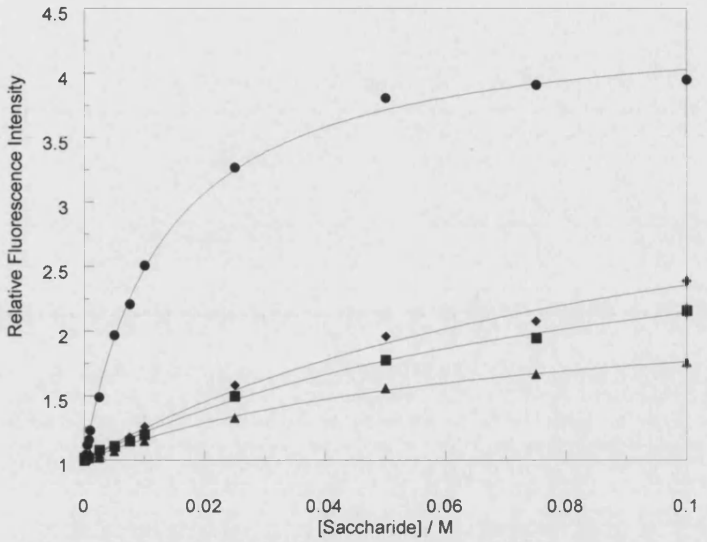

Figure 80: Relative fluorescence intensity *versus* saccharide concentration profile of **14** (4.1×10^{-5} mol.dm^{-3}) with (●) D-fructose, (■) D-glucose, (♦) D-galactose, (▲) D-mannose, in pH 8.21 buffer, λ_{ex} 285 nm, λ_{em} 360 nm.

Table 24: Stability constant *K* (coefficient of determination; r^2) for saccharide complexes of fluorescence sensor **14** at λ_{ex} 285 nm.

	D-Fructose	D-Glucose	D-Galactose	D-Mannose
K mol^{-1}.dm^3 at 285 nm	74 ± 9.0 (0.99)	11 ± 1.4 (0.99)	10 ± 2.7 (0.99)	14 ± 1.9 (0.99)

The spectra of sensor **14** when excited at 285 nm has no isostilbic point but a shift is observed from 410 nm to 368 nm.

The observed order of stability constants (*K*) was D-fructose > D-mannose > D-glucose > D-galactose. Sensor **14** is D-fructose selective.

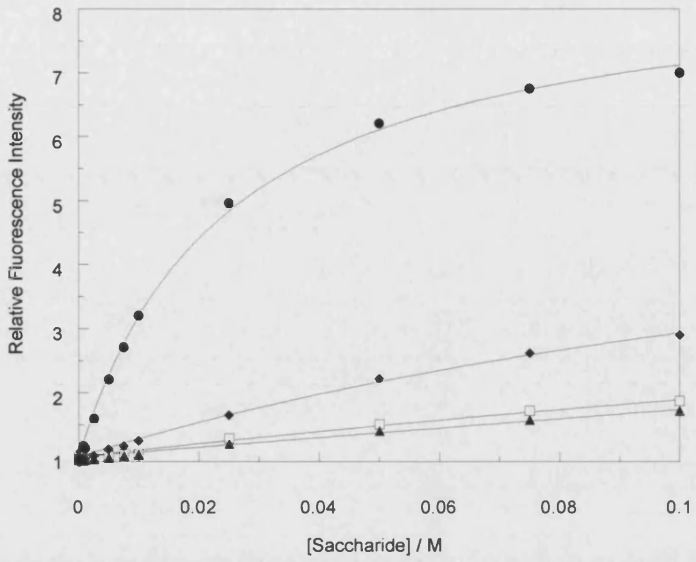

Figure 81: Relative fluorescence intensity *versus* saccharide concentration profile of **14** (4.1×10^{-5} mol.dm^{-3}) with (●) D-fructose, (□) D-glucose, (♦) D-galactose, (▲) D-mannose, in pH 8.21 buffer, λ_{ex} 244 nm, λ_{em} 364 nm.

Table 25: Stability constant *K* (coefficient of determination; r^2) for saccharide complexes of fluorescence sensor **14** at λ_{ex} 244 nm.

	D-Fructose	D-Glucose	D-Galactose	D-Mannose
K mol^{-1}.dm^3	40 ± 2.0 (0.99)	2.1 ± 2.0 (0.98)	5.4 ± 1.2 (0.99)	0.4 ± 2.0 (0.97)

The spectra of sensor **14** when excited at 244 nm have no isostilbic point and no wavelength shift was observed; the maximum of emission is 364 nm.

The observed order of stability constants (*K*) was D-fructose > D-galactose > D-glucose. Sensor **14** is D-fructose selective.

*Evaluation of Sensors **15** and **16***

Sensors **15** and **16** were fully investigated using fluorescence spectroscopy. For all the different experiments presented below, the conditions used are pH 8.21 phosphate buffer[101] for the saccharide binding studies, 4 different monosaccharides (D-fructose, D-glucose, D-galactose and D-mannose) and the sensors concentrations are (4.1×10^{-5} mol.dm^{-3}) for sensors **15** and **16** respectively.

For sensor **15,** only one excitation wavelength was obtained at 244 nm. The fluorescence measurements were carried out at this excitation wavelength. For sensor **16,** two excitation wavelengths were observed: 244 nm and 276 nm. Saccharide binding studies were perfomed at both excitation wavelengths.

The titration of sensors **15** and **16** with 4 saccharides are shown in the graphs (Figure 82-84).

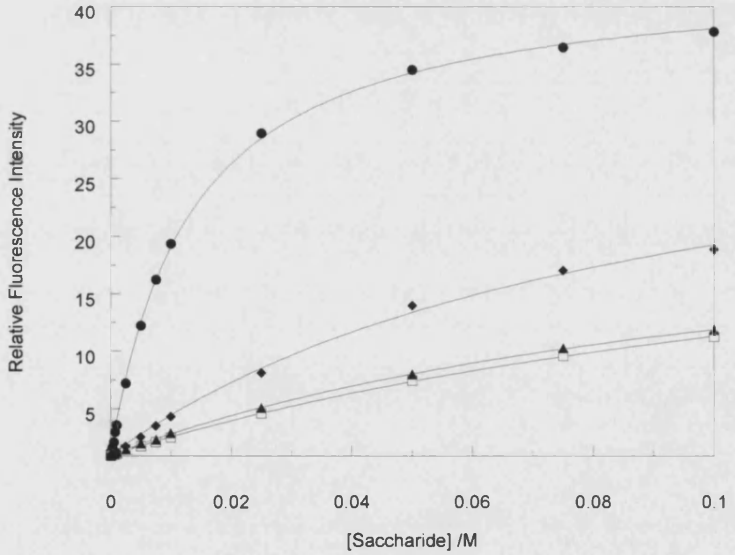

Figure 82: Relative fluorescence intensity *versus* saccharide concentration profile of **15** (4.1×10^{-5} mol.dm^{-3}) with (●) D-fructose, (□) D-glucose, (♦) D-galactose, (▲) D-mannose, in pH 8.21 buffer, λ_{ex} 244 nm, λ_{em} 350 nm.

The spectra of sensor **15** when excited at 244 nm produce no isostilbic point and no wavelength shift was observed; the maximum of emission is 350 nm. The enhancement factor for sensor **15** in the presence of D-fructose is 38 fold.

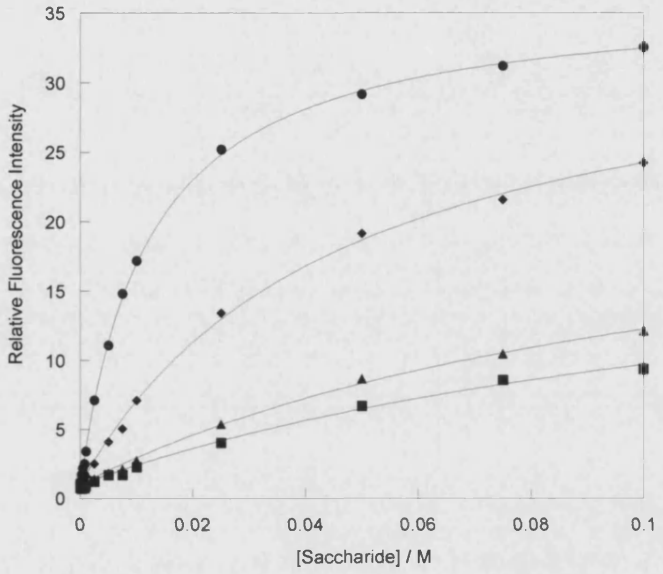

Figure 83: Relative fluorescence intensity *versus* saccharide concentration profile of **16** (4.1×10^{-5} mol.dm^{-3}) with (●) D-fructose, (■) D-glucose, (♦) D-galactose, (▲) D-mannose, in pH 8.21 buffer, λ_{ex} 244 nm, λ_{em} 358 nm.

The spectra of sensor **16** when excited at 244 nm produce no isostilbic point and no wavelength shift was observed; the maximum of emission is 358 nm. The enhancement factor for sensor **16** in the presence of D-fructose is 33 fold.

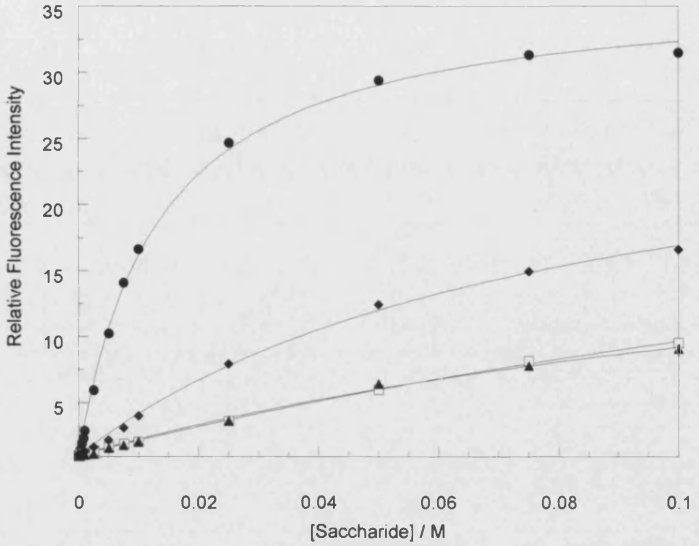

Figure 84: Relative fluorescence intensity *versus* saccharide concentration profile of **16** (4.1×10^{-5} mol.dm^{-3}) with (●) D-fructose, (□) D-glucose, (♦) D-galactose, (▲) D-mannose, in pH 8.21 buffer, λ_{ex} 276 nm, λ_{em} 358 nm.

The spectra of sensor **16** when excited at 276 nm produce no isostilbic point and no wavelength shift was observed; the maximum of emission is 358 nm. The enhancement factor for sensor **16** in the presence of D-fructose is 31 fold.

A summary of the stability constants (*K*) values for sensors **15** and **16** are presented in Table 26.

Table 26: Stability constant *K* (coefficient of determination; r^2) for saccharide complexes of fluorescence sensors **15** at λ_{ex} 244 nm and **16** at λ_{ex} 244 and 276 nm.

Saccharides	**15** (244 nm) *K* mol^{-1}.dm^3	**16** (244 nm) *K* mol^{-1}.dm^3	**16** (276 nm) *K* mol^{-1}.dm^3
D-Glucose	6.3 ± 0.3 (0.99)	7.1 ± 1.5 (0.99)	3.6 ± 0.5 (0.99)
D-Fructose	76 ± 1.8 (0.99)	83 ± 2.1 (0.99)	75 ± 3.4 (0.99)
D-Galactose	11 ± 0.9 (0.99)	22 ± 1.4 (0.99)	12 ± 1.1 (0.99)
D-Mannose	8.3 ± 0.2 (0.99)	8.7 ± 1.0 (0.99)	5.9 ± 1.0 (0.99)

For sensor **16**, similar results were obtained using the two excitation wavelengths. Sensor **15** shows similar result to these obtained with sensor **16**. The observed order of

stability constants (K) was D-fructose > D-galactose > D-mannose > D-glucose. Sensors **15** or **16** are D-fructose selective.

*Evaluation of Sensors **17** and **18***

Sensors **17** and **18** were also fully investigated using fluorescence spectroscopy. For all the different experiments presented below, the conditions used are pH 8.21 phosphate buffer[101] for the saccharide binding study, 4 different monosaccharides (D-fructose, D-glucose, D-galactose and D-mannose) and the sensors concentration are (4.1×10^{-5} mol.dm^{-3}) for sensors **17** and **18** respectively.

For both sensors **17** and **18**, only one excitation wavelength was found at 244 nm. The fluorescence measurements were carried out at this excitation wavelength.

The titration of sensors **17** and **18** with 4 saccharides are shown in the graphs below (Figure 85-86).

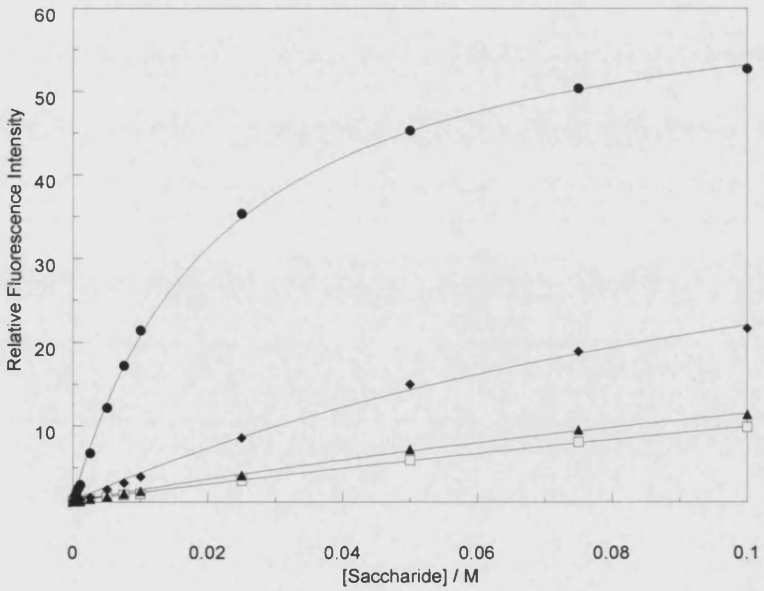

Figure 85: Relative fluorescence intensity *versus* saccharide concentration profile of **17** (4.1×10^{-5} mol.dm^{-3}) with (●) D-fructose, (□) D-glucose, (♦) D-galactose, (▲) D-mannose, in pH 8.21 buffer, λ_{ex} 244 nm, λ_{em} 350 nm.

The spectra of sensor **17** when excited at 244 nm produce no isostilbic point and no wavelength shift was observed; the maximum of emission is 350 nm. The enhancement factor for sensor **17** in the presence of D-fructose is 53 fold.

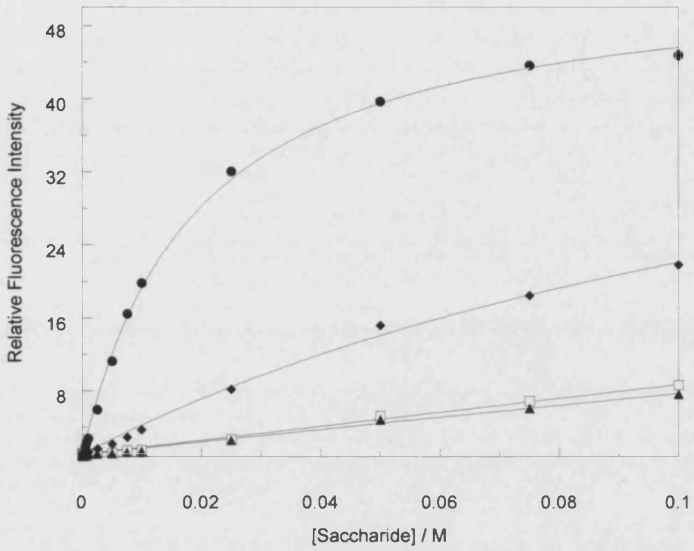

Figure 86: Relative fluorescence intensity *versus* saccharide concentration profile of **18** (4.1×10^{-5} mol.dm^{-3}) with (●) D-fructose, (□) D-glucose, (♦) D-galactose, (▲) D-mannose, in pH 8.21 buffer, λ_{ex} 244 nm, λ_{em} 358 nm.

The spectra of sensor **18** when excited at 244 nm produce no isostilbic point and no wavelength shift was observed; the maximum of emission is 358 nm. The enhancement factor for sensor **18** in the presence of D-fructose is 45 fold.

A summary of the stability constants (K) values for sensors **17** and **18** are shown in Table 27.

Table 27: Stability constant *K* (coefficient of determination; r^2) for saccharide complexes of fluorescence sensors **17** and **18** at λ_{ex} 244 nm.

Saccharides	**17** *K* mol^{-1}.dm^3	**18** *K* mol^{-1}.dm^3	
D-Glucose	1.7 ± 0.4 (0.99)	———	*
D-Fructose	45 ± 1.4 (0.99)	53 ± 2.6 (0.99)	
D-Galactose	7.2 ± 0.9 (0.99)	6.3 ± 1.0 (0.99)	
D-Mannose	3.2 ± 0.6 (0.99)	———	*

* small fluorescence changes

The observed order of stability constants (K) was D-fructose > D-galactose > D-mannose > D-glucose. Sensors **17** or **18** are D-fructose selective.

*Comparison between Sensors **13, 14, 15, 16 , 17** and **18***

All the six-diboronic acid sensors are presented in Figure 87. From this graphical representation, it clearly highlights that the stability constants are highest for the D-glucose complex with sensor **13**.

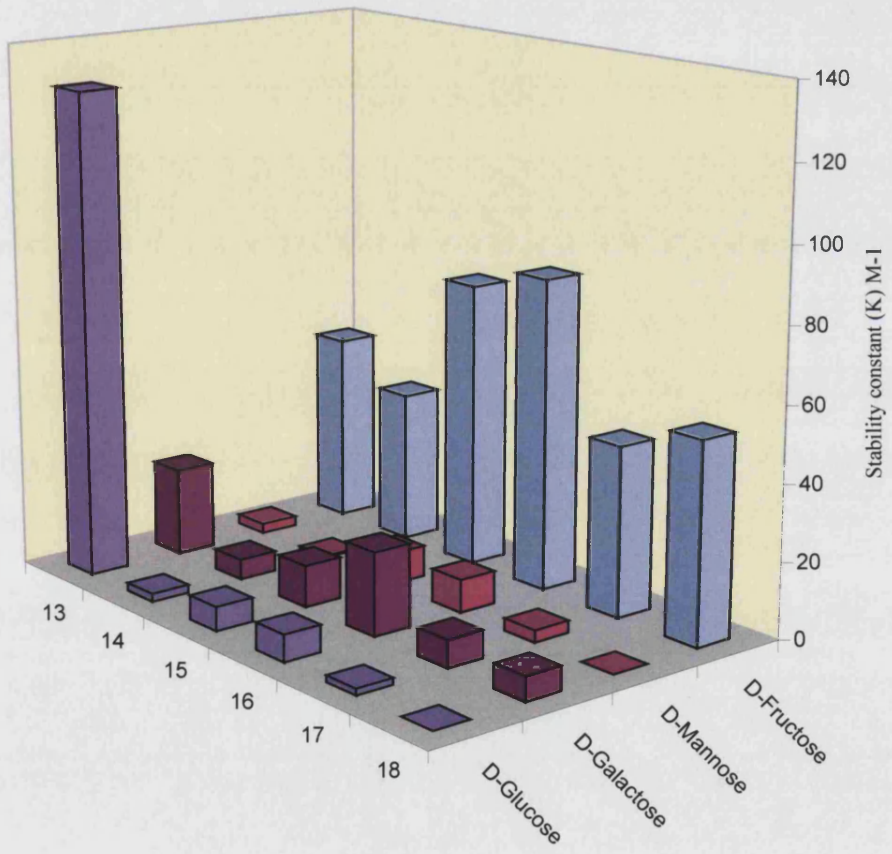

Figure 87: Stability constant (*K*) of the diboronic acid sensors series **13-18,** λ_{ex} 244 nm.

The enhancement factor for all the diboronic acid sensors are given in Table 28 with the boronic acid in *meta* position (sensors **15** and **16**) produce a higher binding constants for D-fructose (Figure 87) while with the boronic acid in the *para* position (sensors **17** and **18**) the largest fluorescence enhancement is observed. With the boronic acid in the *ortho* position (sensors **13** and **14**) a wavelength shift in the spectra is observed. Also, sensor **13** displays enhanced selectivity for D-glucose presumably due to optimal spacing of the boronic acid groups. Study on linker length for a D-glucose selective and sensitive diboronic acid sensor, was reported by James and co-workers[114], in that case ideal linker length is an hexamethylene (C_6) linker.

Table 28: Enhancement Factor (EF) at λ_{em} 358 nm for sensors **16** and **18**, 350 nm for sensors **15** and **17**, 356 nm and 363 nm for sensors **13** and **14** respectively.

Saccharides	**13** EF	**14** EF	**15** EF	**16** EF	**17** EF	**18** EF
D-Glucose	4.2	7	11	9.5	10	8.6
D-Fructose	13	1.9	38	33	**53**	**45**
D-Galactose	6	2.9	19	24	22	22
D-Mannose	2.8	1.7	12	12	11	7.6

*Comparison between Sensors **1** and **13***

The stability constants (K) of sensors **1** and **13** at the excitation wavelength of 244 nm and the ratio[113] diboronic acid sensor / monoboronic acid sensor were summarized in Table 29.

Table 29: Stability constant *K* (coefficient of determination; r^2) for saccharide complexes of fluorescent sensor **1** and **13**, in pH 8.21 buffer at λ_{ex} 244 nm.

Saccharides	**1** K mol^{-1}.dm^3	**13** K mol^{-1}.dm^3	**13 / 1**
D-Glucose	6.4 ± 0.4 (0.99)	129 ± 11 (0.99)	20.2
D-Fructose	79 ± 1.7 (0.99)	50 ± 2.3 (0.99)	0.6
D-Galactose	14 ± 0.6 (0.99)	23 ± 1.9 (0.99)	1.6
D-Mannose	7.8 ± 0.3 (0.99)	2.5 ± 1.0 (0.99)	0.3

In this study, it has been possible to demonstrate that the monoboronic acid sensor **1** was selective for D-fructose (Table 29). This result is the inherent binding of monoboronic acids with the monosaccharides. Sensors **1** and **13** illustrate that it is possible to synthesise an efficient TICT sensor for saccharides.

The ratio **13** / **1** in Table 29 and the graph Figure 88, clearly highlight the high selectivity of sensor **13** for D-glucose. This high selectivity could be explained by formation of 1:1 rigid cyclic complexes. This type of complex in diboronic acid sensors occurred only if the two boronic acids of the receptor site were able to form by cooperative binding, two cyclic esters with a single molecule of D-glucose. This hypothesis will need to be confirmed further using Circular Dichroism (CD) spectroscopy.

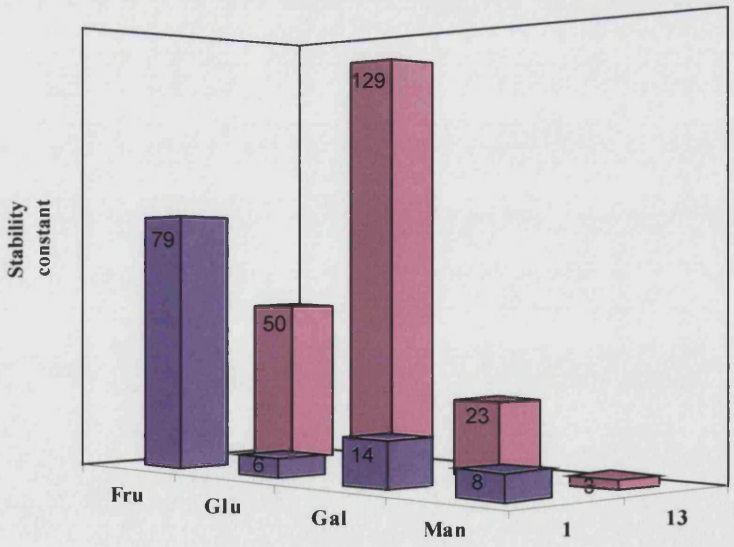

Figure 88: Stability constant (*K*) and saccharides selectivity of the diboronic acid sensors **1** and **13** at excitation 244 nm.

2.4 *Interaction of Boronic Acid Sensors with Fluorides*

This section will examine the interaction of the fluoride anion with some of the monoboronic acid sensors that were used in the saccharide studies. Fluorescence spectroscopy was used to study the binding of potassium fluoride. The effect of others potassium halides were investigated for comparison purposes. The aim was to see if any of those sensors could detect fluoride with a good affinity. There is an interest in following the uptake and metabolism of fluoride in both plant and animals, as well as in the analysis of drinking water. Detection the fluoride ions are also of great interest in the military for the detection of sarin.

Previous systems were based on the Lewis acid-base interaction between boron and anions. The systems achieved an exclusive selectivity for fluorides over other halides ions (KCl, KBr). When boron binds with certain anions the hybridisation changes from sp^2 to sp^3 (see scheme 20).[115,83] The nature of the boron-anion interaction was found to be a covalent bond rather than an ionic interaction.[83] Multiple binding of fluoride to the boron center is possible (Scheme 20). The trifluoro tetrahedral boronate has been shown to be the favoured species in simple boronic acids such as phenylboronic acid and 2-naphthylboronic acid.[115, 116]

A monofluoride adduct has been observed, in the case where this adduct has been stabilised by the presence of additional hydrogen bonding from the protonated amine (Figure 89).[115]

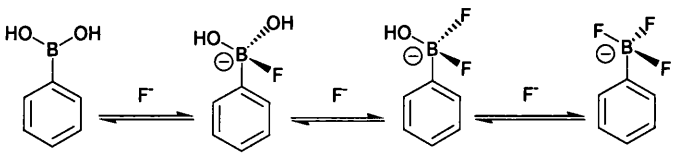

Scheme 20: Interaction of fluoride with simple boronic acids.

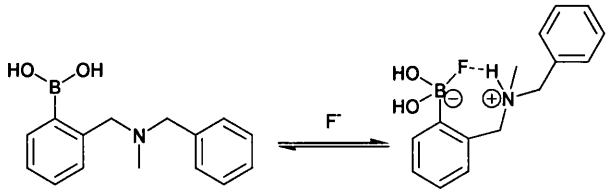

Figure 89: Formation of a hydrogen bonded stabilised mono-fluoride adduct

No studies have been realised on the effect of fluoride on fluorescent sensors with an amine directly attached to the chromophore to date. The following section was designed to explore the fluoride interaction with such system. Sensors **1**, **2**, **3**, **5**, **6**, **7** and **9** were investigated upon fluoride binding, and are described below.

*Evaluation of Sensors **1**, **2**, **3** and **9***

Titrations with solid potassium fluoride, chloride and bromide were performed in HPLC grade methanol to measure the interaction between the anion and the boronic acid in methanol.

The titrations were performed at the best excitation wavelength for each sensor, i.e. 244 nm for sensors **1**, **3**, 240 nm for sensor **2** and 252 nm for sensor **9**. For each sensor, a titration with 3 different potassium halides (KF, KCl and KBr) was achieved. The sensors concentrations used were similar to the one used for saccharide interaction, (2.0×10^{-5} mol.dm^{-3}) for sensors **1**, **2**, **3**, (2.2×10^{-5} mol.dm^{-3}) for sensor **9**.

For each sensor, the titration with KCl or KBr presents no change in fluorescence measurements upon addition of potassium halide.

The emission maximum fluorescence varies for each sensor with KCl or KBr, 391 nm (sensor **1**), 346 nm, 347 nm and 350 nm for sensors **3**, **2** and **9** respectively.

The curves of the fluoride titration for sensors **1**, **2**, **3** and **9** are presented in Figure 90. A summary of the stability constants (K) values and enhancement factors for sensors **1**, **2**, **3** and **9** are shown in Table 30.

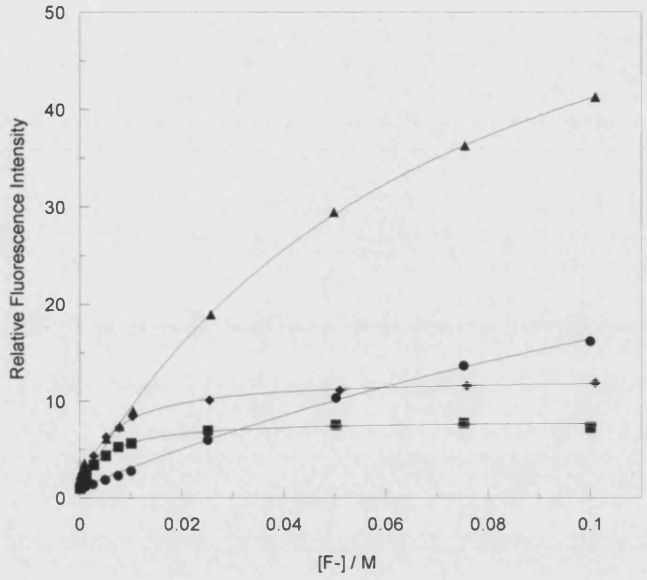

Figure 90: Relative fluorescence intensity *versus* fluoride concentration profile of (●) sensor **1** (2.0×10^{-5} mol.dm^{-3}), (■) sensor **2** (2.0×10^{-5} mol.dm^{-3}), (♦) sensor **3** (2.0×10^{-5} mol.dm^{-3}), (▲) sensor **9** (2.2×10^{-5} mol.dm^{-3}), in methanol, λ_{ex} 244 nm, λ_{em} 352 nm (sensor **1**), λ_{ex} 240 nm, λ_{em} 347 nm (sensor **2**), λ_{ex} 244 nm, λ_{em} 346 nm (sensor **3**) and λ_{ex} 252 nm, λ_{em} 353 nm (sensor **9**).

Table 30: pK_a, Enhancement Factor and Stability constant K (coefficient of determination; r^2) for fluoride complexes of fluorescent sensors **1**, **2**, **3** and **9**, in methanol.

	1	**2**	**3**	**9**
pK_a	10.20	9.30	9.58	10.75
K (mol^{-1}.dm^3)	4 ± 0.5 (0.99)	194 ± 12 (0.99)	163 ± 5 (0.99)	14 ± 1.5 (0.99)
EF	16	8	12	41

The fluorescence emission increased upon addition of fluoride in all the titrations and for all the sensors.

A graphical representation of the stability constants (*K*) values and enhancement factors for fluoride complexes of fluorescent sensors **1**, **2**, **3** and **9** is given Figure 91.

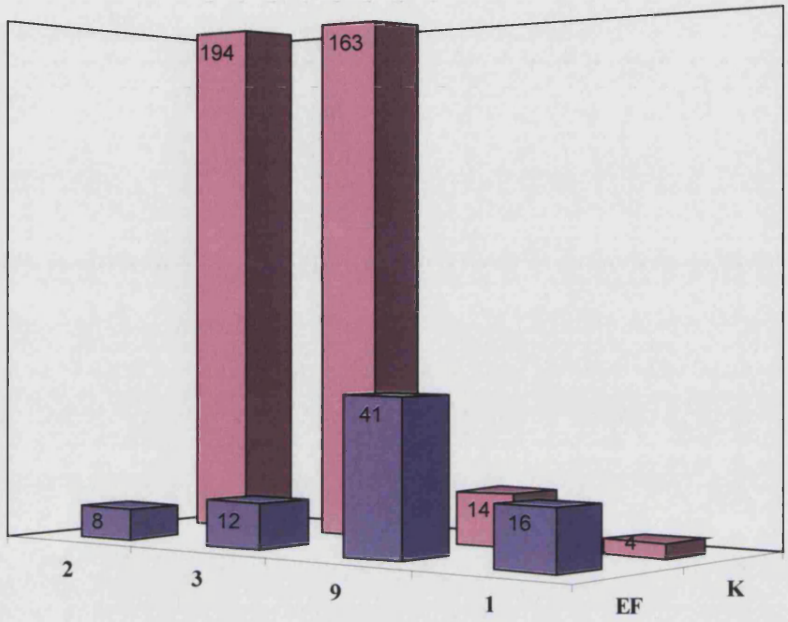

Figure 91: Enhancement Factor and Stability constant (*K*) for fluoride complexes of fluorescent sensors **1**, **2**, **3** and **9**, in methanol.

Sensors **1** and **9** have low stability constants, however sensor **9** has the highest enhancement factor, 41 fold for fluoride.

The curves for sensors **2** and **3** with fluoride anions are very well defined saturation curves, and high values of the stability constants were obtained as a result: 194 $mol.dm^{-3}$ and 163 $mol.dm^{-3}$ for sensors **2** and **3** respectively. The affinity of sensor **2** and **3** are respectively about 50 and 40 times more than the stability constant of sensor **1**. With sensors **2** and **3,** no B-N bond can be formed; the observed stability constant with

fluoride is better than when a B-N interaction is possible. There is also a very clear trend between pK_a and observed stability constant with fluorides. Interestingly, sensor **9**, which contained a N-methyl and the boronic acid is in the *ortho* position, a similar stability constant to sensor **1** is found, but the enhancement factor for fluoride is the highest.

*Evaluation of Sensors **5, 6** and **7***

The anion titrations of sensors **5**, **6** and **7** were performed in the same conditions as described earlier for sensors **1**, **2**, **3** and **9.**

The titrations were performed at the best excitation wavelength for each sensor, i.e. 279 nm for sensors **5**, 244 nm and 289 nm for sensor **6** and 274 nm for sensor **7**. For each sensor, a titration with 3 different potassium halides (KF, KCl and KBr) was performed. The sensors concentration used were similar to the one used for saccharide interaction, (2.0×10^{-5} mol.dm^{-3}) for sensors **5** and **7**, (4.0×10^{-5} mol.dm^{-3}) for sensor **6**.

For each sensor, when titrated with KCl or KBr, no changes in intensity or wavelength in the fluorescence measurements were observed upon addition of increasing concentration of potassium halide.

The emission maximum fluorescence varies for each sensor, 390 nm (λ_{ex} 279 nm) for sensor **5**, 375 nm (λ_{ex} 244 nm and 289 nm) for sensor **6**, and finally 376 nm (λ_{ex} 274 nm) for sensor **7**.

However, when sensor **5** is titrated with fluoride (λ_{ex} 279 nm, λ_{em} 390 nm), the fluorescence is quenched. The curve of the fluoride titration is presented in Figure 92.

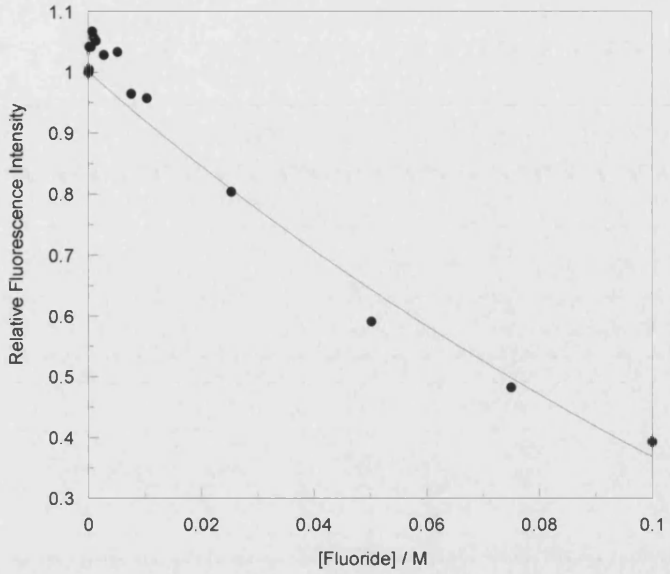

Figure 92: Relative fluorescence intensity *versus* fluoride concentration profile of (●) sensor **5** (2.0×10^{-5} mol.dm^{-3}), λ_{ex} 279 nm, λ_{em} 390 nm

Nevertheless, we were unable to calculate the stability from this curve with a good coefficient of determination (r^2).

When sensor **6** is titrated with fluoride (λ_{ex} 289 nm, λ_{em} 375 nm), the fluorescence increases slowly and the wavelength shifts from 430 to 380 nm. An isostilbic point was observed at 408 nm. The titration curve of the fluoride titration is shown in Figure 93.

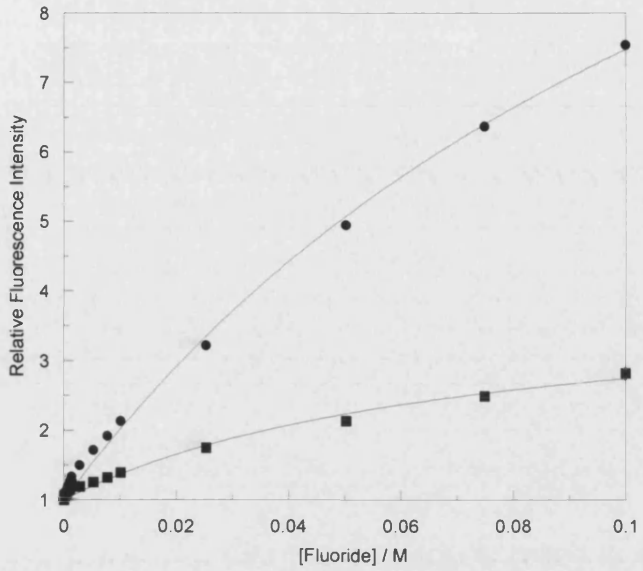

Figure 93: Relative fluorescence intensity *versus* fluoride concentration profile of sensor **6** (4.0×10^{-5} mol.dm^{-3}) (●) at λ_{ex} 244 nm, (■) at λ_{ex} 289 nm, λ_{em} 375 nm

When sensor **6** is titrated with fluoride (λ_{ex} 244 nm, λ_{em} 375 nm), the fluorescence increases upon addition of fluoride and a shift in the maximum is observed from 370 to 375 nm. No isostilbic point was observed. The titration curve of the fluoride titration is shown in Figure 93.

These two types of behaviour have been observed before in the section with the saccharide interaction. The shift observed in the spectra when sensor **6** is excited at 289 nm, can be due to the B-N bond been broken by fixation of fluoride to form the boron fluoride adduct.

The stability constants of sensor **6** are 7 ± 1.1 (0.99) and 14 ± 3.7 (0.98) for excitation wavelengths 244 nm and 289 nm respectively.

Finally, when sensor **7** is titrated with fluoride (λ_{ex} 274 nm, λ_{em} 357 nm), the fluorescence is increased upon addition of fluoride and a shift is observed from 374 to 357 nm. An isostilbic point is observed at 390 nm. The titration curve of the fluoride titration is shown in Figure 94. The stability constant of sensor **7** is 1 ± 1 (0.99).

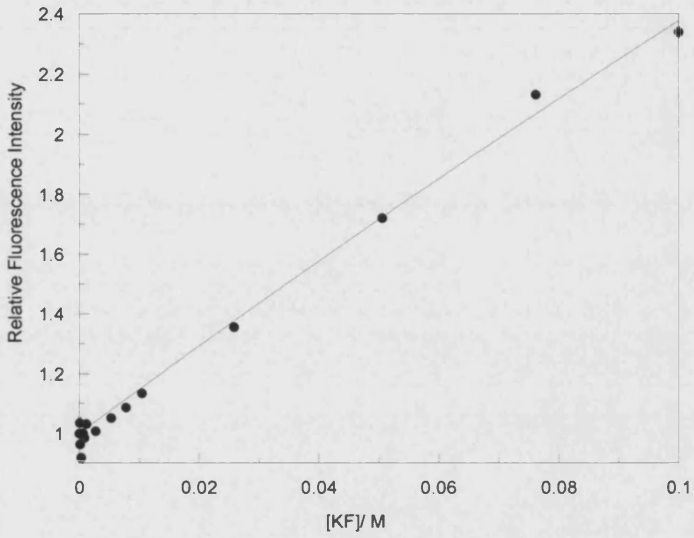

Figure 94: Relative fluorescence intensity *versus* fluoride concentration profile of (●) sensor **7** (2.0×10^{-5} mol.dm^{-3}), λ_{ex} 274 nm, λ_{em} 357 nm

In conclusion, sensors **5**, **6** and **7**, did not present a good affinity for fluoride. However, sensors **2** and **3** turned out to be particularly valuable sensors, high selectivity and good affinity for fluoride. Sensors **9** showed the best fluorescence signal response by giving the best enhancement factor of all sensors in this section. Finally, all the sensors presented here are fluoride selective compared to chloride and bromide.

The fluoride effect on fluorescence of these sensors and others will be investigated further in the group and the stoichiometry of the complex will be investigated by NMR or mass spectroscopy.

2.5 Summary

- Three series of sensors have been synthesised.
- The interaction of saccharide with sensors in phosphate buffer pH 8.21 have been investigated using fluorescence spectroscopy.
- The interaction of fluoride with sensors in methanol has also been investigated using fluorescence.
- Sensor **1**, displays a dual fluorescence, with a TICT state and a LE state (when excited at 274 nm) or only a LE state (when excited at 244 nm).
- Sensors **2** and **3** have only a LE state since B-N bond formation is not possible. Higher stability constant and very good affinity for D-fructose. They also have the best affinity for fluoride and the highest stability constant for fluoride.
- The fluorescence of sensor **5**, is quenched upon addition of saccharides or fluoride. Sensors **6** and **7** display a fluorescence enhancement upon addition of saccharides or fluoride.
- Sensor **9** detects saccharide, but shows the best fluorescence enhancement upon addition of fluoride, but has a low stability constant.
- Modification of the fluorophore, sensor **10** and **11**, did not lead to a major improvement of the system.
- Diboronic acid, sensor **13**, is the only sensor to have a good affinity for D-glucose, and also displays TICT and LE states.
- The crown ether series was synthesised and remains to be investigated.
- Two single crystal X-ray structures were obtained. One of sensor **1** and one of arabinose-phenolboronic acid complex.

Chapter 3

Experimental

"If we knew what it was we were doing, it would not be called research, would it?"

Albert Einstein (1879-1955)

3.1 General procedures

All the solvents and chemicals used as starting materials were reagent grade, unless stated otherwise and supplied by Frontier Scientific Ltd, Aldrich Chemical Co. Ltd., Lancaster Synthesis Ltd. and Fisher Scientific Ltd.

^{1}H and $^{13}C\{^{1}H\}$ NMR spectra were recorded on a Bruker AVANCE 300 (300.13 and 75.47 MHz respectively) and a Jeol-400MHz (399.78 and 100.52 MHz respectively) spectrometer. All the chemical shifts (δ) were reported in ppm using the deuterated solvent and or tetramethylsilane as the internal reference. All the following data use the abbreviations as follow: singlet (s), doublet (d), doublet of doublet (dd), apparent doublet (d app), multiplet (m), broad singlet (brs). *J*-values are given in Hertz.
The mentioned carbon masked by CD_3OD, is a carbon seen under CD_3OD but difficult to assign individually or shown by a 2D ^{1}H-^{13}C correlation.
The $^{13}C\{^{1}H\}$ NMR spectra were subject to the PENDANT technique, resulting in primary and tertiary carbon atoms having a different phase to secondary and quaternary carbon atoms. The phase is presented in the following manner: (+) positive phase, (-) negative phase. Due to quadrupolar relaxation, the aryl carbon atoms attached directly to boron atoms of the boronic acids were not observed by ^{13}C-NMR.

Mass spectra including high-resolution spectra were recorded on a Waters Micromass Autospec Spectrometer using FAB (Fast Atom Bombardment) at the University of Bath and at the EPRSC mass spectrometry centre, Swansea.

Elemental Analysis were performed on a Exeter Analytical CE 440.

Melting points were determined using a Gallenkamp melting point apparatus and are reported uncorrected.

Thin Layer Chromatography (TLC) was performed on precoated aluminium-backed silica plates supplied by Fluka Chemie. Visualisation was achieved by UV light (254 nm).

Organic phases were dried with anhydrous $MgSO_4$, filtered and condensed with a Büchi evaporator. Further evaporation was carried out on high-*vacuum* line where necessary.

All the fluorescence measurements were performed on a Perkin Elmer Luminescence Spectrometer LS 50B with a Starna Silica (quartz) cuvet with 10 mm path lengths and four faces polished. Data was collected *via* the Pekin Elmer FL WinLab 4.00 software package.

UV-Visible absorption measurements used Sigma Spectrophotometer Silica (Quartz) Cuvets with 10 mm path lengths and were recorded on a Perkin-Elmer Lambda 20 UV/VIS spectrometer. The data was collected *via* the Pekin Elmer UV WinLab 2.70 software package.

The association constant K and pKa were analysed with Kaleidagraph 3.51 using nonlinear (Levenberg-Marquardt algorithm) curve fitting. The errors reported are the standard errors obtained from the best fit.

The pH measurements in the pH-titration experiments were taken on a Hanna Instruments HI 9321 Microprocessor pH meter which was calibrated using Fisher Chemicals "colour coded" buffer solutions (pH 4.0- phthalate , pH 7.0- phosphate and pH 10.0- borate).

The pH measurements for the preparation of the HEPES buffer were taken on a Mettler DL 21 Titrator with a Mettler Toledo DG111-SC glass electrode which was calibrated using two 52.1% methanol/water buffers [pH 2.07 (0.01000 m KCl, 0.01101 m HCl) and 9.43 (0.00992 m KCl, 0.004996 m Na borate)].[101]

3.2 Synthesis and Characterisation

Preparation of the (2-boronobenzyl)-aniline (1)

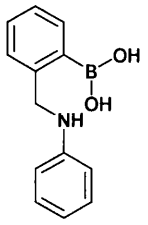

2-Formylphenylboronic acid (1.00 g, 6.67 mmol) was dissolved in a mixture of absolute EtOH/Toluene (90/10) (50 ml) then aniline (621 mg, 6.67 mmol) was added to the reaction. A *Deans and Stark trap* was fixed to the reaction vessel and filled with the same solvent mixture EtOH/Toluene (90/10) (25 ml) to permit the azeotropic removal of water. The reaction was stirred under reflux for 16 hours. After cooling to 0°C with an ice bath, sodium borohydride (1.26 g, 33.35 mmol) was added slowly to the mixture and stirred for 2.5 further hours at room temperature.

The solvent was removed under reduced pressure. Water (100 ml) was added to the residue and the resulting solution was extracted with chloroform (3 × 100 ml). The organic phases were combined, washed with brine (150 ml) and dried over $MgSO_4$. The solvent was then removed *in vacuo*. Precipitation from chloroform/*n*-hexane afforded sensor **1** (813 mg, 54%) as a cream powder.

mp: 125-129°C; Found: C, 74.70; H, 5.97; N, 6.63. $C_{13}H_{14}BNO_2$-H_2O requires C, 74.72; H, 5.80; N, 6.70%; δ_H (300 MHz; CD_3OD) 4.21 (2H, s, C*H*$_2$), 6.60-6.70 (3H, m, Ar*H*), 6.95-7.25 (6H, m, Ar*H*); δ_C (75 MHz; CD_3OD) 51.6, 117.4 (2C), 121.5, 126.9, 127.9, 129.8, 130.2 (2C), 132.7, 146.0, 149.1; *m/z* (FAB) 497.3 ([M+2(3-$HOCH_2C_6H_4NO_2$)-$2H_2O$]$^+$, 100%); $\Phi = 0.0074$ [a], $\Phi = 0.0082$ [b].

[a] (weight curves method to determine the area under the curves)
[b] (kaleidagraph to determine the area under the curves)

Preparation of the (3-boronobenzyl)-aniline (2)

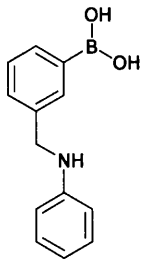

3-Formylphenylboronic acid (200 mg, 1.33 mmol) was dissolved in methanol (20 ml) then aniline (136 mg, 1.46 mmol) was added to the reaction. The reaction was stirred overnight at room temperature. The reduction of the imine product was then carried out by the slow addition of sodium borohydride (250 mg, 6.61 mmol) to the solution. The reaction was stirred for 1.5 further hours at room temperature.

The solvent was removed under reduced pressure. Water (20 ml) was added to the residue and the resulting solution was extracted with chloroform (3 × 40 ml). The organic phases were combined, washed with brine (60 ml) and dried over $MgSO_4$. The solvent was then removed *in vacuo*. Precipitation from chloroform/*n*-hexane afforded sensor **2** (137 mg, 45%) as a white powder.

mp: 166°C; Found: C, 73.90; H, 5.56; N, 6.72. $C_{13}H_{14}BNO_2$-H_2O+0.03 $CHCl_3$ requires C, 73.60; H, 5.70; N, 6.58%); (HRMS: Found $[M+2(3\text{-}HOCH_2C_6H_4NO_2)\text{-}2H_2O]^+$, 497.1776. $C_{27}H_{24}BN_3O_6$ requires 497.1758); δ_H (300 MHz; CD_3OD) 4.31 (2H, s, C*H*$_2$), 6.55-6.65 (3H, m, Ar*H*), 7.00-7.10 (2H, m, Ar*H*), 7.30 (1H, m, Ar*H*), 7.42 (1H, m, Ar*H*), 7.60 (1H, m, Ar*H*), 7.76 (1H, m, Ar*H*); δ_C (75 MHz; CD_3OD) approximately 49.0 carbon masked by CD_3OD, 114.5, 118.3, 129.1, 130.3, 130.8, 133.8, 134.4, 140.8, 150.5; *m/z* (FAB) 498.1 ($[M+H+2(3\text{-}HOCH_2C_6H_4NO_2)\text{-}2H_2O]^+$, 100%); Φ = 0.0085 [a], Φ = 0.0087 [b].

[a] (weight curves method to determine the area under the curves)
[b] (kaleidagraph to determine the area under the curves)

Preparation of the (4-boronobenzyl)-aniline (3)

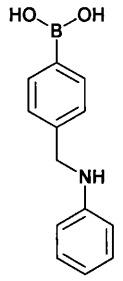

4-formylphenylboronic acid (200 mg, 1.33 mmol) was dissolved in methanol (20 ml) then aniline (137 mg, 1.46 mmol) was added to the reaction. The reaction was stirred overnight at room temperature. The reduction of the imine product was then carried out by the slow addition of sodium borohydride (250 mg, 6.64 mmol) to the solution. The reaction was stirred for 1 further hour at room temperature.

The solvent was removed under reduced pressure. Water (20 ml) was added to the residue and the resulting solution was extracted with chloroform (3 × 40 ml). The organic phases were combined, washed with brine (60 ml) and dried over $MgSO_4$. The solvent was then removed *in vacuo*. Precipitation from chloroform/*n*-hexane afforded sensor **3** (135 mg, 45%) as a white powder.

mp: 164°C; Found: C, 73.90; H, 5.88; N, 6.15. $C_{13}H_{14}BNO_2$-H_2O+0.03 $CHCl_3$ requires C, 73.60; H, 5.70; N, 6.58%); (HRMS: Found $[M+2(3\text{-}HOCH_2C_6H_4NO_2)\text{-}2H_2O]^+$, 497.1772. $C_{27}H_{24}BN_3O_6$ requires 497.1758); δ_H (300 MHz; CD_3OD) 4.30 (2H, s, C*H*$_2$-NH), 6.55-6.65 (3H, m, Ar*H*), 7.00-7.10 (2H, m, Ar*H*), 7.30-7.40 (2H, m, Ar*H*), 7.56 (1H, m, Ar*H*), 7.69 (1H, m, Ar*H*); δ_C (75 MHz; CD_3OD) approximately 49.0 carbon masked by CD_3OD, 114.5, 118.4, 127.9, 130.3, 135.5, 144.1, 150.5; *m/z* (FAB) 497.1 ($[M+2(3\text{-}HOCH_2C_6H_4NO_2)\text{-}2H_2O]^+$, 100%); $\Phi = 0.0069$ [a], $\Phi = 0.0070$ [b].

[a] (weight curves method to determine the area under the curves)
[b] (kaleidagraph to determine the area under the curves)

Preparation of the *N*-phenylbenzylamine (4)

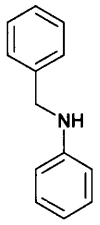

Benzaldehyde (646 mg, 6.08 mmol) was dissolved in toluene (50 ml) then aniline (465 mg, 5.00 mmol) was added to the reaction. A *Deans and Stark trap* was fixed to the reaction vessel and filled with toluene (25 ml). The reaction was heated under reflux overnight. After cooling, the toluene was removed under reduced pressure and the residue was dissolved in methanol (60 ml) and sodium borohydride (946 mg, 25.00 mmol) was added slowly to the mixture and stirred for 2 further hours at room temperature.

The solvent was removed under reduced pressure. Water (60 ml) was added to the residue and extracted with chloroform (3 × 60 ml). The organic phases were combined, washed with brine (60 ml) and dried over $MgSO_4$. The solvent was then removed under *vacuum* and dried under high *vacuum* to afford compound **4** as a brown solid (902 mg, 98%).

mp: 34-36°C; Found: C, 85.00; H, 7.16; N, 7.65. $C_{13}H_{13}N$ requires C, 85.21; H, 7.15; N, 7.64%); (HRMS: Found M^+, 183.1054. $C_{13}H_{13}N$ requires 183.1048); δ_H (300 MHz; $CDCl_3$; Me_4Si) 4.00 (1H, brs, N*H*), 4.30 (2H, s, Ph-CH_2-NH), 6.55-6.75 (3H, m, Ar*H*), 7.10-7.40 (7H, m, Ar*H*); δ_C (75 MHz; $CDCl_3$) 48.3, 112.8, 117.5, 127.2, 127.5, 128.6, 129.2, 139.4, 148.1; *m/z* (FAB) 183.1 (M^+, 100%), 91.0 (C_7H_7, 35%).

Preparation of the (4-chloro-phenyl)-(2-boronobenzyl) amine (5)

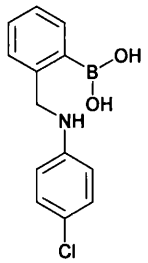

The 4-chloroaniline (84 mg, 0.66 mmol) was dissolved in a mixture of absolute EtOH/Toluene (90/10) (25 ml) then 2-formylphenylboronic acid (100 mg, 0.66 mmol) was added to the solution. A *Deans and Stark trap* was fixed to the reaction vessel and filled with EtOH/Toluene (90/10) mixture (25 ml). The reaction was stirred under reflux overnight. After cooling, sodium borohydride (125 mg, 3.30 mmol) was added slowly to the mixture and stirred for 1.5 further hours at room temperature.

The solvent was removed under reduced pressure. Water (30 ml) was added to the residue and the resulting solution was extracted with chloroform (3 × 30 ml). The organic phases were combined, washed with brine (45 ml) and dried over $MgSO_4$. The solvent was then removed *in vacuo*. Precipitation from chloroform/*n*-hexane afforded sensor **5** (54 mg, 31%) as a white powder.

mp: 148-150°C; (HRMS: Found $[M+2(3\text{-}HOCH_2C_6H_4NO_2)\text{-}2H_2O]^+$, 531.1349. $C_{27}H_{23}BClN_3O_6$ requires 531.1368); δ_H (300 MHz; CD_3OD) 4.19 (2H, s, C*H*$_2$-NH), 6.54 (2H, AA'BB'system, J_{AB} *8.8 Hz* highly second order, Ar*H*), 6.96 (2H, AA'BB'system, $J_{A'B'}$ *8.8 Hz* highly second order, Ar*H*), 7.08-7.25 (4H, m, Ar*H*); δ_C (75 MHz; CD_3OD) 50.8, 117.4 (2C), 124.8, 127.9, 130.0 (4C), 132.9, 145.7, 148.7; *m/z* (FAB) 531.1 ($[M+2(3\text{-}HOCH_2C_6H_4NO_2)\text{-}2H_2O]^+$, 100%); $\Phi = 0.1905$ [a], $\Phi = 0.1921$ [b].

[a] (weight curves method to determine the area under the curves)
[b] (kaleidagraph to determine the area under the curves)

Preparation of the (4-methoxy-phenyl)-(2-boronobenzyl) amine (6)

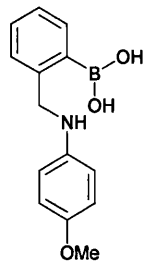

2-Formylphenylboronic acid (200 mg, 1.33 mmol) was dissolved in a mixture absolute EtOH/Toluene (90/10) (25 ml) then *p*-anisidine (164 mg, 1.33 mmol) was added to the solution. A *Deans and Stark trap* was fixed to the reaction vessel and filled with mixture of EtOH/Toluene (90/10) (25 ml). The reaction was heated under reflux overnight. After cooling, sodium borohydride (250 mg, 6.61 mmol) was added slowly to the mixture and stirred for 2 further hours at room temperature.

The solvent was removed under reduced pressure. Water (40 ml) was added to the residue and the resulting solution was extracted with chloroform (3 × 40 ml). The organic phases were combined, washed with brine (60 ml) and dried over $MgSO_4$. The solvent was then removed *in vacuo* and dried under high *vacuum*. The desired sensor **6** (192 mg, 56%) was obtained as a pale brown foam.

Found: C, 69.8; H, 5.76; N, 5.94. $C_{14}H_{16}BNO_3$-H_2O requires C, 70.33; H, 5.90; N, 5.86%; (HRMS: Found $[M+2(3\text{-}HOCH_2C_6H_4NO_2)\text{-}2H_2O]^+$, 527.1858. $C_{28}H_{26}BN_3O_7$ requires 527.1864); δ_H (300 MHz; CD_3OD) 3.63 (3H, s, OCH_3), 4.24 (2H, s, CH_2-NH), 6.72 (2H, AA'BB'system, J_{AB} *9.2 Hz* highly second order, Ar*H*), 6.85 (2H, AA'BB'system, $J_{A'B'}$ *9.2 Hz* highly second order, Ar*H*), 7.08-7.26 (4H, m, Ar*H*); δ_C (75 MHz; CD_3OD) 54.5, 56.4, 116.1 (2C), 121.4 (2C), 128.1 (2C), 129.8, 132.4, 140.0, 145.0, 157.8; m/z (FAB) 527.2 ($[M+2(3\text{-}HOCH_2C_6H_4NO_2)\text{-}2H_2O]^+$, 100%);

$\Phi = 0.0138$ [a], $\Phi = 0.0149$ [b].

[a] (weight curves method to determine the area under the curves)
[b] (kaleidagraph to determine the area under the curves)

Preparation of the (2-borono-5-methoxy-benzyl)-phenyl-amine (7)

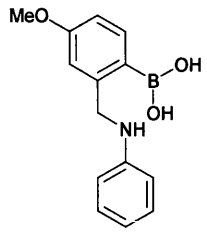

4-Methoxycarbonylphenylboronic acid (275 mg, 1.53 mmol) was dissolved in a mixture absolute EtOH/Toluene (90/10) (25 ml) then aniline (143 mg, 1.53 mmol) was added to the reaction. A *Deans and Stark trap* was fixed to the reaction vessel and filled with a mixture of EtOH/Toluene (90/10) (25 ml). The reaction was heated under reflux for 22 hours. After cooling, sodium borohydride (289 mg, 7.64 mmol) was added slowly to the mixture and stirred for 2.5 further hours at room temperature.

The solvent was removed under reduced pressure. Water (30 ml) was added to the residue and the resulting solution was extracted with chloroform (3 × 30 ml). The organic phases were combined, washed with brine (45 ml) and dried over $MgSO_4$. The solvent was then removed *in vacuo*. Precipitation from chloroform/*n*-hexane afforded sensor **7** (132 mg, 34%) as a yellow solid.

mp: 68-72°C; (HRMS: Found $[M+2(3\text{-}HOCH_2C_6H_4NO_2)\text{-}2H_2O]^+$, 527.1882. $C_{28}H_{26}BN_3O_7$ requires 527.1864); δ_H (300 MHz; CD_3OD) 3.80 (3H, s, OCH_3), 4.30 (2H, s, CH_2-NH), 4.62 (1H, brs, N*H*), 6.72-6.82 (4H, m, Ar*H*), 6.91-6.94 (1H, m, Ar*H*), 7.10-7.16 (2H, m, Ar*H*), 7.21-7.26 (1H, m, Ar*H*); δ_C (75 MHz; CD_3OD) 50.0, 54.5, 115.1 (2C), 117.7, 119.2, 128.6 (4C), 146.2, 147.9, 160.5; *m/z* (FAB) 527.2 ($[M+2(3\text{-}HOCH_2C_6H_4NO_2)\text{-}2H_2O]^+$, 100%); $\Phi = 0.0297$ [a], $\Phi = 0.0330$ [b].

[a] (weight curves method to determine the area under the curves)
[b] (kaleidagraph to determine the area under the curves)

Preparation of the 4-(2-Boronobenzylamino)-benzonitrile (8)

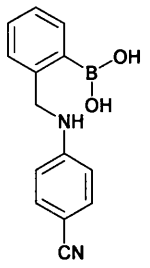

4-Aminobenzonitrile (788 mg, 6.67 mmol) was dissolved in a mixture of absolute EtOH/Toluene (90/10) (50 ml) and then 2-formylbenzeneboronic acid (1.00 g, 6.67 mmol) was added to the reaction. A *Deans and Stark trap* was fixed to the reaction vessel and filled with a mixture of EtOH/Toluene (90/10) (25 ml). The reaction was heated under reflux overnight. After cooling, the solvents were evaporated under reduced pressure and yield to a yellow oil. The latter was dissolved in EtOH (18 ml). After cooling at 0°C with an ice bath, sodium borohydride (1.26 g, 33.35 mmol) was added slowly to the mixture and stirred for 2 further hours at room temperature. Then the solvents were removed under reduced pressure.

Water (100 ml) was added to the residue and the resulting solution was extracted with chloroform (3 × 100 ml). The organic phases were combined, washed with brine (150 ml) and dried over $MgSO_4$. The solvent was removed under reduced pressure to afford a pale yellow powder (crude product, 901.0 mg, 54%).

The crude (745 mg) was mixed with water (120 ml) and aqueous NaOH (3 M) was added to reach pH ≈ 14. The resulting solution was extracted with chloroform (3 × 100 ml), and the combined organic phases were discarded. Aqueous HCl (1 M) was added to the remaining basic aqueous phase to reach pH ≈ 6. This acidic aqueous phase was then extracted with chloroform (3 × 100 ml). These latter organic phases were combined, dried over $MgSO_4$ and concentrated *in vacuo* to afford sensor **8** as a white powder (252 mg, 34% of the used crude product).

mp: 142°C; (HRMS: Found $[M+2(3\text{-}HOCH_2C_6H_4NO_2)\text{-}2H_2O]^+$ 522.1729. $C_{28}H_{23}BN_4O_6$ requires 522.1711); δ_H (300 MHz, CD_3OD) 4.28 (2H, s, C*H*$_2$-NH), 6.53-6.57 (2H, m, Ar*H*), 7.11-7.30 (6H, m, Ar*H*); δ_C (75 MHz; CD_3OD) approximately 49.0 carbon masked by CD_3OD, 99.6, 114.7 (2C), 121.8, 128.0, 128.4, 130.3, 133.1, 134.8 (2C), 144.5, 154.2; *m/z* (FAB) 522.2 ($[M+2(3\text{-}HOCH_2C_6H_4NO_2)\text{-}2H_2O]^+$, 12%), 73.0 (100%); ν_{max} (film)/cm^{-1} 3370 (NH), 2213 (CN), 1605 (Ar).

Preparation of the (2-boronobenzyl)-methyl-*m*-tolylamine (9)

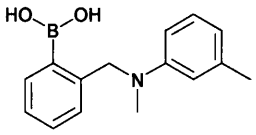

A sample of (2-boronobenzyl)-methyl-*m*-tolylamine has been synthesised, described and characterised in the thesis of Christopher J. Ward. [96] This compound has been used in the fluorescence titrations described herein.

$\Phi = 0.0038$ [a], $\Phi = 0.0045$ [b].

[a] (weight curves method to determine the area under the curves)
[b] (kaleidagraph to determine the area under the curves)

Preparation of the 2-(boronobenzyl)-naphthalen-1-yl-amine (10)

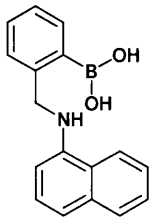

A sample of (2-boronobenzyl)-naphthalen-1-yl-amine has been synthesised, described and characterised in the thesis of Christopher J. Ward.[96]

This compound has been used in the fluorescence titrations described herein.

Preparation of the (2-boronobenzyl)-pyren-1-yl-amine (11)

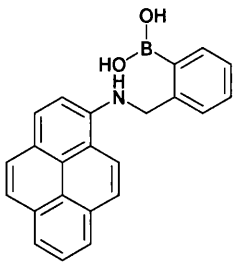

1-Pyrenemethylamine hydrochloride salt was added to aqueous NaOH (1 M) solution. The mixture was stirred for 30 min and the precipitate was extracted with ether. The organic layers were combined, dried over $MgSO_4$, filtered and evaporated to afford the product used in the next step.

1-pyrenemethylamine (200 mg, 0.92 mmol) was dissolved in a mixture of THF/MeOH (50/50) (10 ml) and 2-formylphenylboronic acid (165 mg, 1.10 mmol) was added to the solution. The solution was stirred at room temperature for 24 hours under nitrogen atmosphere. Sodium borohydride (125 mg, 3.30 mmol) was added slowly to the mixture and stirred for 1 further hour at room temperature. Then the solvent was removed under reduced pressure.

The residue was dissolved in chloroform (10 ml), washed with water (10 ml) and dried over $MgSO_4$. The solvent was removed under reduced pressure. Precipitation from chloroform/*n*-hexane afforded sensor **11** (151 mg, 47%) as an olive green powder.

mp: 129-130°C dec; Found: C, 81.8; H, 5.16; N, 4.25. $C_{23}H_{18}BNO_2$-H_2O+0.1$CHCl_3$ requires C, 82.07; H, 4.81; N, 4.14%; (HRMS: Found $[M+2(3\text{-}HOCH_2C_6H_4NO_2)\text{-}2H_2O]^+$, 621.2098. $C_{37}H_{28}BN_3O_6$ requires 621.2071); δ_H (400 MHz; CD_3OD+$CDCl_3$; Me_4Si) 4.68 (2H, s, C*H*$_2$-NH_2), 7.24-7.48 (4H, m, Ar*H*), 7.71-8.17 (9H, m, Ar*H*); δ_C (100 MHz; CD_3OD+$CDCl_3$) 49.7, 120.3, 123.3, 123.5, 123.7, 125.5, 125.8, 125.9, 126.0, 126.7, 127.6, 131.8, 132.3; *m/z* (FAB) 621.2 ($[M+2(3\text{-}HOCH_2C_6H_4NO_2)\text{-}2H_2O]^+$, 100%).

Preparation of the Benzyl-(2-borono-benzyl)-amine (12)

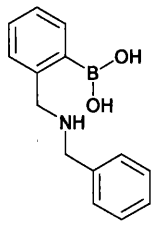

2-Formylphenylboronic acid (3.00 g, 20.00 mmol) was dissolved in a mixture of absolute EtOH/Toluene (90/10) (100 ml) then benzylamine (2.14 g, 20.00 mmol) was added to the reaction. A *Deans and Stark trap* was fixed to the reaction vessel and filled with a mixture of EtOH/Toluene (90/10) (25 ml). The reaction was heated under reflux for 10 hours. After cooling, the solution was diluted with EtOH (50 ml) and cooled to 0°C with an ice bath. Sodium borohydride (3.78 g, 100.00 mmol) was then added slowly to the mixture, which was allowed to warm to room temperature.

The solvent was removed under reduced pressure. Water (100 ml) was added to the residue and the resulting solution was extracted with chloroform (3 × 100 ml). The organic phases were combined, washed with brine (150 ml) and dried over $MgSO_4$. The solvent was then removed *in vacuo*. Precipitation from chloroform/*n*-hexane afforded sensor **12** (1.78 g, 37%) as a white powder.

mp: 118-125°C; (HRMS: Found $[M+H+2(3\text{-}HOCH_2C_6H_4NO_2)\text{-}2H_2O]^+$, 512.1998. $C_{28}H_{27}BN_3O_6$ requires 512.1993); δ_H (300 MHz; CD_3OD) 3.88 (2H, s, C*H*$_2$-NH), 3.99 (2H, s, C*H*$_2$-NH), 7.07-7.11 (1H, m, Ar*H*), 7.21-7.23 (2H, m, Ar*H*), 7.35-7.49 (6H, m, Ar*H*); δ_C (75 MHz; CD_3OD) 52.6, 54.6, 124.7, 128.1, 128.7, 129.9, 130.3 (2C), 131.3 (2C), 132.1, 136.6, 142.7; *m/z* (FAB) 512.2 ($[M+H+2(3\text{-}HOCH_2C_6H_4NO_2)\text{-}2H_2O]^+$, 34%), 359.2 ($[M\text{-}OH+3\text{-}HOCH_2C_6H_4NO_2\text{-}H_2O]^+$, 37%), 91.1 (100%).

Preparation of the *N,N'*-(2-boronobenzyl)-3,3'-methylenedianiline (13)

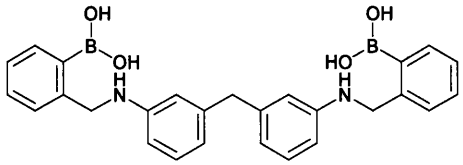

3,3'-Methylenedianiline (131 mg, 0.66 mmol) was dissolved in methanol (8 ml) and 2-formylbenzeneboronic acid (198 mg, 1.32 mmol) was added slowly. The reaction was stirred overnight at room temperature.

The reduction of the diimine was then carried out *in situ* by the slow addition of sodium borohydride (125 mg, 3.30 mmol) to the solution. The reaction was stirred for 1 further hour at room temperature.

The solvent was removed under reduced pressure. Water (30 ml) was added to the solid residue then extracted with chloroform (3 × 30 ml). The organic phases were combined, washed with brine (40 ml) and dried over $MgSO_4$. The solvent was then removed *in vacuo*. The crude product was precipitated from chloroform/*n*-hexane to afford sensor **13** as a yellow solid (174 mg, 56%).

mp: 130°C dec; (Found: C, 70.20; H, 6.08; N, 5.99. $C_{27}H_{28}B_2N_2O_4$+0.15 C_6H_{14} requires C, 69.95; H, 6.33; N, 5.85%); (HRMS: Found $[M+4(3\text{-}HOCH_2C_6H_4NO_2)\text{-}4H_2O]^+$, 1006.3570. $C_{55}H_{48}B_2N_6O_{12}$ requires 1006.3516); δ_H (300 MHz; CD_3OD) 3.70 (2H, s, Ph-C*H*$_2$-Ph), 4.28 (4H, s, PhC*H*$_2$-NH-Ph), 6.45-6.73 (6H, m, Ar*H*), 6.90-7.10 (2H, m, Ar*H*), 7.15-7.33 (8H, m, Ar*H*); δ_C (75 MHz; CD_3OD) 43.8, 51.6, 115.0, 118.0, 120.9, 121.7, 127.6, 129.1, 130.4, 134.0, 144.0, 145.8; *m/z* (FAB) 1006.3 ($[M+4(3\text{-}HOCH_2C_6H_4NO_2)\text{-}4H_2O]^+$, 100%).

Preparation of the *N,N'*-(2-boronobenzyl)-4,4'-methylenedianiline (14)

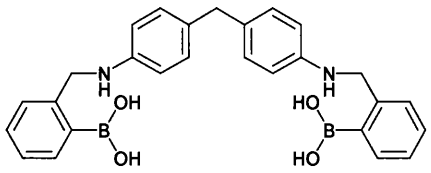

4,4'-Methylenedianiline (131 mg, 0.66 mmol) was dissolved in methanol (8 ml) and 2-formylbenzeneboronic acid (198 mg, 1.32 mmol) was added slowly. The reaction was stirred at room temperature overnight. The reduction of the diimine was then carried out directly *in situ* by the slow addition of sodium borohydride (125 mg, 3.30 mmol) to the solution. The reaction was stirred for 3 further hours at room temperature.

The reaction was poured into ice-water (5 ml) and stirred for 10 minutes. The organic solvent was removed under reduced pressure. Chloroform (2 × 30 ml) was added to the previous aqueous solution and the product was extracted, dried over $MgSO_4$, filtered and evaporated under reduced pressure. The crude product was precipitated from chloroform with *n*-hexane twice to give sensor **14** (90 mg, 29%) as a white powder.

mp: 170°C dec; (Found: C, 73.10; H, 5.80; N, 6.21 $C_{27}H_{28}B_2N_2O_4$-1.2 H_2O requires C, 72.95; H, 5.80; N, 6.30%); (HRMS: Found $[M+4(3\text{-}HOCH_2C_6H_4NO_2)\text{-}4H_2O]^+$ 1006.3555. $C_{55}H_{48}B_2N_6O_{12}$ requires 1006.3516); δ_H (300 MHz; CD_3OD) 3.80 (2H, s, Ph-C*H*$_2$-Ph), 4.30 (4H, s, PhC*H*$_2$-NH-Ph), 6.70-6.80 (4H, m, Ar*H*), 6.90-7.10 (4H, m, Ar*H*), 7.15-7.35 (8H, m, Ar*H*); δ_C (75 MHz; CD_3OD) 40.1 (+), 51.1 (+), 116.8 (-), 125.0 (-), 126.4 (-), 128.1 (-), 129.0 (-), 131.1 (-), 134.8 (+), 144.2 (+), 144.8 (+); *m/z* (FAB) 1006.3 ($[M+4(3\text{-}HOCH_2C_6H_4NO_2)\text{-}4H_2O]^+$, 100%).

Preparation of the *N,N'*-(3-boronobenzyl)-3,3'-methylenedianiline (15)

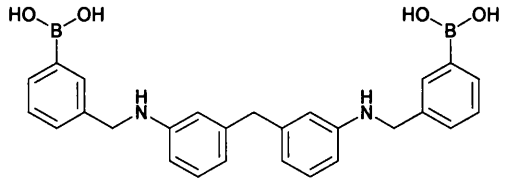

3,3'-Methylenedianiline (200 mg, 1.01 mmol) and 3-formylbenzeneboronic acid (300 mg, 2.00 mmol) were dissolved in a mixture of absolute EtOH/Toluene (90/10) (25 ml). A *Dean and Stark trap* was fitted, filled with of the same mixture EtOH/Toluene (90/10) (25 ml). The reaction was heated at reflux overnight (18 hours). After cooling, sodium borohydride (152 mg, 4.02 mmol) was added slowly to the mixture and stirred for 2 further hours at room temperature.

The solvent was removed under reduced pressure. Water (30 ml) was added to the residue and stirred for a few minutes. Chloroform (30 ml) was added and stirred for a few minutes. The product precipitated and after drying lead to sensor **15** as a cream solid (172 mg, 37%).

mp: >212°C dec; (HRMS: Found $[M+4(3\text{-}HOCH_2C_6H_4NO_2)\text{-}4H_2O]^+$, 1006.3580. $C_{55}H_{48}B_2N_6O_{12}$ requires 1006.3516); δ_H (300 MHz; CD_3OD) 3.69 (2H, s, Ph-C*H*$_2$-Ph), 4.22 (4H, s, PhC*H*$_2$-NH-Ph), 6.35-6.60 (6H, m, Ar*H*), 6.90-7.00 (2H, m, Ar*H*), 7.18-7.33 (4H, m, Ar*H*), 7.45-7.70 (4H, m, Ar*H*); δ_C (100 MHz; CD_3OD + NaOD) 43.3, approximately 49.0 carbon masked by CD_3OD shown by 2D ^1H-^{13}C correlation, 111.9, 115.1, 118.7, 125.3, 127.4, 129.6, 132.7, 133.4, 138.1, 143.2, 150.2; *m/z* (FAB) 1007.0 ($[M+H+4(3\text{-}HOCH_2C_6H_4NO_2)\text{-}4H_2O]^+$, 55%), 603.0 ($[M+(3\text{-}HOCH_2C_6H_4NO_2)\text{-}H_2O]^+$, 40%), 274.0 and 170.0 (100%).

Preparation of *N,N'*-(3-boronobenzyl)-4,4'-methylenedianiline (16)

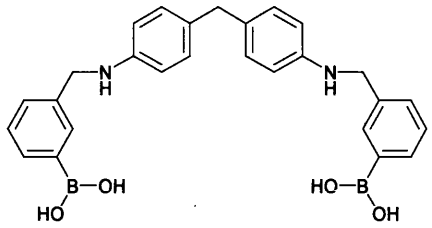

4,4'-methylenedianiline (131 mg, 0.66 mmol) was dissolved in methanol (8 ml) and 3-formylbenzeneboronic acid (198 mg, 1.32 mmol) was added slowly. The reaction was stirred overnight at room temperature. The reduction of the diimine was then carried out directly *in situ* by the slow addition of sodium borohydride (125 mg, 3.30 mmol) to the solution. The reaction was stirred for 2 further hours at room temperature.

The solvent was concentrated under reduced pressure. Water (10 ml) was added to the mixture, then a few drop of aqueous HCl (1 M) were added to reach pH 9. A precipitate was formed and collected by filtration. The precipitate was dried under high *vacuum* to afford the light sensitive sensor **16** as a white powder (192.0 mg, 62%), which became light green when exposed to natural light.

mp: >180°C dec; (HRMS Found: $[M+4(3\text{-}HOCH_2C_6H_4NO_2)\text{-}4H_2O]^+$, 1006.3537. $C_{55}H_{48}B_2N_6O_{12}$ requires 1006.3516); δ_H (300 MHz; CD_3OD) 3.64 (2H, s, Ph-C*H*$_2$-Ph), 4.24 (4H, s, 2PhC*H*$_2$-NH-Ph), 6.50-6.60 (4H, m, Ar*H*), 6.85-6.90 (4H, m, Ar*H*), 7.23-7.40 (4H, m, Ar*H*), 7.45-7.80 (4H, m, Ar*H*); δ_C (100 MHz; CD_3OD) 41.2, approximately 49.0 carbon masked by CD_3OD shown by 2D ^1H-^{13}C correlation, 114.3, 116.8, 128.4, 130.1, 132.0, 140.1, 147.8; *m/z* (FAB) 1006.1 ($[M+4(3\text{-}HOCH_2C_6H_4NO_2)\text{-}4H_2O]^+$, 100%), 1007.1 ($[M+H+4(3\text{-}HOCH_2C_6H_4NO_2)\text{-}4H_2O]^+$, 50%).

Preparation of *N,N'*-(4-boronobenzyl)-3,3'-methylenedianiline (17)

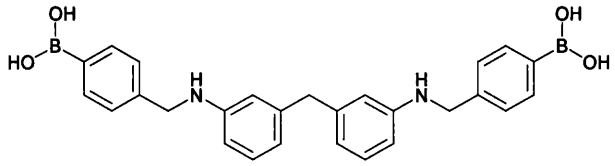

3,3'-Methylenedianiline (131 mg, 0.66 mmol) was dissolved in methanol (8 ml) and 4-formylbenzeneboronic acid (198 mg, 1.32 mmol) was added slowly. The reaction was stirred overnight at room temperature. The reduction of the diimine was then carried out *in situ* by slow addition of sodium borohydride (125 mg, 3.30 mmol) to the solution. The reaction was stirred for 2 further hours at room temperature.

The solvent was concentrated under reduced pressure. Water (10 ml) was added to the mixture, then aqueous HCl (1 ml, 1 M) was added to reach pH 9. A precipitate was formed and collected by filtration. The precipitate was dried under high *vacuum* to afford sensor **17** as a white powder (138 mg, 44%).

mp: 198-204°C dec; (HRMS: Found $[M+4(3\text{-}HOCH_2C_6H_4NO_2)\text{-}4H_2O]^+$, 1006.3596. $C_{55}H_{48}B_2N_6O_{12}$ requires 1006.3516); δ_H (300 MHz; CD_3OD) 3.66 (2H, s, Ph-C*H*$_2$-Ph), 4.22 (4H, s, 2PhC*H*$_2$-NH-Ph), 6.35-6.50 (6H, m, Ar*H*), 6.88-7.00 (2H, m, Ar*H*), 7.20-7.30 (4H, m, Ar*H*), 7.60 (4H, brs, Ar*H*); δ_C (100 MHz; CD_3OD) 42.1, approximately 49.0 carbon masked by CD_3OD shown by 2D ^1H-^{13}C correlation, 110.7, 113.8, 117.8, 126.3, 128.7, 133.7, 142.4, 148.9; *m/z* (FAB) 1006.9 ($[M+4(3\text{-}HOCH_2C_6H_4NO_2)\text{-}4H_2O]^+$, 75%), 1007.1 ($[M+H+4(3\text{-}HOCH_2C_6H_4NO_2)\text{-}4H_2O]^+$, 60%), 330.0 (100%).

Preparation of the *N,N'*-(4-boronobenzyl)-4,4'-methylenedianiline (18)

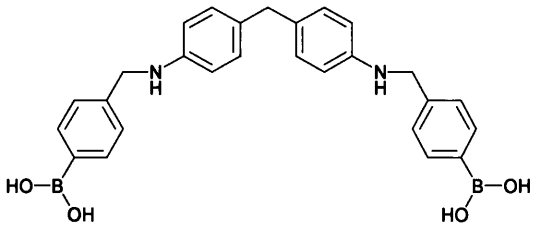

4,4'-Methylenedianiline (131 mg, 0.66 mmol) was dissolved in methanol (8 ml) and 4-formylbenzeneboronic acid (198 mg, 1.32 mmol) was added slowly. The reaction was stirred overnight at room temperature. The reduction of the diimine was then carried out *in situ* by the slow addition of sodium borohydride (125 mg, 3.30 mmol) to the solution. The reaction was stirred for 2 further hours at room temperature.

The solvent was concentrated under reduced pressure. Water (10 ml) was added to the mixture, then a few drop of aqueous HCl (1 M) were added to reach pH 8. A precipitate was formed and collected by filtration. The precipitate was dried under high *vacuum* to afford sensor **18** as a white powder (227 mg, 74%).

mp: >220°C dec; (HRMS: Found $[M+4(3\text{-}HOCH_2C_6H_4NO_2)\text{-}4H_2O]^+$, 1006.3591. $C_{55}H_{48}B_2N_6O_{12}$ requires 1006.3516); δ_H (300 MHz; CD_3OD) 3.65 (2H, s, Ph-C*H*$_2$-Ph), 4.20 (4H, s, 2PhC*H*$_2$-NH-Ph), 6.45-6.55 (4H, m, Ar*H*), 6.80-6.92 (4H, m, Ar*H*), 7.20-7.35 (4H, m, Ar*H*), 7.60 (4H, brs, Ar*H*); δ_C (100 MHz; CD_3OD) 40.1, 48.5, 113.2, 126.2, 129.0, 131.0, 133.6, 146.8; *m/z* (FAB) 1006.0 ($[M+4(3\text{-}HOCH_2C_6H_4NO_2)\text{-}4H_2O]^+$, 100%), 1007.0 ($[M+H+4(3\text{-}HOCH_2C_6H_4NO_2)\text{-}4H_2O]^+$, 100%).

Preparation of the (2-boronobenzyl)-(6,7,9,10,12,13,15,16-octahydro-5,8,11,14,17-pentaoxa-benzocyclopentadecen-2-yl) amine (19)

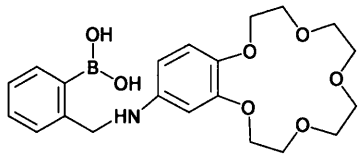

2-Formylbenzeneboronic acid (75 mg, 0.50 mmol) dissolved in THF/MeOH (50/50) (2 ml) was added to a stirred solution of 4-amino-benzo-15-crown-5 (142 mg, 0.50 mmol) in THF/MeOH (50/50) (8 ml). The mixture was stirred overnight at room temperature. Sodium borohydride (95 mg, 2.51 mmol) was slowly added to the solution and stirred for 4 further hours.

After removing the solvents under reduced pressure, the residue was dissolved in chloroform (20 ml), washed with water (2 × 10 ml), brine (10 ml), then dried over $MgSO_4$. The remaining solvent was removed *in vacuo* to afford a brown oil.

The latter was dissolved in water (6 ml) and aqueous NaOH (3 M) was added to reach pH 14. The resulting basic aqueous phase was extracted with diethylether (3 × 5 ml) and the combined organic phases were discarded. The remaining basic aqueous phase was acidified with aqueous HCl (1 M) to reach pH 6. This acidic aqueous phase was extracted with diethylether (3 × 5 ml), the combined organic phases were dried over $MgSO_4$ and concentrated under *vacuo* to afford sensor **19** (59 mg, 28%), as a brown oil. (HRMS Found: $[M+H]^+$, 418.2030. $C_{21}H_{29}BNO_7$ requires 418.2032); δ_H (300 MHz, CD_3OD) 3.70 (8H, s, $4OCH_2$); 3.81-3.85 (4H, m, $2OCH_2$), 4.03-4.06 (4H, m, $2OCH_2$), 4.34 (2H, s, CH_2NH), 6.44 (1H, dd, *J 8.48 and 2.45 Hz*, Ar*H* benzocrown ether), 6.57 (1H, d, *J 2.45 Hz*, Ar*H* benzocrown ether), 6.82 (1H, d, *J 8.48 Hz*, Ar*H* benzocrown ether), 7.20-7.34 (4H, m, Ar*H* boronic acid); δ_C (100 MHz; CD_3OD) 51.6, 68.3, 69.0,

69.4, 69.7, 69.9, 70.0, 70.2, 104.1, 109.1, 115.8, 126.4, 128.1, 131.1, 141.6, 143.4, 143.8, 149.5; *m/z* (ES^+) 418.1 ($[M+H]^+$, 95%), 440.0 ($[M+Na]^+$, 100%).

Preparation of the [3-(5,5'-dimethyl-[1,2,3] dioxaborinan-2-yl)-benzyl]-(6,7,9,10,12,13,15,16-octahydro-5,8,11,14,17-pentaoxa-benzocyclopentadecen-2-yl) amine (20)

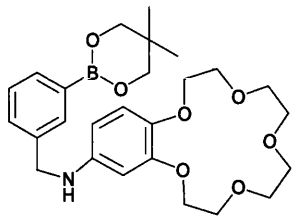

3-Formylphenylboronic acid (75 mg, 0.50 mmol) was dissolved in toluene (12 ml) then 2,2'-dimethyl-1,3-propanediol (57 mg, 0.55 mmol) was added to the reaction. The reaction was heated at reflux for 2 hours. The solvent was removed under reduced pressure to afford the protected boronic acid as a yellow oil with 100% conversion. The protected boronic acid was dissolved in a mixture THF/MeOH (50/50) (10 ml), then the 4-aminobenzo-15-crown-5 (142 mg, 0.50 mmol) was added to the solution. The reaction was stirred overnight at room temperature. The reduction of the imine product was then carried out by the slow addition of sodium borohydride (95 mg, 2.51 mmol) to the solution. The reaction was stirred for 3 further hours at room temperature.

The solvent was removed under reduced pressure. Chloroform (20 ml) was added to the residue and the resulting solution (after 10 min stirring) was washed with water (2 × 20 ml), brine (20 ml) and dried over $MgSO_4$. The solvent was then removed under reduced pressure to afford sensor **20** (143 mg, 59%) as an apricot oil.

Found: C, 61.8; H, 7.39; N, 3.00. $C_{26}H_{36}BNO_7 + 0.19\ CHCl_3$ requires C, 61.91; H, 7.18; N, 2.76%); (HRMS: Found $[M]^+$, 485.2605. $C_{26}H_{36}BNO_7$ requires 485.2585); δ_H (300 MHz; $CDCl_3$; Me_4Si) 0.95 (6H, s, $2CH_3$), 3.67 (8H, s, $4OCH_2$), 3.69 (4H, s, $2OCH_2$ protected boronic acid), 3.78-3.85 (4H, m, $2OCH_2$), 3.97-4.03 (4H, m, $2OCH_2$), 4.18 (2H, s, CH_2-NH), 6.09 (1H, dd, *J 8.48 Hz and 2.64 Hz*, Ar*H*), 6.17 (1H, d app, *J 2.64*

Hz, Ar*H*), 6.69 (1H, d app, *J 8.48 Hz*, Ar*H*), 7.26 (1H, t, *J 7.7 Hz*, Ar*H BA*), 7.36 (1H, d app, *J 7.7 Hz*, Ar*H BA*), 7.64 (1H, d app, *J 7.3 Hz*, Ar*H BA*), 7.72 (1H, m, Ar*H BA*); δ_C (75 MHz; $CDCl_3$) 22.3 (2C), 32.3 (2C), 49.6, 69.0, 70.0, 70.4, 70.8, 71.2, 72.7 (2C), 101.0, 105.0, 117.7, 128.3, 130.5, 133.2, 133.5, 138.86, 141.6, 144.4, 150.8; *m/z* (FAB^+) 485.2 ($[M]^+$, 100%).

Preparation of [4-(5,5'-dimethyl- [1,2,3] dioxaborinan-2-yl)-benzyl]-(6,7,9,10,12,13,15,16-octahydro-5,8,11,14,17-pentaoxa-benzocyclopentadecen-2-yl) amine (21)

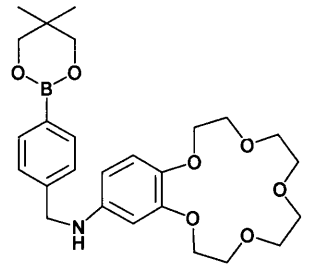

4-Formylphenylboronic acid (75 mg, 0.50 mmol) was dissolved in toluene (15 ml) then 2,2'-dimethyl-1,3-propanediol (57 mg, 0.55 mmol) was added to the reaction. The reaction was heated under reflux for 2 hours. The solvent was removed under reduced pressure to afford the protected boronic acid as a white solid (100% conversion). The protected boronic acid was dissolved in a mixture THF/MeOH (50/50) (10 ml), then the 4-aminobenzo-15-crown-5 (142 mg, 0.50 mmol) was added to the solution. The reaction was stirred overnight at room temperature. The reduction of the imine product was then carried out by the slow addition of sodium borohydride (95 mg, 2.51 mmol) to the solution. The reaction was stirred for 3 further hours at room temperature.

The solvent was removed under reduced pressure. Chloroform (20 ml) was added to the residue and the resulting solution (after 10 min stirring) was washed with water (2 × 20 ml), brine (20 ml) and dried over $MgSO_4$. The solvent was then removed under reduced pressure, drying under high *vacuum* for 1 hour leading to sensor **21** (101 mg, 42%) as white foam.

Found: C, 60.40; H, 7.08; N, 2.75. $C_{26}H_{36}BNO_7$ + 0.31 $CHCl_3$ requires C, 60.49; H, 7.00; N, 2.68%); (HRMS: Found $[M]^+$, 485.2602. $C_{26}H_{36}BNO_7$ requires 485.2585); δ_H (300 MHz; $CDCl_3$; Me_4Si) 0.95 (6H, s, $2CH_3$), 3.67 (8H, s, $4OCH_2$), 3.70 (4H, s,

2OC*H*$_2$ protected boronic acid), 3.79-3.82 (4H, m, 2OC*H*$_2$), 3.97-4.00 (4H, m, 2OC*H*$_2$), 4.20 (2H, s, C*H*$_2$-NH), 6.08 (1H, dd, *J 8.48 and 2.64 Hz*, Ar*H*), 6.16 (1H, d, *J 2.45 Hz*, Ar*H*), 6.69 (1H, d, *J 8.48 Hz*, Ar*H*), 7.28 (2H, d, *J 7.91 Hz*, Ar*H* boronic acid), 7.70 (2H, d, *J 7.91 Hz*, Ar*H* boronic acid); δ_C (75 MHz; $CDCl_3$) 22.3 (2C), 32.3 (2C), 49.5, 69.00, 70.0, 70.4, 70.9, 71.2, 72.7, 101.0, 105.0, 118.0, 127.2 (2C), 134.6 (2C), 141.6, 142.4, 144.3, 151.0; *m/z* (FAB^+) 485.2 ($[M]^+$, 100%).

Preparation of the crystal of β-D-Arabinose diphenylboronic acid complex (22)

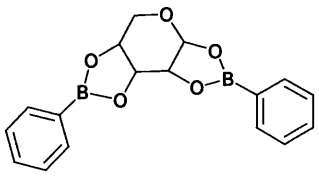

Phenylboronic acid (244 mg, 2.00 mmol) was put in solution in toluene (25 ml) then β-D-arabinose (150 mg, 1.00 mmol) was added to the reaction. A *Deans and Stark trap* was fitted to the vessel and the side arm was filled with toluene (25 ml). The reaction was heated under reflux for 2 hours.

The solvent was removed under reduced pressure to afford compound **22** as a white crystal (338 mg, quantitative). Some of this solid (30 mg) was crystallised from toluene/hexane (1/2) to afford the single crystal analysed by X-ray.

mp: 160-162°C; (HRMS: Found $[M]^+$, 322.1181 $C_{17}H_{16}B_2O_5$ requires 322.1178); δ_H (300 MHz; $CDCl_3$; Me_4Si) 3.65 (1H, dd, *J* 13.74 and 1.89 *Hz*, *H5*), 3.82 (1H, d, *J* 13.74 *Hz*, *H5'*), 4.63 (1H, dd, *J* 8.46 and 1.71 *Hz*, *H4*), 4.74 (1H, dd, *J* 6.03 and 2.46 *Hz*, *H2*), 5.00 (1H, dd, *J* 8.46 and 2.46 *Hz*, *H3*), 5.89 (1H, d, *J* 6.03 *Hz*, *H1*), 7.30-7.51 (5H, m, Ar*H*), 7.74-7.84 (5H, m, Ar*H*); δ_C (75 MHz; $CDCl_3$) 60.7, 72.5, 72.8, 72.9, 97.7, 128.3 (2C), 128.4 (2C), 132.2, 132.8, 135.4 (2C), 135.7 (2C); *m/z* (EI) 322.2 ($[M]^+$, 70%), (CI) 340.2 ($[M+NH_4]^+$, 100%).

3.3 Fluorescence measurements

The osmotic buffer solutions were prepared with HPLC grade methanol (33.3wt% or 52.1wt%), deionized water and NaCl·0.05 $mol.dm^{-3}$ and stored in a dark cool place.

The pH 8.21 buffer was prepared according to literature procedure [101] as follows. 52.1wt% HPLC grade methanol in deionized water with KCl, 0.01000 $mol.dm^{-3}$; KH_2PO_4, 0.002752 $mol.dm^{-3}$; Na_2HPO_4, 0.002757 $mol.dm^{-3}$ and stored in a dark cool place.

The HEPES buffer (0.1 M, methanol/water 50/50 v/v) was made from a HEPES buffer (1 M, in water) as follow. HEPES salt (23.83 g) were weighed and dissolved in deionized and degassed water in a 100 ml volumetric flask. In order to make 500 ml of HEPES buffer (0.1 M, methanol/water 50/50 v/v), 50 ml of the HEPES (1 M, in water), 250 ml of HPLC methanol and 43.6 ml of aqueous NaOH (0.974 M), were measured, and made up to exactly 500 ml with deionized and degassed water to lead to the HEPES buffer used in the titration described herein. The pH of this buffer has been measured and the value is pH = 8.53.

The experiments in organic media were carried out in HPLC grade methanol.

Stock solutions of sensors were prepared at a concentration of 1.0×10^{-2} $mol.dm^{-3}$, 1.09×10^{-2} $mol.dm^{-3}$ and 2.2×10^{-2} $mol.dm^{-3}$ for sensors **1, 2, 3, 4, 5, 6, 7,** sensor **9,** and sensors **13, 14, 15, 16, 17, 18** respectively in 10.0 ml of HPLC grade methanol prepared prior to use and stored at 5°C in the dark until required.

Fluorescence pH-titrations of **1, 2, 3, 5, 6, 7** and **9**

The fluorescence emission spectra of **1**, **2**, **3**, **5**, **6**, **7** and **9** (1.0×10^{-5} mol.dm^{-3}) in an osmotic buffer (52.1wt% methanol in water with NaCl 0.05 mol.dm^{-3}) were recorded as the pH varied from pH 2 to 12 in approximate intervals of 0.5 pH units. The pH was controlled using minimal volumes of sodium hydroxide and hydrochloric acid solutions. The same experiment was repeated with **1** (1.0×10^{-5} mol.dm^{-3}) in an osmotic buffer (33.3 wt% methanol in water with NaCl 0.05 mol.dm^{-3}).

Fluorescence pH-titrations of **1, 2, 3, 5, 6, 7** and **9** in the presence of D-fructose

The previous experiments were repeated with the addition of 0.05 mol.dm^{-3} of D-fructose to the solution in all cases prior to start.

Fluorescence pH-titrations of **13** and **14**

The fluorescence emission spectra of **13** and **14** (4.2×10^{-5} mol.dm^{-3}) in an osmotic buffer (52.1wt% methanol in water with NaCl 0.05 mol.dm^{-3}) were recorded as the pH varied from pH 2 to 12 in approximate intervals of 0.5 pH units. The pH was controlled using minimal volumes of sodium hydroxide and hydrochloric acid solutions.

Fluorescence pH-titrations of **13** and **14** in the presence of D-fructose

The previous experiments were repeated with the addition of 0.05 mol.dm^{-3} of D-fructose to the solution in all cases prior to start.

Fluorescence Saccharide titrations of **1**, **2**, **3**, **5**, **6**, **7** and **9** at pH 8.21

The sensor molecules were evaluated by the use of fluorescence spectroscopy. The fluorescence emission spectra of each sensor in a pH 8.21 buffer (52.1wt% methanol in water with KCl, 0.01000 mol.dm^{-3}; KH_2PO_4, 0.002752 mol.dm^{-3}; Na_2HPO_4, 0.002757 mol.dm^{-3})[101] was recorded as increasing amounts of D-monosaccharide were added to the solution to reach the saccharide concentration of 0 to 0.1 mol.dm^{-3}.

The fluorescence emission spectra of sensors **1**, **5**, **7** (2.0×10^{-5} mol.dm^{-3}), **2**, **3** (1.0×10^{-5} mol.dm^{-3}), **9** (2.2×10^{-5} mol.dm^{-3}) and **6** (4.0×10^{-5} mol.dm^{-3}) in a pH 8.21 buffer were recorded as increasing amounts of various saccharides (D-fructose, D-glucose, D-galactose and D-mannose) were added to the solution.

Fluorescence Saccharide titrations of **1** in HEPES and in ionic buffer

The fluorescence emission spectra of sensors **1** (2.0×10^{-5} mol.dm^{-3}), in a pH 8.53 (0.1 mol.dm^{-3}, 50 v/v MeOH/water) HEPES buffer or in an ionic buffer (52.1wt% MeOH/water and NaCl 0.05 mol.dm^{-3}) were recorded as increasing amounts of D-fructose, were added to the solution.

Fluorescence Saccharide titrations of **8** at pH 8.21

The fluorescence emission spectra of sensor **8** (2.0×10^{-5} mol.dm^{-3}) in a pH 8.21 buffer were recorded with increasing amounts of D-fructose. No fluorescence changes were detected.

Fluorescence Saccharide titrations of **10** and **11** at pH 8.21

The fluorescence emission spectra of sensors **10** (2.0×10^{-6} mol.dm^{-3}) and **11** (2.5×10^{-7} mol.dm^{-3}) in a pH 8.21 buffer were recorded as increasing amounts of various saccharides (D-fructose, D-glucose, D-galactose and D-mannose) were added to the solution.

Fluorescence Saccharide titrations of **13, 14, 15, 16, 17** and **18** at pH 8.21

The fluorescence emission spectra of sensors **13, 14** (4.2×10^{-5} mol.dm^{-3}), **15, 16, 17, 18** (4.0×10^{-5} mol.dm^{-3}) in a pH 8.21 buffer were recorded as increasing amounts of various saccharides (D-fructose, D-glucose, D-galactose and D-mannose) were added to the solution.

Fluorescence Potassium Halide titrations of **1, 2, 3, 5, 6, 7** and **9** at pH 8.21

The fluorescence emission spectra of **1, 2, 3, 5, 7** (2.0×10^{-5} mol.dm^{-3}), **6** (4.0×10^{-5} mol.dm^{-3}) and **9** (2.2×10^{-5} mol.dm^{-3}) in HPLC grade methanol, were recorded as increasing amounts of various potassium halides (KF, KCl and KBr) were added to the solution. After each addition of salt, the solutions were allowed to stir for at least 2 minutes before fluorescence measurements were taken, to allow complete dissolution of the salt.

Fluorescence measurements for the quantum yield of **1, 2, 3, 5, 6, 7, 9,** and aniline

Fluorescence emission measurements were recorded for compounds **1, 2, 3, 5, 6, 7, 9** and aniline at the concentration of (2×10^{-5} mol.dm^{-3}), in HPLC grade methanol.

Fluorescence measurements in methanol of **1** and **4**

The experiment was performed with compound **4** (4.7×10^{-5} mol.dm^{-3}) and sensor **1** (4.7×10^{-5} mol.dm^{-3}) successively at two different excitation wavelengths 244 and 274 nm. An emission spectrum was recorded for each wavelength and for compound **4** and sensor **1**.

A drop of base (NaOH 3 M) was added in solution of sensor **1** and then emission spectra of sensor **1** were recorded respectively at excitation wavelengths of 244 and 274 nm.

Excitation spectra of compound **4** were recorded by choosing the emission wavelength at 342 nm. Excitation spectra of sensor **1** were recorded at emission wavelength 393 nm in the absence and in the presence of base. The experimental conditions are the same as the one above.

Fluorescence excitation Saccharide titrations of **1** and **13**

The fluorescence excitation spectra of sensor **1** (2.0×10^{-5} mol.dm^{-3}) at emission wavelength 393 nm, and sensor **13** (4.2×10^{-5} mol.dm^{-3}) at emission wavelength 400 nm in a pH 8.21 buffer were recorded as increasing amounts of D-fructose were added to the solution (0 to 0.1 mol.dm^{-3}).

3.4 UV-Visible measurements

UV-Visible titration of 1 with D-fructose

The UV-visible absorption spectra of **1** (5.0×10^{-5} mol.dm^{-3}) in a pH 8.21 buffer (52.1wt% methanol in water with KCl, 0.01000 mol.dm^{-3}; KH_2PO_4, 0.002752 mol.dm^{-3}; Na_2HPO_4, 0.002757 mol.dm^{-3}) [101] were recorded as increasing amounts of D-fructose was added to the solution (0 to 0.1 mol.dm^{-3}).

UV-Visible measurements for the quantum yield of **1, 2, 3, 5, 6, 7, 9,** and aniline

Absorbance measurements were recorded for compounds **1**, **2**, **3**, **5**, **6**, **7**, at the 3 different concentration of (1×10^{-2} mol.dm^{-3}), (2×10^{-4} mol.dm^{-3}), (2×10^{-5} mol.dm^{-3}), except for **9** the concentration were as followed (1.09×10^{-2} mol.dm^{-3}), (2.18×10^{-4} mol.dm^{-3}), (2.18×10^{-5} mol.dm^{-3}) and aniline (2.2×10^{-2} mol.dm^{-3}), (2×10^{-4} mol.dm^{-3}), (2×10^{-5} mol.dm^{-3}). Each solution was prepared in HPLC grade methanol. The two highest dilutions were prepared in serial dilution from the concentrated solution.

Chapter 4

Conclusions

" One never notices what has been done; one can only see what remains to be done."

Marie Curie (1867 – 1934)

Conclusions and future work

A series of boronic acid based sensors for saccharides and fluoride were designed and successfully synthesised.

Saccharide investigation

Sensor **1** (excited at 274 nm) turned to be a TICT system displaying dual fluorescence, involving TICT (band at 404 nm) and LE (band at 360 nm) states. The change from TICT to LE state is due to the breakdown of the B-N bond when the complex with saccharide is formed. Therefore, two species are observed, the unbound and bound. Sensor **1** can also display only a LE state (band at 360 nm) when excited at 244 nm.

Sensors **2** and **3** display only LE (band at 350 nm) state, high fluorescence enhancements (18 and 25 fold respectively) and large affinity for D-Fructose (212 $mol^{-1}.dm^3$ for **2** and 128 $mol^{-1}.dm^3$ for **3**) when excited at 240 and 244 nm respectively. Fluorescence enhancements are attributed to the fluorescence recovery of the aniline fluorophore. With these systems in the absence of saccharides, fluorescence (band at 350 nm) of the LE state of the aniline donor is quenched by energy transfer to the phenylboronic acid acceptor. When saccharides are added, a negatively charged boronate anion is formed and under these conditions, energy transfer from aniline donor is unfavourable and fluorescence recovery of LE state is observed. Quantum yield measurements confirmed this hypothesis.

Sensor **5** is the only sensor where the fluorescence is quenched. The decrease of fluorescence observed is due to the decrease of the unbound species (TICT state), as the bound species (LE state) in this case is non-fluorescent.

Addition of electron-donating group do not alter the system significantly. Changing the fluorophore from benzene to naphathalene (**10**) or pyrene (**11**) reduces sensitivity but extends the working wavelength of the sensors.

Diboronic acid sensor **13** displays enhanced selectivity for D-glucose, due to optimal spacing of boronic acid groups and form a 1:1 rigid complex.

A higher stability constant for D-fructose with boronic acid groups in *meta*-position (sensors **15** and **16**) is observed, while the largest fluorescence enhancement is observed with boronic acid groups in *para*-position (sensors **17** and **18**).

Fluoride investigation

Sensors **2** and **3** turned out to be highly selective sensors and displayed high affinity for fluoride. Sensors **2** and **3** are 50 and 40 times more selective for fluoride than sensor **1**. There is a clear trend between pK_a and observed stability constant with fluoride. However, sensor **5, 6, 7** do not have a good affinity for fluoride. Sensor **5** quenched the fluorescence on addition of fluoride. Other potassium halides (KCl, KBr) do not lead to change in fluorescence behaviour, so all sensors are fluoride selective.

Crown ether sensors were designed to work as logic gate sensors, as the crown ether and the boronic acid can recognize two different guests. Future work will involve the investigation of these possible logic gates (sensors **19, 20** and **21**).

Chapter 5

References

"If I have seen further than others, it is by standing upon the shoulders of giants."

Newton, Isaac (1642-1727)

1. Granda-Valdés, M., Badía, R., Pina-Luis, G., and Díaz-García, M.E., *Quim. Anal.*, 2000, **19**, 38.
2. Wayne, C.E. and Wayne, R.P. *Photochemistry*; Oxford University Press, 1996.
3. Nassau, K. *The Physics and Chemistry of Color*; J. Wiley & Sons, 1983.
4. UK Prospective Diabetes Study Group, *The Lancet*, 1998, **352**, 837.
5. James, T.D., Linnane, P., and Shinkai, S., *Chem. Commun.*, 1996, 281.
6. James, T.D., Sandanayake, K.R.A.S., and Shinkai, S., *Angew. Chem., Int. Ed.*, 1996, **35**, 1911.
7. Cattrall, R.W. *Chemical Sensors*; Oxford University Press: Oxford, 1997; Vol. 52.
8. Vyas, N.K., Vyas, M.N., and Quiocho, F.A., *Science*, 1988, **242**, 1290.
9. Davis, A.P. and Wareham, R.S., *Angew. Chem., Int. Ed.*, 1999, **38**, 2979.
10. Davis, A.P. and Wareham, R.S., *Angew. Chem., Int. Ed.*, 1998, **37**, 2270.
11. Lecollinet, G., Dominey, A.P., Velasco, T., and Davis, A.P., *Angew. Chem., Int. Ed.*, 2002, **41**, 4093.
12. Tamaru, S., Yamamoto, M., Shinkai, S., Khasanov, A., and Bell, T.W., *Chem. Eur. J.*, 2001, **7**, 5270.
13. Mazik, M., Radunz, W., and Sicking, W., *Org. Lett.*, 2002, **4**, 4579.
14. Rusin, O., Lang, K., and Kral, V., *Chem. Eur. J.*, 2002, **8**, 655.
15. Droz, A., Neidlein, U., Anderson, S., Seiler, P., and Diederich, F., *Helv. Chem. Acta*, 2001, **84**, 2243.
16. Nagase, T., Nakata, E., Shinaki, S., and Hamachi, I., *Chem. Eur. J.*, 2003, **9**, 3660.
17. Segura, M., Bricoli, B., Casnati, A., Munoz, E.M., Sansone, F., Ungaro, R., and Vincent, C., *J. Org. Chem.*, 2003, **68**, 6296.
18. Michaelis, A. and Becker, P., *Ber. Dtsch. Chem. Ges.*, 1880, **13**, 58.
19. Kuivila, H.G., Keough, A.H., and Soboczenski, E.J., *J. Org. Chem.*, 1954, **19**, 780.
20. Sugihara, J.M. and Bowman, C.M., *J. Am. Chem. Soc.*, 1958, **80**, 2443.
21. Lorand, J.P. and Edwards, J.O., *J. Org. Chem.*, 1959, **24**, 769.
22. Bielęcki, M., Eggert, H., and Norrild, J.C., *J. Chem. Soc., Perkin Trans. 2*, 1999, 449.
23. Hartley, J.H., James, T.D., and Ward, C.J., *J. Chem. Soc., Perkin Trans. 1*, 2000, 3155.
24. James, T.D. and Shinkai, S., *Host-Guest Chemistry*, 2002, **218**, 159.
25. de Silva, A.P., Gunaratne, H.Q.N., Gunnlaugsson, T., Huxley, A.J.M., McCoy, C.P., Rademacher, J.T., and Rice, T.E., *Chem. Rev.*, 1997, **97**, 1515.
26. Wang, W., Gao, X., and Wang, B., *Curr. Org. Chem.*, 2002, **6**, 1285.
27. Striegler, S., *Curr. Org. Chem.*, 2003, **7**, 81.
28. Hartley, J.H., *Saccharide accelerated hydrolysis of boronic acid imines*, in *Ph.D Thesis University of Birmingham, UK.* 2001, Birmingham.
29. Hartley, J.H., Phillips, M.D., and James, T.D., *New J. Chem.*, 2002, **26**, 1228.
30. Wulff, G., *Pure Appl. Chem.*, 1982, **54**, 2093.
31. Rettig, W., *Angew. Chem., Int. Ed. Engl.*, 1986, **25**, 971.
32. Yoon, J. and Czarnik, A.W., *J. Am. Chem. Soc.*, 1992, **114**, 5874.
33. Yoon, J. and Czarnik, A.W., *Biorg. Med. Chem.* , 1993, **1**, 267.
34. Nagai, Y., Kobayashi, K., Toi, H., and Aoyama, Y., *Bull. Chem. Soc. Jpn.*, 1993, **66**, 2965.
35. Suenaga, H., Mikami, M., Sandanayake, K.R.A.S., and Shinkai, S., *Tetrahedron Lett.*, 1995, **36**, 4825.

36. Suenaga, H., Yamamoto, H., and Shinkai, S., *Pure Appl. Chem.*, 1996, **68**, 2179.
37. Shinmori, H., Takeuchi, M., and Shinkai, S., *Tetrahedron*, 1995, **51**, 1893.
38. DiCesare, N. and Lakowicz, J.R., *J. Phys. Chem. A* 2001, **105**, 6834.
39. Sandanayake, K.R.A.S., Imazu, S., James, T.D., Mikami, M., and Shinkai, S., *Chem. Lett.*, 1995, 139.
40. DiCesare, N. and Lakowicz, J.R., *J. Biomed. Opt.*, 2002, **7**, 538.
41. Di Cesare, N. and Lakowicz, J.R., *J. Photochem. Photobiol., A*, 2001, **143**, 39.
42. DiCesare, N. and Lakowicz, J.R., *Chem. Commun.*, 2001, 2022.
43. DiCesare, N. and Lakowicz, J.R., *Tetrahedron Lett.*, 2001, **42**, 9105.
44. DiCesare, N. and Lakowicz, J.R., *Tetrahedron Lett.*, 2002, **43**, 2615.
45. Gao, X., Zhang, Y., and Wang, B., *Org. Lett.*, 2003, **5**, 4615.
46. James, T.D., Sandanayake, K.R.A.S., and Shinkai, S., *J. Chem. Soc., Chem. Commun.*, 1994, 477.
47. Cooper, C.R. and James, T.D., *J. Chem. Soc., Perkin Trans. 1*, 2000, 963.
48. Bissell, R.A., deSilva, A.P., Gunaratne, H.Q.N., Linch, P.L.M., McCoy, C.P., Maguire, G.E.M., and Sandanayake, K.R.A.S. *Fluorescent Chemosensors of Ion and Molecule Recognition*; American Chemical Society: Washington, 1993; Vol. 206.
49. James, T.D., Sandanayake, K.R.A.S., Iguchi, R., and Shinkai, S., *J. Am. Chem. Soc.*, 1995, **117**, 8982.
50. James, T.D., Sandanayake, K.R.A.S., and Shinkai, S., *Angew. Chem., Int. Ed.*, 1994, **33**, 2207.
51. Sandanayake, K.R.A.S., James, T.D., and Shinkai, S., *Chem. Lett.*, 1995, 503.
52. Arimori, S., Phillips, M.D., and James, T.D., *Tetrahedron Lett.*, 2003, in press.
53. Arimori, S., Consiglio, G.A., Phillips, M.D., and James, T.D., *Tetrahedron Lett.*, 2003, **44**, 4789.
54. Arimori, S., Bell, M.L., Oh, C.S., and James, T.D., *Org. Lett.*, 2002, **4**, 4249.
55. Cooper, C.R. and James, T.D., *Chem. Commun.*, 1997, 1419.
56. Takeuchi, M., Yamamoto, M., and Shinkai, S., *Chem. Commun.*, 1997, 1731.
57. Yamamoto, M., Takeuchi, M., and Shinkai, S., *Tetrahedron*, 1998, **54**, 3125.
58. Yang, W., Yan, J., Fang, H., and Wang, B., *Chem. Commun.*, 2003, 792.
59. Brown, G.J., DeSilva, A.P., and Pagliari, S., *Chem. Commun.*, 2002, **21**, 2461.
60. de Silva, A.P. and McClenaghan, N.D., *Chem.Eur. J.*, 2002, **8**, 4935.
61. de Silva, A.P., Gunaratne, H.Q.N., and Sandanayake, K.R.A.S., *Tetrahedron Lett.*, 1990, **31**, 5193.
62. de Silva, A.P., Gunaratne, H.Q.N., and McCoy, C.P., *Nature*, 1993, **364**, 42.
63. Beer, P.D. and Gale, P.A., *Angew. Chem., Int. Ed.*, 2001, **40**, 486.
64. Martinez-Manez, R. and Sancenon, F., *Chem. Rev.*, 2003, **103**, 4419.
65. Miyaji, H. and Sessler, J.L., *Angew. Chem., Int. Ed.*, 2001, **40**, 154.
66. Metzger, A. and Anslyn, E.V., *Angew. Chem., Int. Ed.*, 1998, **37**, 649.
67. Lavigne, J.J. and Anslyn, E.V., *Angew. Chem., Int. Ed.*, 1999, **38**, 3666.
68. Wiskur, S.L. and Anslyn, E.V., *J. Am. Chem. Soc.*, 2001, **123**, 10109.
69. Wiskur, S.L., Ait-Haddou, H., Lavigne, J.J., and Anslyn, E.V., *Acc. Chem. Res.*, 2001, **34**, 963.
70. Huston, M.E., Engin, U.A., and Czarnik, A.W., *J. Am. Chem. Soc.*, 1989, **111**, 8735.
71. Gale, P.A., Special issue, *Coordination Chemistry Reviews*, 2003, **240**, 1.
72. Kissa, E., *Clin. Chem.*, 1987, **33**, 253.
73. Geddes, C.D., *Meas. sci. Technol.*, 2001, **12**, R53.

74. Kirk, K.L. *Biochemistry of the Elemental Halogens and Inorganic Halides*; Plenum Press, 1991.
75. Sonh, H., Letant, S., Sailor, M.J., and Trogler, W.C., *J. Am. Chem. Soc.*, 2000, **122**, 5399.
76. Noort, D., Benschop, H.P., and Black, R.M., *Toxicol. Appl. Pharmacol.*, 2002, **184**, 116.
77. Frant, M.S. and Ross, J.W., *Science*, 1966, **154**, 1533.
78. Miyaji, H., Anzenbacher, P., Sessler, J.L., Bleasdale, E.R., and Gale, P.A., *Chem. Commun.*, 1999, 1723.
79. Anzenbacher, P., Jr,, Jursikova, K., and Sessler, J.L., *J. Am. Chem. Soc.*, 2000, **122**, 9350.
80. Kim, S.K. and Yoon, J., *Chem. Commun.*, 2002, 770.
81. Camiolo, S., Gale, P.A., Hursthouse, M.B., Light, M.E., and Warriner, C.N., *Tetrahedron Lett.*, 2003, **44**, 1367.
82. Shao, S., Guo, Y., Jiang, S., and Yu, X., *Tetrahedron Lett.*, 2003, **44**, 2175.
83. Jacobson, S. and Pizer, R., *J. Am. Chem. Soc.*, 1993, 11216.
84. Paugam, M.F. and Smith, B.D., *Tetrahedron Lett.*, 1993, **34**.
85. Katz, H.E., *J. Org. Chem.*, 1985, **50**, 5027.
86. Katz, H.E., *J. Am. Chem. Soc.*, 1985, **107**, 1420.
87. Ward, C.J., Patel, P., and James, T.D., *Chem. Lett.*, 2001, 406.
88. Ward, C.J., Patel, P., Ashton, P.R., and James, T.D., *Chem. Commun.*, 2000, 229.
89. DiCesare, N. and Lakowicz, J.R., *Anal. Biochem.*, 2002, **301**, 111.
90. Dusemund, C., Sandanayake, K.R.A.S., and Shinkai, S., *J. Chem. Soc., Chem. Commun.*, 1995, 333.
91. Ori, A. and Shinkai, S., *J. Chem. Soc., Chem. Commun.*, 1995, 1771.
92. Yamamoto, H., Ori, A., Ueda, K., Dusemund, C., and Shinkai, S., *Chem. Commun.*, 1996, 407.
93. Norrild, J.C. and Sotofte, I., *J. Chem. Soc., Perkin Trans. 2*, 2002, 303.
94. Norrild, J.C. and Sotofte, I., *J. Chem. Soc., Perkin Trans. 2*, 2001, 727.
95. Seaman, W. and Johnson, J.R., *J. Am. Chem. Soc.*, 1931, **53**, 711.
96. Ward, C.J., *The Design and Synthesis of Boronic acid Dye Molecules,* in *Ph.D Thesis University of Bath, UK,* 2001, Bath.
97. Reetz, M.T., Huff, J., and Goddard, R., *Tetrahedron Lett.*, 1994, **35**, 2521.
98. Bates, R.G. *Determination of pH, Theory and practice*; John Wiley & Sons, Inc.: London, 1964.
99. De Ligny, C.S. and Rehbach, M., *Rec. trav. chim. Pays-Bas*, 1960, **79**, 727.
100. Arimori, S., Bosch, L.I., Ward, C.J., and James, T.D., *Tetrahedron Lett.*, 2001, **42**, 4553.
101. Perrin, D.D. and Dempsey, B. *Buffers for pH and Metal Ion Control*; Chapman and Hall: London, 1974.
102. Collins, P. and Ferrier, R. *Monosaccharides: Their Chemistry and Their Roles in Natural Products*; John Wiley & Sons Ltd: Chichester, 1995.
103. Eggert, H., Frederiksen, J., Morin, C., and Norrild, J.C., *J. Org. Chem.*, 1999, **64**, 3846.
104. Norrild, J.C. and Eggert, H., *J. Am. Chem. Soc.*, 1995, **117**, 1479.
105. Norrild, J.C. and Eggert, H., *J. Chem. Soc., Perkin Trans. 2*, 1996, 2583.
106. Bosch, L.I., Fyles, T.M., and James, T.D., *J. Phys. Chem.*, 2003, submitted.
107. Rettig, W. and Chandross, E.A., *J. Am. Chem. Soc.*, 1985, **107**, 5617.

108. Grabowski, Z.R., Rotkiewicz, K., Siemiarczuk, A., Cowley, D.J., and Baumann, W., *Nouv. J. Chim*, 1979, **3**, 443.
109. Joedicke, C.J. and Luethi, H.P., *J. Am. Chem. Soc.*, 2003, **125**, 252.
110. Bosch, L.I. and James, T.D., *Tetrahedron Lett.*, 2003, in press.
111. Perichet, G., Chapelon, R., and Pouyet, B., *J. Photochem.*, 1980, **13**, 67.
112. Schulman, S.G. *Fluorescence and Phosphorescence Spectroscopy: Physicochemical Principles and Practice*; Pergamon press: Oxford, 1977; Vol. 59.
113. Arimori, S., Bosch, L.I., Ward, C.J., and James, T.D., *Tetrahedron Lett.*, 2002, **43**, 911.
114. Arimori, S., Bell, M.L., Oh, C.S., Frimat, K.A., and James, T.D., *J. Chem. Soc., Perkin Trans. 1*, 2002, 803.
115. Cooper, C.R., Spencer, N., and James, T.D., *Chem. Commun.*, 1998, 1365.
116. Yuchi, A., Tatebe, A., Kani, S., and James, T.D., *Bull. Chem. Soc. Jpn.*, 2001, **74**, 509.

Appendix

"Science may set limits to knowledge, but should not set limits to imagination. "

Russell, Bertrand (1872 - 1970)

Appendix 1. Crystal structure of sensor **1**.

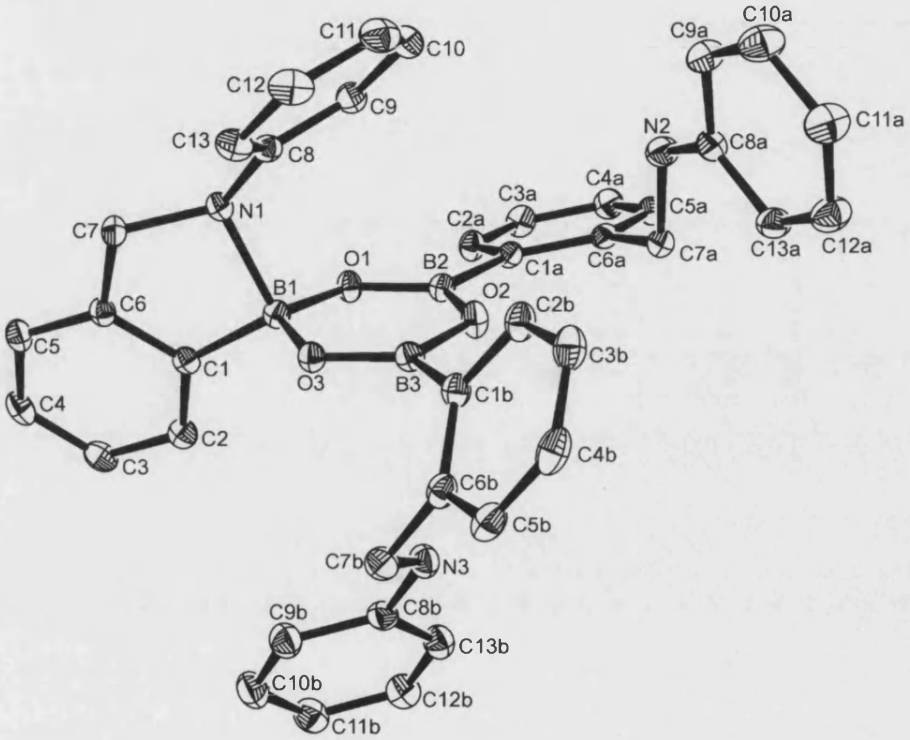

Table 1: Crystal data and structure refinement for of sensor **1**.

Identification code	k02tdj4
Empirical formula	$C_{39}H_{36}B_3N_3O_3$
Formula weight	627.14
Temperature	150(2) K
Wavelength	0.71073 Å
Crystal system	Triclinic
Space group	P-1
Unit cell dimensions	a = 9.9370(2)Å α = 111.598(1)°
	b = 12.2360(2)Å β = 95.196(1)°
	c = 15.1760(4)Å γ = 106.565(1)°
Volume	1604.42(6) $Å^3$
Z	2
Density (calculated)	1.298 Mg/m^3
Absorption coefficient	0.081 mm^{-1}
F(000)	660
Crystal size	0.30 x 0.25 x 0.18 mm
Theta range for data collection	3.54 to 27.58°.
Index ranges	-12<=h<=12; -15<=k<=15; -19<=l<=19
Reflections collected	29404
Independent reflections	7340 [R(int) = 0.0544]
Reflections observed (>2σ)	4954
Data Completeness	0.987
Absorption correction	Semi-empirical from equivalents
Max. and min. transmission	0.990 and 0.926
Refinement method	Full-matrix least-squares on F^2
Data / restraints / parameters	7340 / 3 / 446
Goodness-of-fit on F^2	1.023
Final R indices [I>2σ(I)]	R_1 = 0.0498 wR_2 = 0.1052
R indices (all data)	R_1 = 0.0906 wR_2 = 0.1224
Largest diff. peak and hole	0.259 and -0.243 $eÅ^{-3}$

Notes: hydrogen atoms attached to nitrogens were located and refined at a distance of 0.89 Å from the relevant parent atoms

Table 2. Atomic coordinates (x 10^4) and equivalent isotropic displacement parameters ($Å^2$ x 10^3) for **1**.U(eq) is defined as one third of the trace of the orthogonalized Uij tensor.

Atom	x	y	z	U(eq)
O(1)	9139(1)	4236(1)	1828(1)	27(1)
O(2)	7450(1)	2328(1)	1666(1)	33(1)
O(3)	8347(1)	4017(1)	3243(1)	26(1)
N(1)	11042(1)	4849(1)	3318(1)	25(1)
N(2)	7821(2)	-337(1)	-49(1)	34(1)
N(3)	4961(2)	3435(1)	2819(1)	35(1)
C(1)	9654(2)	6256(1)	3358(1)	25(1)
C(2)	8896(2)	6961(2)	3145(1)	30(1)
C(3)	9435(2)	8263(2)	3608(1)	35(1)
C(4)	10734(2)	8868(2)	4282(1)	35(1)
C(5)	11503(2)	8190(2)	4515(1)	31(1)
C(6)	10946(2)	6891(1)	4050(1)	25(1)
C(7)	11631(2)	6021(1)	4236(1)	28(1)
C(8)	11122(2)	3685(1)	3332(1)	26(1)
C(9)	11067(2)	2747(2)	2446(1)	31(1)
C(10)	11061(2)	1594(2)	2402(2)	38(1)
C(11)	11100(2)	1372(2)	3232(2)	41(1)
C(12)	11167(2)	2308(2)	4109(2)	40(1)
C(13)	11178(2)	3472(2)	4167(1)	33(1)
C(1A)	8161(2)	2535(1)	132(1)	26(1)
C(2A)	8780(2)	3428(2)	-227(1)	31(1)
C(3A)	8756(2)	3114(2)	-1204(1)	35(1)
C(4A)	8114(2)	1882(2)	-1858(1)	35(1)
C(5A)	7494(2)	984(2)	-1530(1)	31(1)
C(6A)	7506(2)	1284(2)	-550(1)	26(1)
C(7A)	6800(2)	230(2)	-272(1)	29(1)
C(8A)	7337(2)	-1291(2)	274(1)	30(1)
C(9A)	8323(2)	-1744(2)	607(1)	38(1)
C(10A)	7855(2)	-2721(2)	884(2)	47(1)
C(11A)	6416(2)	-3274(2)	837(2)	46(1)
C(12A)	5441(2)	-2824(2)	515(2)	42(1)
C(13A)	5883(2)	-1851(2)	233(1)	35(1)
C(1B)	6583(2)	1897(2)	3047(1)	28(1)
C(2B)	6767(2)	742(2)	2833(1)	34(1)
C(3B)	5997(2)	-115(2)	3161(1)	38(1)
C(4B)	5001(2)	167(2)	3705(1)	40(1)
C(5B)	4764(2)	1288(2)	3905(1)	37(1)
C(6B)	5536(2)	2153(2)	3581(1)	31(1)
C(7B)	5240(2)	3347(2)	3747(1)	36(1)
C(8B)	4696(2)	4481(2)	2775(1)	32(1)
C(9B)	5249(2)	5665(2)	3549(1)	41(1)
C(10B)	4970(2)	6671(2)	3452(2)	45(1)
C(11B)	4137(2)	6529(2)	2618(2)	43(1)
C(12B)	3594(2)	5353(2)	1847(2)	42(1)
C(13B)	3886(2)	4358(2)	1922(1)	38(1)
B(1)	9322(2)	4779(2)	2872(1)	25(1)
B(2)	8253(2)	3052(2)	1257(1)	25(1)
B(3)	7485(2)	2826(2)	2655(1)	27(1)

Table 3. Bond lengths [Å] and angles [°] for **1**.

O(1)-B(2)	1.354(2)	O(1)-B(1)	1.445(2)
O(2)-B(2)	1.378(2)	O(2)-B(3)	1.390(2)
O(3)-B(3)	1.359(2)	O(3)-B(1)	1.448(2)
N(1)-C(8)	1.456(2)	N(1)-C(7)	1.498(2)
N(1)-B(1)	1.747(2)	N(2)-C(8A)	1.407(2)
N(2)-C(7A)	1.462(2)	N(3)-C(8B)	1.401(2)
N(3)-C(7B)	1.460(2)	C(1)-C(6)	1.393(2)
C(1)-C(2)	1.395(2)	C(1)-B(1)	1.599(2)
C(2)-C(3)	1.392(2)	C(3)-C(4)	1.386(3)
C(4)-C(5)	1.387(2)	C(5)-C(6)	1.391(2)
C(6)-C(7)	1.509(2)	C(8)-C(13)	1.384(2)
C(8)-C(9)	1.394(2)	C(9)-C(10)	1.386(2)
C(10)-C(11)	1.384(3)	C(11)-C(12)	1.380(3)
C(12)-C(13)	1.392(2)	C(1A)-C(6A)	1.408(2)
C(1A)-C(2A)	1.409(2)	C(1A)-B(2)	1.570(2)
C(2A)-C(3A)	1.384(2)	C(3A)-C(4A)	1.378(2)
C(4A)-C(5A)	1.381(2)	C(5A)-C(6A)	1.392(2)
C(6A)-C(7A)	1.508(2)	C(8A)-C(13A)	1.395(2)
C(8A)-C(9A)	1.396(2)	C(9A)-C(10A)	1.382(3)
C(10A)-C(11A)	1.379(3)	C(11A)-C(12A)	1.377(3)
C(12A)-C(13A)	1.379(2)	C(1B)-C(2B)	1.399(2)
C(1B)-C(6B)	1.410(2)	C(1B)-B(3)	1.568(2)
C(2B)-C(3B)	1.389(2)	C(3B)-C(4B)	1.382(3)
C(4B)-C(5B)	1.386(3)	C(5B)-C(6B)	1.393(2)
C(6B)-C(7B)	1.507(2)	C(8B)-C(13B)	1.395(3)
C(8B)-C(9B)	1.399(3)	C(9B)-C(10B)	1.392(3)
C(10B)-C(11B)	1.371(3)	C(11B)-C(12B)	1.391(3)
C(12B)-C(13B)	1.370(3)		
B(2)-O(1)-B(1)	122.63(13)	B(2)-O(2)-B(3)	120.39(13)
B(3)-O(3)-B(1)	121.17(13)	C(8)-N(1)-C(7)	118.91(13)
C(8)-N(1)-B(1)	114.80(12)	C(7)-N(1)-B(1)	105.56(11)
C(8A)-N(2)-C(7A)	118.14(14)	C(8B)-N(3)-C(7B)	120.76(14)
C(6)-C(1)-C(2)	118.15(15)	C(6)-C(1)-B(1)	112.17(14)
C(2)-C(1)-B(1)	129.55(15)	C(3)-C(2)-C(1)	120.42(16)
C(4)-C(3)-C(2)	120.11(16)	C(3)-C(4)-C(5)	120.67(16)
C(4)-C(5)-C(6)	118.48(16)	C(5)-C(6)-C(1)	122.15(15)
C(5)-C(6)-C(7)	124.95(15)	C(1)-C(6)-C(7)	112.89(13)
N(1)-C(7)-C(6)	103.79(13)	C(13)-C(8)-C(9)	120.31(15)
C(13)-C(8)-N(1)	122.65(14)	C(9)-C(8)-N(1)	116.96(15)
C(10)-C(9)-C(8)	119.79(17)	C(11)-C(10)-C(9)	120.11(17)
C(12)-C(11)-C(10)	119.83(17)	C(11)-C(12)-C(13)	120.78(18)
C(8)-C(13)-C(12)	119.17(17)	C(6A)-C(1A)-C(2A)	117.06(15)
C(6A)-C(1A)-B(2)	126.85(14)	C(2A)-C(1A)-B(2)	116.08(14)
C(3A)-C(2A)-C(1A)	122.54(16)	C(4A)-C(3A)-C(2A)	119.33(16)
C(3A)-C(4A)-C(5A)	119.59(16)	C(4A)-C(5A)-C(6A)	121.82(16)
C(5A)-C(6A)-C(1A)	119.65(15)	C(5A)-C(6A)-C(7A)	117.42(15)
C(1A)-C(6A)-C(7A)	122.93(15)	N(2)-C(7A)-C(6A)	111.57(13)
C(13A)-C(8A)-C(9A)	118.17(16)	C(13A)-C(8A)-N(2)	122.22(16)
C(9A)-C(8A)-N(2)	119.53(15)	C(10A)-C(9A)-C(8A)	120.18(17)
C(11A)-C(10A)-C(9A)	121.37(18)	C(12A)-C(11A)-C(10A)	118.56(18)
C(11A)-C(12A)-C(13A)	121.12(18)	C(12A)-C(13A)-C(8A)	120.61(17)

C(2B)-C(1B)-C(6B)	117.68(15)	C(2B)-C(1B)-B(3)	119.60(15)
C(6B)-C(1B)-B(3)	122.66(14)	C(3B)-C(2B)-C(1B)	121.97(17)
C(4B)-C(3B)-C(2B)	119.45(17)	C(3B)-C(4B)-C(5B)	119.98(17)
C(4B)-C(5B)-C(6B)	120.86(17)	C(5B)-C(6B)-C(1B)	120.00(16)
C(5B)-C(6B)-C(7B)	121.61(16)	C(1B)-C(6B)-C(7B)	118.34(15)
N(3)-C(7B)-C(6B)	109.22(14)	C(13B)-C(8B)-C(9B)	118.17(17)
C(13B)-C(8B)-N(3)	119.36(16)	C(9B)-C(8B)-N(3)	122.45(17)
C(10B)-C(9B)-C(8B)	119.60(19)	C(11B)-C(10B)-C(9B)	121.61(18)
C(10B)-C(11B)-C(12B)	118.74(18)	C(13B)-C(12B)-C(11B)	120.44(19)
C(12B)-C(13B)-C(8B)	121.39(18)	O(1)-B(1)-O(3)	114.42(14)
O(1)-B(1)-C(1)	115.07(13)	O(3)-B(1)-C(1)	117.70(13)
O(1)-B(1)-N(1)	104.75(12)	O(3)-B(1)-N(1)	105.79(12)
C(1)-B(1)-N(1)	95.74(12)	O(1)-B(2)-O(2)	119.97(15)
O(1)-B(2)-C(1A)	118.78(14)	O(2)-B(2)-C(1A)	121.25(14)
O(3)-B(3)-O(2)	120.83(15)	O(3)-B(3)-C(1B)	123.09(15)
O(2)-B(3)-C(1B)	115.88(15)		

Symmetry transformations used to generate equivalent atoms:

Table 4. Anisotropic displacement parameters ($Å^2$ x 10^3) for **1**. The anisotropic displacement factor exponent takes the form: $-2\ gpi^2\ [\ h^2\ a^{*2}\ U11 + ... + 2\ h\ k\ a^*\ b^*\ U$

Atom	U11	U22	U33	U23	U13	U12
O(1)	32(1)	24(1)	21(1)	9(1)	6(1)	4(1)
O(2)	39(1)	27(1)	24(1)	9(1)	8(1)	2(1)
O(3)	28(1)	25(1)	23(1)	9(1)	7(1)	6(1)
N(1)	28(1)	23(1)	23(1)	10(1)	9(1)	8(1)
N(2)	30(1)	34(1)	42(1)	18(1)	10(1)	12(1)
N(3)	37(1)	34(1)	29(1)	9(1)	4(1)	12(1)
C(1)	28(1)	27(1)	21(1)	11(1)	10(1)	10(1)
C(2)	34(1)	33(1)	26(1)	14(1)	8(1)	12(1)
C(3)	47(1)	33(1)	34(1)	18(1)	16(1)	21(1)
C(4)	49(1)	22(1)	32(1)	9(1)	16(1)	11(1)
C(5)	35(1)	27(1)	25(1)	6(1)	8(1)	6(1)
C(6)	28(1)	26(1)	20(1)	9(1)	8(1)	7(1)
C(7)	28(1)	25(1)	24(1)	5(1)	1(1)	6(1)
C(8)	23(1)	25(1)	33(1)	14(1)	9(1)	8(1)
C(9)	31(1)	31(1)	31(1)	12(1)	5(1)	11(1)
C(10)	36(1)	29(1)	45(1)	10(1)	7(1)	13(1)
C(11)	39(1)	32(1)	63(1)	27(1)	16(1)	16(1)
C(12)	44(1)	47(1)	51(1)	34(1)	23(1)	22(1)
C(13)	37(1)	37(1)	36(1)	20(1)	16(1)	17(1)
C(1A)	23(1)	27(1)	25(1)	10(1)	4(1)	7(1)
C(2A)	32(1)	30(1)	26(1)	10(1)	5(1)	5(1)
C(3A)	36(1)	39(1)	29(1)	17(1)	7(1)	8(1)
C(4A)	36(1)	43(1)	24(1)	12(1)	6(1)	13(1)
C(5A)	32(1)	31(1)	25(1)	5(1)	3(1)	11(1)
C(6A)	23(1)	29(1)	25(1)	9(1)	3(1)	9(1)
C(7A)	26(1)	27(1)	29(1)	9(1)	3(1)	8(1)
C(8A)	33(1)	29(1)	28(1)	10(1)	8(1)	12(1)
C(9A)	29(1)	44(1)	45(1)	22(1)	8(1)	13(1)
C(10A)	42(1)	58(1)	55(1)	35(1)	11(1)	24(1)
C(11A)	44(1)	50(1)	59(1)	36(1)	15(1)	18(1)
C(12A)	34(1)	45(1)	55(1)	28(1)	14(1)	13(1)
C(13A)	32(1)	35(1)	42(1)	17(1)	9(1)	15(1)
C(1B)	32(1)	29(1)	21(1)	10(1)	3(1)	7(1)
C(2B)	37(1)	31(1)	27(1)	12(1)	5(1)	4(1)
C(3B)	45(1)	31(1)	33(1)	15(1)	0(1)	5(1)
C(4B)	38(1)	41(1)	33(1)	21(1)	-1(1)	-4(1)
C(5B)	29(1)	48(1)	26(1)	16(1)	4(1)	3(1)
C(6B)	29(1)	35(1)	22(1)	11(1)	2(1)	5(1)
C(7B)	35(1)	42(1)	28(1)	12(1)	10(1)	13(1)
C(8B)	31(1)	32(1)	34(1)	12(1)	13(1)	11(1)
C(9B)	43(1)	39(1)	34(1)	11(1)	9(1)	12(1)
C(10B)	53(1)	32(1)	43(1)	9(1)	14(1)	12(1)
C(11B)	51(1)	37(1)	48(1)	20(1)	18(1)	17(1)
C(12B)	46(1)	43(1)	39(1)	20(1)	12(1)	15(1)
C(13B)	41(1)	35(1)	33(1)	12(1)	9(1)	11(1)
B(1)	27(1)	27(1)	20(1)	11(1)	6(1)	9(1)
B(2)	26(1)	25(1)	23(1)	11(1)	4(1)	7(1)
B(3)	29(1)	28(1)	26(1)	12(1)	8(1)	9(1)

Table 5. Hydrogen coordinates (x 10^4) and isotropic displacement parameters ($Å^2$ x 10^3) for **1**.

Atom	x	y	z	U(eq)
H(21)	8007	6550	2681	36
H(31)	8910	8736	3461	42
H(4)	11102	9757	4589	42
H(5)	12389	8604	4982	37
H(7A)	12693	6376	4359	34
H(7B)	11360	5860	4800	34
H(9)	11034	2898	1875	37
H(10)	11029	955	1799	45
H(11)	11081	577	3200	49
H(12)	11205	2155	4679	48
H(13)	11224	4113	4772	40
H(2A)	9231	4279	219	37
H(3A)	9178	3741	-1422	42
H(4A)	8097	1653	-2530	42
H(5A)	7048	138	-1985	38
H(7A1)	6394	554	303	34
H(7A2)	5997	-417	-813	34
H(9A)	9320	-1380	643	45
H(10A)	8538	-3017	1112	56
H(11A)	6104	-3950	1023	55
H(12A)	4448	-3189	486	50
H(13A)	5191	-1560	8	41
H(2B)	7440	538	2452	40
H(3B)	6152	-888	3013	46
H(4B)	4481	-407	3941	48
H(5B)	4065	1469	4268	44
H(7B1)	4395	3351	4046	43
H(7B2)	6079	4075	4196	43
H(9B)	5812	5781	4138	49
H(10B)	5367	7477	3975	54
H(11B)	3934	7220	2569	52
H(12B)	3018	5239	1263	50
H(13B)	3528	3567	1381	45
H(2)	8685(18)	225(17)	312(14)	52(6)
H(1)	11556(18)	5020(16)	2911(12)	32(5)
H(3)	4310(20)	2689(16)	2340(14)	57(6)

Appendix 2. Crystal structure of compound **22**.

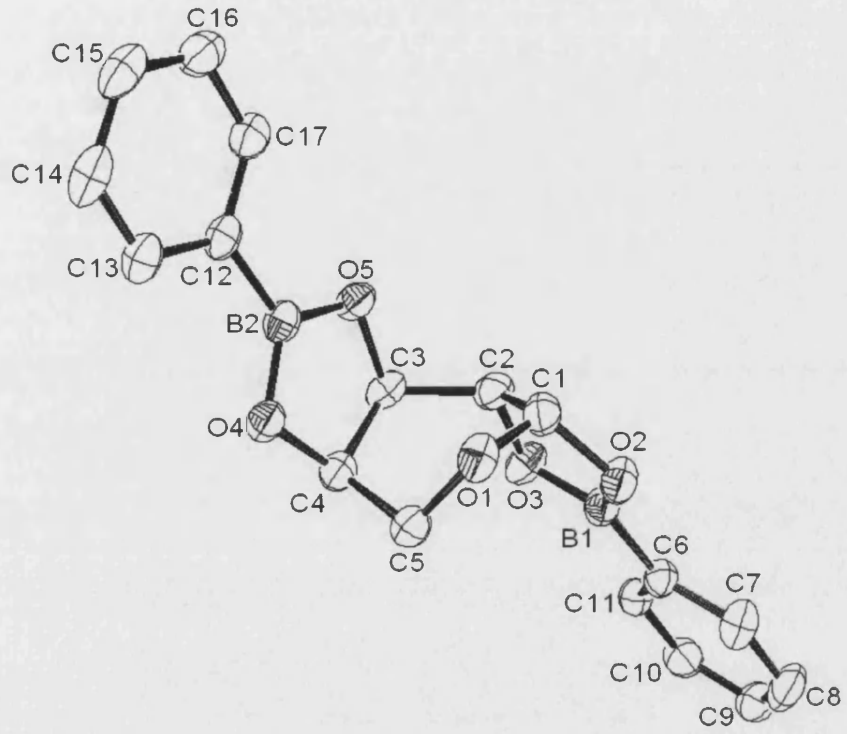

Table 1. Crystal data and structure refinement for **22.**

Identification code	k02kcm29
Empirical formula	$C_{17}H_{16}B_2O_5$
Formula weight	321.92
Temperature	170(2) K
Wavelength	0.71073 Å
Crystal system	Orthorhombic
Space group	$P2_12_12_1$
Unit cell dimensions	a = 9.2780(2)Å α = 90°
	b = 10.1300(2)Å β = 90°
	c = 16.9910(3)Å γ = 90°
Volume	1596.92(5) $Å^3$
Z	4
Density (calculated)	1.339 Mg/m^3
Absorption coefficient	0.095 mm^{-1}
F(000)	672
Crystal size	0.40 x 0.30 x 0.25 mm
Theta range for data collection	3.13 to 27.50°.
Index ranges	-12<=h<=12; -13<=k<=13; -22<=l<=22
Reflections collected	21791
Independent reflections	3645 [R(int) = 0.0493]
Reflections observed (>2σ)	3225
Data Completeness	0.994
Max. and min. transmission	0.9765 and 0.9628
Refinement method	Full-matrix least-squares on F^2
Data / restraints / parameters	3645 / 0 / 218
Goodness-of-fit on F^2	0.596
Final R indices [I>2σ(I)]	R_1 = 0.0334 wR_2 = 0.0981
R indices (all data)	R_1 = 0.0409 wR_2 = 0.1093
Absolute structure parameter	-0.6(8)
Largest diff. peak and hole	0.227 and -0.139 $eÅ^{-3}$

Table 2. Atomic coordinates ($\times 10^4$) and equivalent isotropic displacement parameters ($Å^2 \times 10^3$) for **22**.U(eq) is defined as one third of the trace of the orthogonalized Uij tensor.

Atom	x	y	z	U(eq)
B(1)	404(2)	1654(2)	-518(1)	30(1)
B(2)	-222(2)	-2679(2)	1336(1)	30(1)
C(1)	654(2)	-579(2)	-414(1)	36(1)
C(2)	952(2)	95(2)	386(1)	34(1)
C(3)	133(2)	-505(2)	1071(1)	31(1)
C(4)	-1446(2)	-882(2)	884(1)	30(1)
C(5)	-1758(2)	-815(2)	10(1)	33(1)
C(6)	133(2)	3042(2)	-881(1)	30(1)
C(7)	-4(2)	3238(2)	-1692(1)	41(1)
C(8)	-284(2)	4487(2)	-1996(1)	48(1)
C(9)	-416(2)	5553(2)	-1492(1)	43(1)
C(10)	-259(2)	5384(2)	-692(1)	38(1)
C(11)	11(2)	4133(2)	-387(1)	31(1)
C(12)	131(2)	-4115(2)	1590(1)	31(1)
C(13)	-942(2)	-5088(2)	1648(1)	36(1)
C(14)	-585(2)	-6388(2)	1815(1)	43(1)
C(15)	846(3)	-6738(2)	1929(1)	43(1)
C(16)	1913(2)	-5787(2)	1901(1)	41(1)
C(17)	1557(2)	-4486(2)	1730(1)	35(1)
O(1)	-586(1)	-1365(1)	-426(1)	35(1)
O(2)	517(1)	511(1)	-953(1)	37(1)
O(3)	528(1)	1451(1)	275(1)	35(1)
O(4)	-1572(1)	-2241(1)	1146(1)	33(1)
O(5)	827(1)	-1737(1)	1263(1)	32(1)

Table 3. Bond lengths [Å] and angles [°] for **22**.

B(1)-O(3)	1.367(2)	B(1)-O(2)	1.377(2)
B(1)-C(6)	1.556(2)	B(2)-O(4)	1.368(2)
B(2)-O(5)	1.368(2)	B(2)-C(12)	1.553(2)
C(1)-O(1)	1.399(2)	C(1)-O(2)	1.4399(18)
C(1)-C(2)	1.547(2)	C(2)-O(3)	1.4414(19)
C(2)-C(3)	1.516(2)	C(3)-O(5)	1.4422(18)
C(3)-C(4)	1.547(2)	C(4)-O(4)	1.4516(18)
C(4)-C(5)	1.514(2)	C(5)-O(1)	1.429(2)
C(6)-C(11)	1.391(2)	C(6)-C(7)	1.399(2)
C(7)-C(8)	1.391(3)	C(8)-C(9)	1.383(3)
C(9)-C(10)	1.377(3)	C(10)-C(11)	1.392(2)
C(12)-C(17)	1.396(2)	C(12)-C(13)	1.404(2)
C(13)-C(14)	1.387(2)	C(14)-C(15)	1.387(3)
C(15)-C(16)	1.382(3)	C(16)-C(17)	1.390(2)
O(3)-B(1)-O(2)	113.33(14)	O(3)-B(1)-C(6)	122.66(14)
O(2)-B(1)-C(6)	124.00(14)	O(4)-B(2)-O(5)	113.84(14)
O(4)-B(2)-C(12)	124.23(14)	O(5)-B(2)-C(12)	121.90(15)
O(1)-C(1)-O(2)	110.78(14)	O(1)-C(1)-C(2)	114.30(13)
O(2)-C(1)-C(2)	103.68(12)	O(3)-C(2)-C(3)	110.27(14)
O(3)-C(2)-C(1)	104.81(12)	C(3)-C(2)-C(1)	114.06(13)
O(5)-C(3)-C(2)	107.30(13)	O(5)-C(3)-C(4)	104.80(12)
C(2)-C(3)-C(4)	114.57(12)	O(4)-C(4)-C(5)	109.12(12)
O(4)-C(4)-C(3)	104.33(12)	C(5)-C(4)-C(3)	111.79(13)
O(1)-C(5)-C(4)	110.20(13)	C(11)-C(6)-C(7)	118.31(15)
C(11)-C(6)-B(1)	119.45(13)	C(7)-C(6)-B(1)	122.23(15)
C(8)-C(7)-C(6)	120.73(17)	C(9)-C(8)-C(7)	119.86(16)
C(10)-C(9)-C(8)	120.25(17)	C(9)-C(10)-C(11)	119.97(17)
C(6)-C(11)-C(10)	120.86(14)	C(17)-C(12)-C(13)	118.10(15)
C(17)-C(12)-B(2)	119.95(14)	C(13)-C(12)-B(2)	121.89(15)
C(14)-C(13)-C(12)	120.79(17)	C(15)-C(14)-C(13)	119.92(17)
C(16)-C(15)-C(14)	120.22(16)	C(15)-C(16)-C(17)	119.82(18)
C(16)-C(17)-C(12)	121.09(16)	C(1)-O(1)-C(5)	113.30(12)
B(1)-O(2)-C(1)	108.04(12)	B(1)-O(3)-C(2)	107.22(13)
B(2)-O(4)-C(4)	107.84(12)	B(2)-O(5)-C(3)	107.85(13)

Symmetry transformations used to generate equivalent atoms:

Table 4. Anisotropic displacement parameters ($Å^2 \times 10^3$) for **22**. The anisotropic displacement factor exponent takes the form: $-2\ gpi^2\ [\ h^2\ a^{*2}\ U11 + ... + 2\ h\ k\ a^*\ b^*\ U$

Atom	U11	U22	U33	U23	U13	U12
B(1)	33(1)	28(1)	30(1)	3(1)	4(1)	0(1)
B(2)	37(1)	31(1)	22(1)	0(1)	-1(1)	-2(1)
C(1)	42(1)	28(1)	37(1)	5(1)	11(1)	7(1)
C(2)	35(1)	29(1)	39(1)	8(1)	-3(1)	1(1)
C(3)	38(1)	25(1)	29(1)	3(1)	-5(1)	1(1)
C(4)	35(1)	29(1)	27(1)	2(1)	1(1)	2(1)
C(5)	36(1)	33(1)	29(1)	2(1)	-3(1)	-1(1)
C(6)	31(1)	29(1)	30(1)	5(1)	1(1)	-3(1)
C(7)	55(1)	37(1)	30(1)	3(1)	2(1)	-9(1)
C(8)	55(1)	53(1)	35(1)	20(1)	-4(1)	-9(1)
C(9)	40(1)	36(1)	52(1)	19(1)	2(1)	1(1)
C(10)	37(1)	29(1)	49(1)	3(1)	6(1)	1(1)
C(11)	32(1)	29(1)	33(1)	3(1)	3(1)	-3(1)
C(12)	42(1)	29(1)	21(1)	2(1)	1(1)	-2(1)
C(13)	46(1)	35(1)	27(1)	5(1)	-2(1)	-6(1)
C(14)	68(1)	32(1)	29(1)	5(1)	-3(1)	-14(1)
C(15)	72(1)	30(1)	26(1)	3(1)	1(1)	4(1)
C(16)	51(1)	38(1)	33(1)	4(1)	2(1)	11(1)
C(17)	43(1)	33(1)	30(1)	3(1)	3(1)	1(1)
O(1)	51(1)	27(1)	28(1)	-2(1)	4(1)	1(1)
O(2)	51(1)	28(1)	31(1)	4(1)	11(1)	4(1)
O(3)	48(1)	25(1)	31(1)	3(1)	-6(1)	-3(1)
O(4)	36(1)	32(1)	31(1)	6(1)	-2(1)	-2(1)
O(5)	35(1)	28(1)	33(1)	7(1)	-4(1)	1(1)

Table 5. Hydrogen coordinates (× 10^4) and isotropic displacement parameters ($Å^2$ × 10^3) for **22**.

Atom	x	y	z	U(eq)
H(1)	1506	-1126	-566	43
H(2)	2009	59	500	41
H(3)	165	103	1534	37
H(4)	-2127	-303	1182	36
H(5A)	-2653	-1309	-108	39
H(5B)	-1905	116	-148	39
H(7)	94	2509	-2040	49
H(8)	-383	4609	-2547	57
H(9)	-616	6405	-1699	51
H(10)	-335	6121	-349	46
H(11)	113	4022	165	38
H(13)	-1923	-4854	1571	43
H(14)	-1320	-7039	1851	52
H(15)	1092	-7633	2027	51
H(16)	2889	-6023	1998	49
H(17)	2296	-3838	1709	42

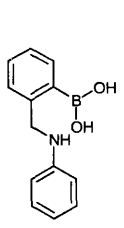

1

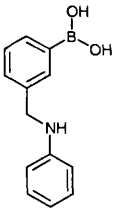

2

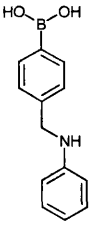

3

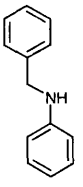

4

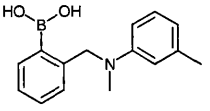

9

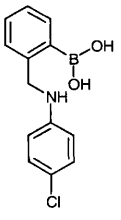

5

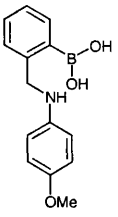

6

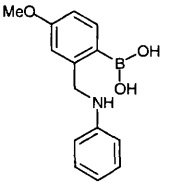

7

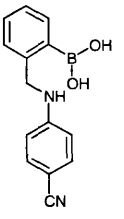

8

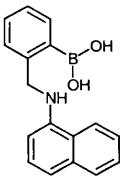

10

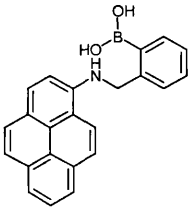

11

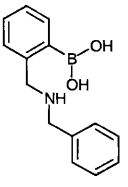

12

Monoboronic acid sensors series

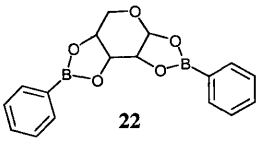

22

Arabinose-phenylboronic acid complex

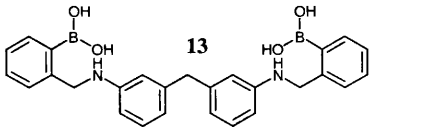

13

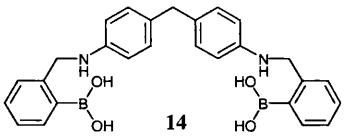

14

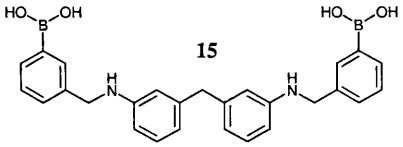

15

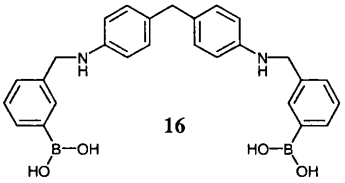

16

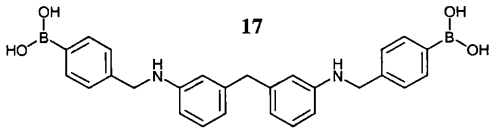

17

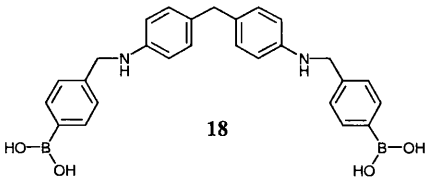

18

Diboronic acid sensors series

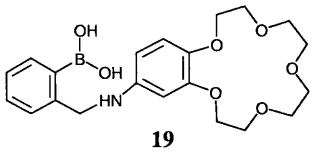

19

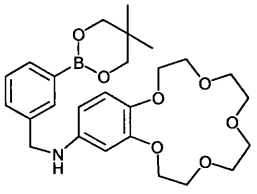

20

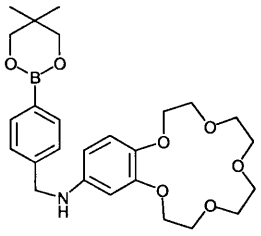

21

Crown ether sensors series